

Phosphate homeostasis and posttranscriptional gene regulation
during arbuscular mycorrhizal symbiosis in *Medicago truncatula*

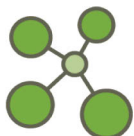
Dissertation

zur Erlangung des akademischen Grades
"doctor rerum naturalium"
(Dr. rer. nat.)
in der Wissenschaftsdisziplin "Biochemie"

eingereicht an der
Mathematisch-Naturwissenschaftlichen Fakultät
der Universität Potsdam

von
Anja Branscheid
geb. am 03.12.1979 in Templin

Potsdam, Februar 2012



IMPRS
Primary Metabolism
and Plant Growth



MAX-PLANCK-GESELLSCHAFT

Published online at the
Institutional Repository of the University of Potsdam:
URL <http://opus.kobv.de/ubp/volltexte/2012/6210/>
URN <urn:nbn:de:kobv:517-opus-62106>
<http://nbn-resolving.de/urn:nbn:de:kobv:517-opus-62106>

CONTENTS

1	INTRODUCTION	1
1.1	PHOSPHORUS IN PLANT NUTRITION	1
1.1.1	<i>P_i-homeostasis in plants</i>	2
1.2	ARBUSCULAR MYCORRHIZAL SYMBIOSIS (AMS)	3
1.2.1	<i>State of the art - Phosphate homeostasis and AMS- development</i>	5
1.3	MICRORNAS AND POSTTRANSCRIPTIONAL REGULATION OF GENES	6
1.3.1	<i>miRNAs involved in plant-microbe interactions</i>	7
1.3.2	<i>Identification of new miRNA targets with degradome analysis</i>	8
1.4	AIM OF THE WORK	10
2	MATERIAL AND METHODS	11
2.1	MATERIALS	11
2.1.1	<i>Chemicals</i>	11
2.1.1.1	Enzymes	11
2.1.1.2	Reaction kits	11
2.1.1.3	Other kits	12
2.1.1.4	Antibiotics	12
2.1.1.5	Buffers and solutions	12
2.1.1.6	Synthetic oligonucleotides and genes	15
2.1.1.7	Other chemicals	16
2.1.2	<i>Growth media</i>	16
2.1.2.1	Bacterial growth media	16
2.1.2.2	Plant growth substrates, media and solutions	17
2.1.3	<i>Biological material</i>	18
2.1.3.1	Bacterial strains	18
2.1.3.2	Fungal inoculum	18
2.1.3.3	Plant material	18
2.1.3.4	Plasmids	18
2.2	METHODS	19
2.2.1	<i>Plant growth and transformation of Medicago truncatula</i>	19
2.2.1.1	Surface sterilization and germination of seeds	19
2.2.1.2	Inoculation with <i>Glomus intraradices</i>	19
2.2.1.3	Nodulation of <i>M. truncatula</i> plants	19
2.2.1.4	Plant growth conditions	19
2.2.1.5	Time course experiment	20
2.2.1.6	P _i -gradient experiment	20
2.2.1.7	Plant root transformation using <i>A. rhizogenes</i>	20
2.2.1.8	Infiltration of transformed <i>A. tumefaciens</i> into <i>Nicotiana benthamiana</i>	21
2.2.2	<i>Biomolecular methods</i>	21
2.2.2.1	Cloning strategies and preparation of plasmids	21
2.2.2.2	Transformation of microorganisms	24

2.2.2.3	DNA isolation methods	24
2.2.2.4	RNA isolation methods.....	25
2.2.2.5	cDNA synthesis for real-time quantification of mRNAs	25
2.2.2.6	cDNA synthesis for real-time quantification of small RNAs.....	25
2.2.2.7	Polymerase-chain-reaction (PCR)	26
2.2.2.8	Modified 5'- RLM-RACE to determine miRNA target cleavage	27
2.2.2.9	Degradome library preparation.....	27
2.2.3	<i>Biochemistry</i>	27
2.2.3.1	Determination of soluble phosphate	27
2.2.3.2	<i>In situ</i> hybridization using LNA detection probes	28
2.2.3.3	Non-radioactive RNA-RNA Gelshift assay.....	28
2.2.3.4	Staining of fungal structures in roots	30
2.2.4	<i>Bioinformatic methods</i>	30
2.2.4.1	Processing of Illumina SBS high-throughput sequencing data	30
3	RESULTS	32
3.1	IDENTIFICATION OF NOVEL miRNA CLEAVAGE TARGETS IN <i>M. TRUNCATULA</i> ROOTS USING DEGRADOME HIGH-THROUGHPUT SEQUENCING	32
3.1.1	<i>Construction and quality control of degradome libraries of G. intraradices colonized and non-colonized roots</i>	32
3.1.2	<i>Mapping of degradome sequence tags to Medicago truncatula genome resources</i>	33
3.1.2.1	The degradome sequences are correlated to transcriptome data of mycorrhizal and non-mycorrhizal roots	34
3.1.3	<i>Identification of miRNA/miRNA* cleavage targets</i>	35
3.1.4	<i>MiRNA/miRNA*-mediated mRNA cleavage of genes involved in root endosymbioses</i>	38
3.1.5	<i>The distribution of degradome tags provides information about miRNA precursor processing and regulation of miRNA abundance</i>	41
3.2	INVOLVEMENT OF PLANT P _i -HOMEOSTASIS SIGNALLING COMPONENTS IN AMS DEVELOPMENT	44
3.2.1	<i>PHR1 as transcriptional regulator of the low phosphate response and its putative function during AMS</i>	44
3.2.1.1	Identification of putative <i>AtPhr1</i> homologues in <i>M. truncatula</i>	44
3.2.1.2	Functional characterization of <i>MtPhr1</i> during AMS	45
3.2.2	<i>The role of Mt4 during AMS – characterization of a functional Mt4 knock-out mutant</i>	48
3.2.2.1	Identification of a <i>Mt4 Tnt1</i> insertional knock-out mutant	48
3.2.2.2	Overexpression of <i>Mt4</i> transcripts.....	50
3.2.2.3	Identification of a putative <i>Mt4</i> homologue in <i>M. truncatula</i>	51
3.2.2.4	<i>Mt4-2</i> interacts with mature miR399	52
3.2.3	<i>Involvement of miR399 in AMS regulation</i>	54
3.2.3.1	Localization of mature miR399 in roots using <i>in situ</i> hybridization.....	54
3.2.3.2	Localization of miR399 promoter activity	57
3.2.3.3	Regulation of miR399 transcription at different stages of AMS development	59
3.2.3.4	P _i -gradient experiment - effects of the symbiotic P _i -uptake on plant P _i -homeostasis	61
3.2.3.5	Crosstalk of P _i -homeostasis, AMS development and photosynthates.....	64
3.2.4	<i>Identification of a novel miR399 target by degradome analysis</i>	65

3.2.4.1	<i>In vivo</i> validation of miR399-mediated cleavage of <i>MtPt8</i> transcripts	66
3.2.4.2	Conservation of miR399 binding sites in the P _i -transporter family in <i>M. truncatula</i>	69
3.2.4.3	Conservation of miR399-mediated regulation of P _i -transporters in the Viridiplantae kingdom	71
3.2.5	<i>MiR399 - MtPt8 interaction links P_i-homeostasis and AMS</i>	73
3.2.5.1	Expression analysis of <i>MtPt8</i> transcripts.....	73
3.2.5.2	Localization of <i>MtPt8</i> promoter activity.....	75
4	DISCUSSION	77
4.1	DEGRADOME DEEP SEQUENCING PROVIDES INFORMATION ABOUT REGULATION OF mRNA ABUNDANCE, miRNA CLEAVAGE TARGETS AND miRNA PRECURSOR PROCESSING.....	77
4.1.1	<i>mRNA abundance is regulated through general and specific degradation mechanisms</i>	77
4.1.2	<i>miRNA*-mediated target cleavage</i>	78
4.1.3	<i>miRNAs modulate the defence response upon mycorrhizal infection</i>	80
4.1.4	<i>Regulation of symbiosis relevant transcripts by miRNAs</i>	80
4.1.5	<i>Combined analysis of degradome and small RNA data for insight into miRNA precursor processing and regulation</i>	82
4.2	PHOSPHATE HOMEOSTASIS SIGNALLING IS DIRECTLY LINKED TO AMS AND IS SUBJECTED TO A COMPLEX REGULATION IN RESPONSE TO THE SYMBIOTIC INTERACTION	84
4.2.1	<i>Overexpression of MtPhr1 positively influences colonization with AMF</i>	84
4.2.2	<i>Mt4 transcript abundance cannot be modulated through overexpression</i>	85
4.2.3	<i>Identification of a Mt4 Tnt1 knockout mutant</i>	86
4.2.4	<i>Dynamics of AMS development and components of the P_i-homeostasis signalling pathway</i>	87
4.2.5	<i>Interplay of photosynthetic carbon, P_i-homeostasis and AMS development</i>	90
4.2.6	<i>Cell-specific accumulation of mature miR399 in arbuscule-containing cells – pros and cons of miR399 movement</i>	91
4.2.7	<i>The novel miR399 target MtPt8 directly links P_i-homeostasis signalling and AMS</i>	93
5	SUMMARY	95
6	LITERATURE	96
7	ACKNOWLEDGEMENT	106
8	SUPPLEMENTARY	107
9	EIDESSTATTLICHE ERKLÄRUNG	112

The following parts of this work were published:

Stars and symbiosis: microRNA and microRNA*-mediated transcript cleavage involved in arbuscular mycorrhizal symbiosis.

Branscheid A, Devers EA, May P, Krajinski F.
Plant Phys. 2011, 156 (4): 1990-2011

Distribution pattern of small RNA and degradome reads provides information on miRNA gene structure and regulation.

Branscheid A, Devers EA, May P, Krajinski F.
Plant Signal Behav. 2011, 6 (10): 1609-1611

Expression pattern suggests a role of MiR399 in the regulation of the cellular response to local P_i increase during arbuscular mycorrhizal symbiosis.

Branscheid A, Sieh D, Pant BD, May P, Devers EA, Elkrog A, Schauser L, Scheible WR, Krajinski F.
Mol Plant Microbe Interact. 2010, 23(7): 915-26

Other publications

Evidence that SNF1-related kinase and hexokinase are involved in separate sugar-signalling pathways modulating post-translational redox activation of ADP-glucose pyrophosphorylase in potato tubers.

Tiessen A, Prescha K, Branscheid A, Palacios N, McKibbin R, Halford NG, Geigenberger P.
Plant J. 2003, 35(4): 490-500.

Starch synthesis in potato tubers is regulated by post-translational redox modification of ADP-glucose pyrophosphorylase: a novel regulatory mechanism linking starch synthesis to the sucrose supply.

Tiessen A, Hendriks JH, Stitt M, Branscheid A, Gibon Y, Farré EM, Geigenberger P.
Plant Cell. 2002, 14(9): 2191-213.

ABBREVIATIONS

ac	arbuscule containing cell
AMS	arbuscular mycorrhizal symbiosis
ATP	adenosine-5'-triphosphate
BCIP	5-bromo-4-chloro-3-indolyl phosphate
bp	base pairs
bs	binding site
CDS	coding sequence
cDNA	complementary deoxyribonucleic acid
CIP	calf intestine phosphatase
cm	centimeter
Ct	threshold cycle
DCL	Dicer-like protein
ddH ₂ O	double distilled water
deg tag	degradome tag
DEPC	diethylpyrocarbonate
DIG	digoxigenin
DNA	deoxyribonucleic acid
DNase	deoxyribonuclease
dNTPs	deoxyribonucleotides
dpi	days post inoculation
DPU	direct phosphate uptake system
dsRNA	double stranded ribonucleic acid
DTT	dithiothreitol
<i>E. coli</i>	<i>Escherichia coli</i>
EDC	1-ethyl-3-(3-dimethylaminopropyl) carbodiimide
EDTA	ethylenediaminetetraacetic acid
eGFP	enhanced green fluorescent protein
EST	expressed sequence tag
<i>et al.</i>	and others
EtBr	ethidium bromide

ABBREVIATIONS

EtOH	ethanol
g	gram
gDNA	genomic deoxyribonucleic acid
h	hour
GdmCl	guanidinium chloride
kb	kilo base pairs
l	litre
LFC	log ₂ -fold change
LNA	locked nucleic acid
M	molar
MES	2-(N-morpholino)ethanesulfonic acid
MFS	major facilitator superfamily
mg	milligram
min	minutes
miRNA	micro ribonucleic acid
miR	mature micro ribonucleic acid
miR*	micro ribonucleic acid star strand
ml	milliliter
mM	millimolar
mRNA	messenger ribonucleic acid
myc	mycorrhizal
NBT	nitro blue tetrazolium
nt	nucleotides
nmyc	non-mycorrhizal
ORF	open reading frame
PBS	phosphate buffered saline
PCR	polymerase chain reaction
P _i	inorganic phosphate
PR	pathogen-related
Pri-miR	miRNA primary transcript
qRT-PCR	quantitative real time PCR
RISC	RNA-induced silencing complex

ABBREVIATIONS

RLM-RACE	RNA ligase mediated rapid amplification of cDNA-ends
RNA	ribonucleic acid
RNase	ribonuclease
rpm	rotations per minute (centrifuge)/ reads per million (small RNAs)
rRNA	ribosomal ribonucleic acid
RT	room temperature
RT-	reverse transcription (prefix)
SD	standard deviation
sr	small ribonucleic acids
TAE	Tris-acetate-EDTA
TAP	tobacco acid pyrophosphatase
TF	transcription factor
Tris	Tris(hydroxymethyl)aminomethane
<i>Tnt1</i>	transposon 1 of <i>Nicotiana tabacum</i>
UTR	untranslated region
W/V	weight/volume
wpi	weeks post-inoculation
V/V	volume/volume
Vol	volume
µg	microgram
µl	microliter
λ	wavelength

1 Introduction

1.1 Phosphorus in plant nutrition

Beside nitrogen, phosphorus (P) is the most limiting macro nutrient for plant growth, development and reproduction. Phosphorus is gathered up by plants as inorganic phosphate (P_i) and is predominantly metabolized as such. The growing cells need P_i for the synthesis of ATP, a crucial energy source needed for many metabolic, signal transduction and transport processes. The composition of essential macromolecules such as nucleic acids and phospholipids requires the incorporation of P_i . Although the total amount of P_i in the soil might be high, most of the P_i is unavailable for the plants. Inorganic phosphate forms pH-dependent insoluble complexes with positively charged mineral and organic ions and is often adsorbed to soil particles². The very slow diffusion of P_i in the soil compared to the uptake of P_i by plants leads to the depletion of soluble P_i in the rhizosphere³. Hence, the accessible concentration of P_i in most soils is less than $10 \mu\text{M}$ ⁴, which is insufficient for normal plant growth². To sustain constantly limited accessible P_i in the soil, plants have evolved several strategies. This involves the recycling, remobilization and coordinated allocation of internal P_i and an altered root morphology and architecture. Through the exudation of protons, organic acids and phosphatases the soil is acidified in order to solubilize P_i from organic resources, which can contribute up to 50% of the P_i -content of soils⁵. One major strategy is the formation of symbiotic associations with mycorrhizal fungi of which the arbuscular mycorrhizal symbiosis (AMS) is the most common one. This symbiotic interaction between plant roots and mycorrhizal fungi improves the P_i -status and growth of the plant by enhanced P_i -uptake via the extensive fungal network in the soil^{6,7}. With respect to the environmental protection, the investigation of adaptations to low nutrient availability is from great interest. Since artificial fertilizers have been widely used to increase crop yield, natural P resources became very limited⁸. The symbiotic association with soil-born AM fungi improves the nutrient status of plants in a natural manner and is a possibility to reduce the application of fertilizers in order to protect our environment.

1.1.1 P_i -homeostasis in plants

Because of the crucial role of P_i for plant growth and development, the plant P_i -homeostasis must be highly controlled and regulated which is mediated by the PHR1-PHO2-dependent P_i homeostasis signalling pathway⁹⁻¹¹ (figure 1). Although it is currently not known, how cellular P_i is sensed, recent investigations elicited major steps in the maintenance of P_i homeostasis in plants. Low cellular P_i induces the MYB transcription factor PHR1 (phosphate starvation response 1)¹² which is probably sumoylated by SIZ1 for activation¹³ PHR1 binds to a palindromic DNA-motif present in the promoter region of many P_i -starvation responsive genes such as the miRNA399 (miR399) gene family¹². Binding of PHR1 induces the transcription of the miR399 genes whereof 17 are known so far for *Medicago truncatula* (miRBase v.18). The miR399 primary transcripts (pri-miR399) are subsequently processed by DCL1¹⁴ in order to release mature miRNA399 molecules, which are long-distance shoot-to-root P_i -signals transported via the phloem^{15,16}. Mature miR399 mediate the cleavage of the *PHO2* transcript, which encodes for the constitutively expressed E2 ubiquitin conjugase enzyme repressing the P_i -starvation response under P_i -replete conditions¹⁷. The miR399-mediated decline of PHO2 levels leads therefore to the activation of the P_i -starvation response. This involves amongst others the establishment of high affinity P_i -transporters of the PHT1 family¹⁷ in order to increase the P_i -uptake rate. Additionally, it has been demonstrated that the non-coding RNA *At4/IPS1* sequesters mature miR399 by a mechanism called target mimicry¹⁸ in order to regulate the miRNA activity with regard to changing P_i -concentrations. The findings imply a complex regulation of P_i -homeostasis in response to P_i -deprivation.

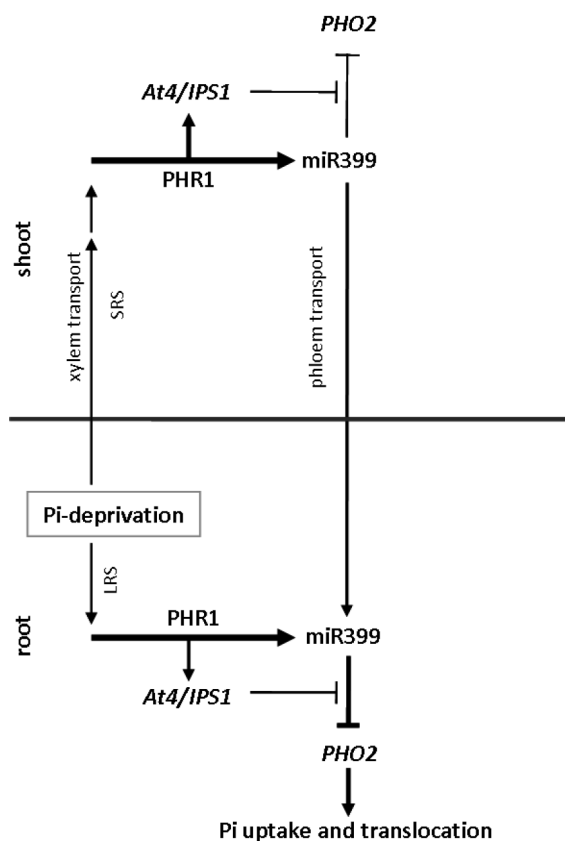


Figure 1. Proposed model of the systemic regulation by the PHR1-miR399-PHO2 signalling pathway in response to P_i -deprivation. It is suggested that P_i -deprivation-derived root born signals locally (LRS) and systemically (SRS) induce miR399 transcription in roots and shoots via PHR1, respectively. Mature miR399 are transported from shoots to roots through the phloem where they mediate the cleavage of PHO2 mRNA. By down-regulation of PHO2, the mechanisms for P_i -uptake and translocation are re-repressed. *IPS1*, which is a P_i -starvation induced non-coding RNA, negatively influences the mature miR399 activity and depends on activation by PHR1. Model adapted to Lin *et al.*, 2008.

1.2 Arbuscular mycorrhizal symbiosis (AMS)

The formation of symbiotic associations with mycorrhizal fungi is one major strategy of plants to overcome a low P_i availability in the soil. The AMS is a very widespread and ancient root endosymbiosis formed between plant roots and the obligate biotrophic arbuscular mycorrhizal fungi (AMF), aiming an improved supply with nutrients for the plant as well as for the fungus. Whereas the fungus provides the plant primarily with inorganic phosphate, nitrogen and water, the plant allocates up to 20 % of its photosynthetic carbohydrates to the fungus. The establishment of an AMS requires fundamental physiological and morphological changes in root cortical cells which precedes an intense molecular communication involving diffusible compounds, e.g. strigolactones and myc factors^{19,20}. The resulting reprogramming of cortex cells allows the fungus to penetrate the plant root and to grow into the inner

cortex²¹⁻²³. Here, the fungus forms the typical tree-like structures called arbuscules, which are supposed to be the place of nutrient exchange. The arbuscules are surrounded by the plant derived periarbuscular membrane (PAM)²⁴. Although the PAM is continuous from the plasma membrane it has a different composition of proteins²⁵, which is probably due to the different constitution of phospholipids compared to the cells usual plasma membrane. Several specific transport proteins are located in the PAM^{26, 27}, for example MtPT4, a mycorrhizal induced P_i transporter indispensable for AMS²⁸. The fact, that hundreds of plant genes are up-regulated during AMS establishment²⁹⁻³⁴ also suggests, that the plant actively regulates the tolerance to fungal colonization and determines development and degree of AMF colonization. Many factors directly or indirectly influence colonization levels, for example hormones^{35, 36}, photosynthesis rates³⁷ and nutrient status of the plant^{38, 39}. Especially the phosphate status has an impact on mycorrhizal development, but only little is known about the P_i-mediated regulation of AMS so far.

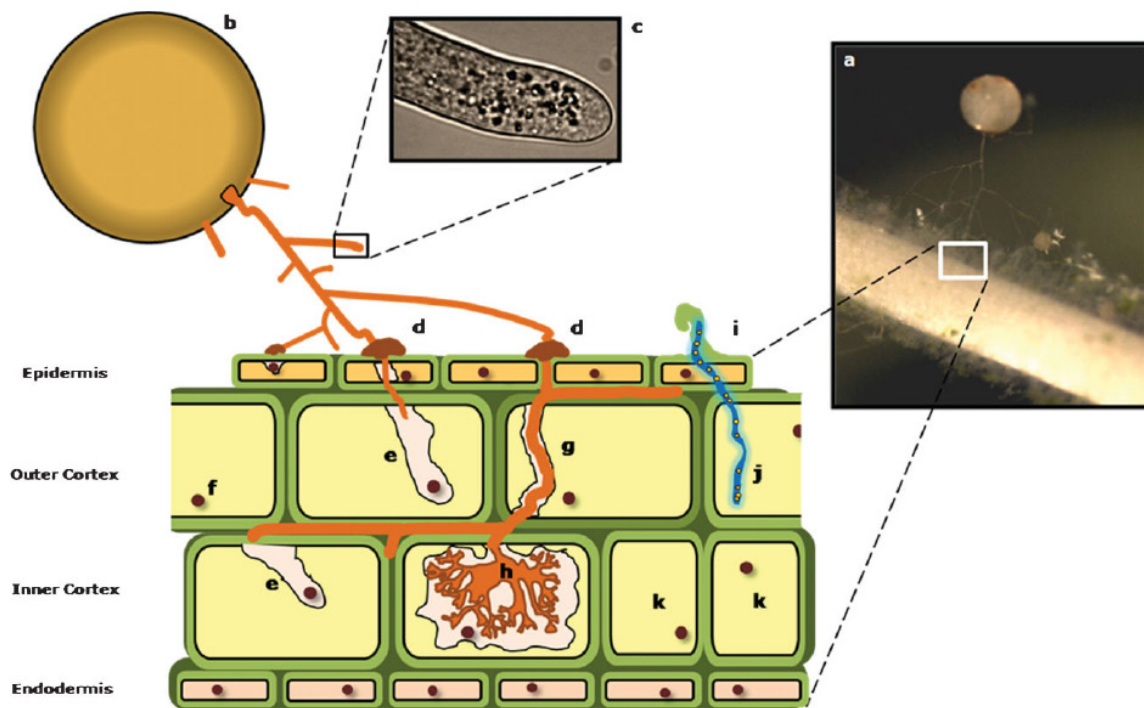


Figure 2. Overview of arbuscular mycorrhizal symbiosis development. A typical example of a leguminous plant root colonized with AM fungi (a) The germination of fungal spores (b) and an extensive hyphal branching is initiated upon perception of plant root exudates. The fungus releases diffusible compounds, namely myc-factors, triggering a calcium-dependent signalling in rhizodermal cells. Once fungal tips (c) touches the root surface, appressoria (d) and the prepenetration apparatus (PPA) (e) is formed to allow the fungal growth into the inner cortex (g). Here the typical tree-like structures, the arbuscules (h), develop and are supposed to be the place of nutrient exchange. Model from Lima *et al.*, 2009¹.

1.2.1 State of the art - Phosphate homeostasis and AMS-development

The symbiotic interaction with mycorrhizal fungi has a positive influence on plant P_i -nutrition and growth. Although there is a significant positive effect on mycorrhizal plant growth under P_i limitation, there is hardly any visible effect on growth in P_i -repleted mycorrhizal plants. Moreover, P_i -repleted plants are much less colonized by mycorrhizal fungi⁴⁰. This P_i -dependent AMS-repression is systemically regulated as demonstrated in split root cultures or by foliar application of P_i ^{40, 41}. Obviously, there must be a link between the regulatory mechanisms of P_i -sensing and homeostasis and AMS development. In a recent study⁴² we could demonstrate that the expression of key components of the P_i homeostasis signalling pathway is modulated upon colonization with the AMF *Glomus intraradices*. The transcription of seven members of the miR399 family was upregulated in leaves of mycorrhizal plants. Additionally, the mature miR399 accumulate to higher levels in mycorrhizal roots than in non-mycorrhizal roots under P_i -deplete conditions. Further, we observed a constantly low level of the miR399 target *MtPho2* in mycorrhizal roots despite increasing P_i levels caused by the symbiotic P_i uptake. Based on the results we suggested the mature miR399 being mobile P_i signals in the systemic P_i -dependent regulation of AMS development. Our hypothesis was further supported by the specific downregulation of the *AT4/IPS1* orthologue *Mt4* in *M. truncatula* by AM symbiosis⁴³. Downregulation of *Mt4* in colonized roots might positively influence the activity of mature miR399 molecules and, in addition to increased miR399 transcription in the shoots, this could be a mechanism to keep genes of the P_i -starvation response at high levels (figure 3). Interestingly, *IPS1* and its orthologue *Mt4*, miR399 and many other P_i -starvation and mycorrhizal-induced genes such as *MtPt4* exhibit one or more P1BS (Phr1 binding site) motifs in their promoter regions^{10, 12, 42} implying a PHR1 dependent initiation of transcription. In their very recent study Chen *et al.*⁴⁴ demonstrated that besides PHR1 another cis-acting element namely MYCS is required for the efficient activation of mycorrhizal induced P_i -transporters of the Pht1;4 family. Taken together, there are several lines of evidence that the regulation of P_i homeostasis and AM development are systemically affiliated but the mechanisms are still poorly understood and need to be elucidated.

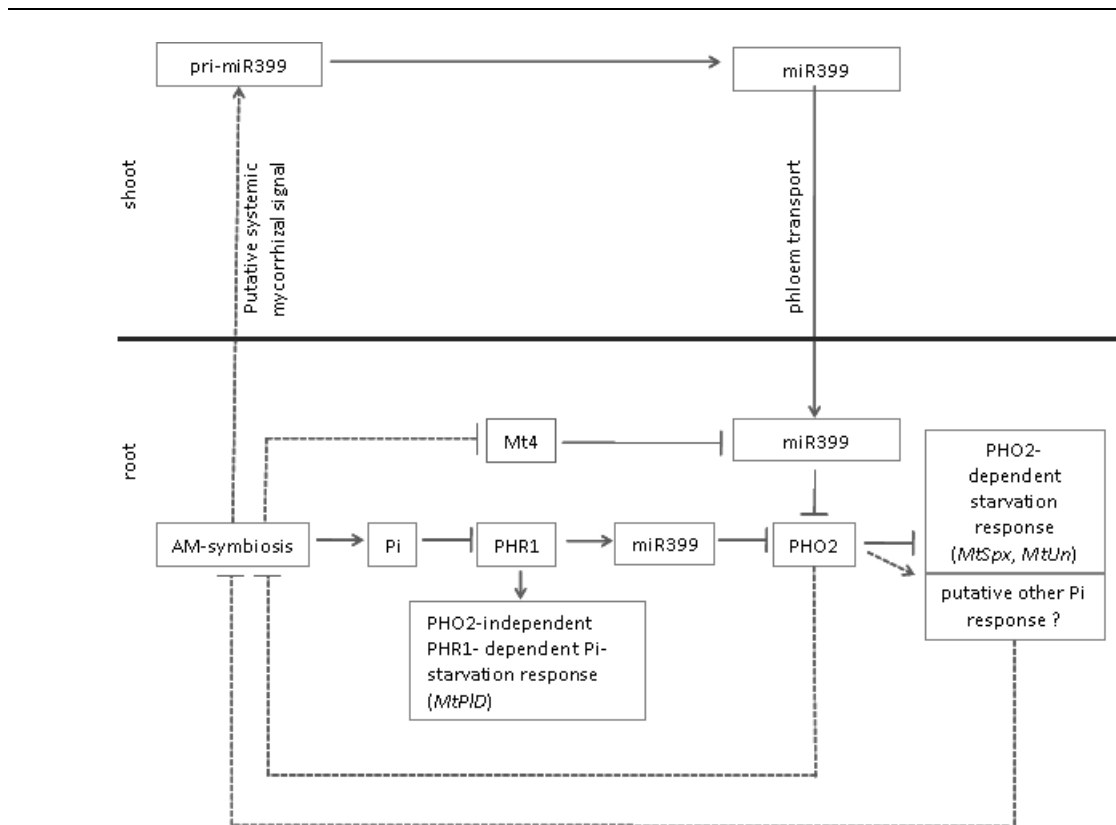


Figure 3. Hypothetical model of the influence of the symbiotic P_i -uptake to the systemic regulation of P_i -homeostasis. AM symbiosis improves the P_i -status in colonized roots. Hence, PHR1 will be downregulated and consistently, PHR1-dependent P_i -stress markers and pri-miR399 synthesis are repressed. In parallel, a hypothetical systemic mycorrhizal signal leads to increased pri-miR399 synthesis in shoots resulting in an increased accumulation of mature miR399 in mycorrhizal roots after phloem transport. Here, mature miR399 mediate the cleavage of their target PHO2, which has despite locally increased P_i and decreased miR399 transcription constantly low expression levels. This might be a mechanism of plants to keep PHO2 and other high responsive genes on low levels that might otherwise suppress AM symbiosis due to symbiotically provided P_i -increase in mycorrhizal roots. Yet unknown pathways are indicated in dashed lines. Model adapted to Branscheid *et al.*, 2010.

1.3 MicroRNAs and posttranscriptional regulation of genes

Small regulatory RNAs such as the microRNAs play a crucial role in the post-transcriptional and translational gene regulation in both plants and animals. miRNAs in plants, mostly 20-24 nts in length, are predominantly transcribed from intergenic located *MIR* genes through RNA polymerase II activity⁴⁵. The resulting 5' capped and 3' poly(A)-tailed primary transcript^{45,46} is processed in the nucleus by the ribonuclease III enzyme DICER-LIKE1 (DCL1) yielding in a miRNA/miRNA* duplex^{14,47,48}. The duplex is subsequently methylated by HUA ENHANCER1 (HEN1)^{49,50} and exported to the cytosol presumably by HASTY⁵¹. The mature strand then binds to the AGO1 protein and directs the miRNA-mediated inhibition of target transcripts⁵².

Post-transcriptional gene silencing (PTGS) is a mechanism based on RNA *interference* (RNAi) of most eucaryots to downregulate gene activity at the RNA level. It has been demonstrated that miRNAs are key players in the PTGS by affecting their target transcripts through two major mechanisms: mRNA cleavage and translational repression. The transcript cleavage is mediated by the complementary binding of the miRNA to its target mRNA. The miRNA-mRNA duplex is cleaved between the 10th and 11th nucleotide of the miRNA⁵³ by the endonuclease activity of AGO1^{54,55}. In the second mode of repression plant miRNAs mediate the translational inhibition of target mRNAs. This was shown in several studies where miRNA abundance, target transcript levels and target protein levels were examined^{10,56-58}. Although the target mRNA abundance was high the protein level of the appropriate target was significantly decreased. Translational repression is a widespread mode of action for plant miRNAs which was shown by Brodersen *et al.*⁵⁹ by the isolation of mutants that specifically deregulate miRNA-mediated translational inhibition.

1.3.1 miRNAs involved in plant-microbe interactions

RNA *interference* (RNAi) was originally thought to be a mechanism preventing the plant against viral attacks. It was supposed that the intrusion of exogenous viral small RNAs activates the plant immune response and mediates the silencing of viral genes to limit viral infection⁶⁰. Over the last years, it became obvious that the impact of small RNAs is not only related to virus-host infection but more to a wide range of plant-microbe interactions including bacteria and fungi. Plants often trigger their immune response by miRNAs as it has been shown by Navarro *et al.*⁶¹. The bacterial infection of Arabidopsis plants with infectious *Pseudomonas syringae* strongly induces the miR393 expression⁶¹. It turned out that the bacterial effector Flg22, a flagellin-derived pathogen-associated molecular pattern (PAMP), is responsible for the induction of miR393 which then targets transcripts involved in auxin signalling such as TIR1 (transport inhibitor response 1), AFB2 and AFB3 (auxin signalling F-Box protein). Overexpression of ath-miR393a resulted in decreased mRNA levels of TIR1 accompanied with restricted bacterial growth in those plants⁶². Several other miRNAs, such as miR160 and miR167, were up-regulated upon pathogenic bacterial infection and also regulate transcripts of the auxin signalling⁶³, suggesting that the basal plant immune response is based in the suppression of auxin signalling components. Interestingly, miR393 and miR167 were highly abundant in infiltrated zones after infection with the tumor-

inducing *Agrobacterium tumefaciens* but greatly reduced in tumor tissue⁶⁴. This indicates a tissue-specific action of these miRNAs.

Several studies gave evidence for the important role of miRNAs and their specific regulation of relevant genes in symbiotic interactions of plants with bacteria and fungi in the nodule or the arbuscular mycorrhizal symbiosis, respectively^{42, 65-69}. Transcription factors relevant for a functional nodule symbiosis like MtHAP2-1 and MtNSP2 are degraded by miR169 and miR172, respectively^{65, 67}. *In situ* hybridization revealed a differential and tissue specific expression of these miRNAs in nodules indicating the need for transcript regulation in distinct cells or tissues in response to the interaction with microbes. In recent studies, we suggested a role of the P_i-responsive miR399 in the systemic regulation of AMS development. We observed an increased accumulation of mature miR399 in mycorrhizal roots as compared to non-mycorrhizal roots⁴² and a cell-specific downregulation of its target transcript *MtPho2* in arbuscule containing cells⁷⁰. To what extent particularly this miRNA is involved in symbiosis development and its specific role in the linkage of P_i homeostasis and AMS needs to be further investigated.

1.3.2 Identification of new miRNA targets with degradome analysis

The establishment of the AMS and the formation of arbuscules involves a complex reprogramming of distinct root cortex cells resulting in massive changes in the transcriptome of mycorrhizal roots and arbuscule containing cells⁷¹⁻⁷³. Changes in transcript abundances can be realized by activation or repression of the transcription or by posttranscriptional regulation, for instance the miRNA-mediated degradation of mRNA. The entirety of all degraded transcripts, either by miRNAs or other mechanisms, is collectively named as degradome. The high-throughput sequencing of the degradome is one method to identify cleaved mRNA by detecting 5'-ends of degraded mRNA⁷⁴. The cleavage of mRNA by miRNA-AGO complexes or other endonucleases leaves a phosphate residue at the 5'-end of the degraded transcript, which is the basis for the construction of special cDNA libraries (figure 4)⁷⁵. cDNA libraries can be sequenced by next generation sequencing approaches, for example by the sequencing-by-synthesis (SBS) method by Illumina. SBS is a reversible terminator-based method enabling the detection of single bases as they are incorporated into growing DNA strands. The fluorescent-labelled terminator is imaged after binding of the appropriate dNTP and afterwards cleaved before the next base is incorporated. The resulting sequencing data are then computational

processed using the Cleaveland pipeline v2.0⁷⁶ a program to trim adapter sequences, remove structural RNAs (e.g. rRNA, tRNA), align the degradome sequence tags to genomic and cDNA databases to identify the corresponding mRNA and, finally, to determine transcripts which were cleaved by small RNAs.

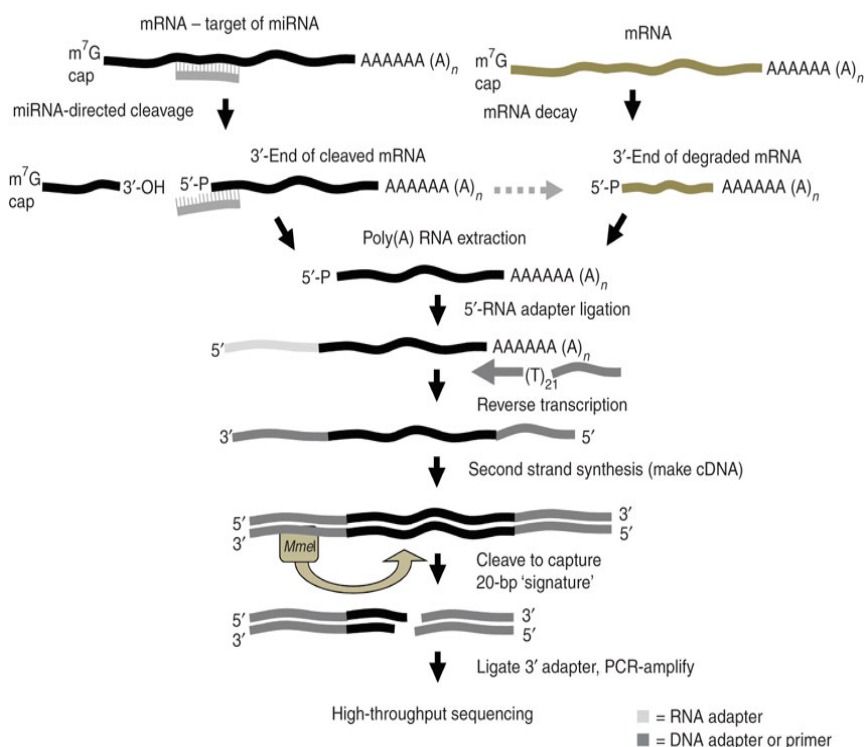


Figure 4. Schematic depiction of Degradome cDNA library construction for miRNA target identification. After extraction of polyadenylated an RNA adapter is ligated to the 5′-ends of the single-stranded cleaved or degraded RNA molecules that are ligation competent (with a 5′-monophosphate). Reverse transcription is carried out to generate the first strand of cDNA using an oligo (dT) with a 3′-adapter sequence. A short PCR is applied to amplify the cDNA that is afterwards digested with MmeI to generate equal-sized fragments that are recovered by PAGE (step not shown). A double-stranded 3′-DNA adapter with degenerate nucleotides in the overhang region is ligated to the MmeI digestion products that are recovered by PAGE (step not shown). The resulting material is PCR-amplified, gel-purified and used for high-throughput sequencing. Figure from German et al, 2009.

1.4 Aim of the work

A high P_i status systemically represses AMS development indicated by split root and foliar P_i treatment experiments. Therefore, we assume a link between the signalling pathway of the plant P_i homeostasis and AMS development. Recently we could show, that the miR399 as systemic regulators of the P_i homeostasis were increased upon colonization and accumulate to higher levels in shoots and roots of mycorrhizal plants. We suggested that miR399 might have a role in the systemic P_i -dependent regulation of AMS development and establishment. Still the underlying mechanisms of the P_i -mediated AM regulation and the specific role of miR399 are poorly understood and are thus the central aspect of this PhD thesis.

This work will focus on the investigation of the miR399 gene family and its modulators *MtPhr1* and *Mt4*, which are orthologues of *AtPhr1* and *At4/AtIPS1*. Using promoter studies and a LNA *in situ* hybridization based approach, the miR399 transcription site and mature miR399 accumulation in AM colonized roots will be localized, respectively. Furthermore, the modulation of *MtPhr1* and *Mt4* expression via stable or transient transformation of *M. truncatula* and the subsequent detailed analysis of the molecular and the mycorrhizal phenotype of these plants will indicate a putative role of these components in the linkage of P_i -status and AM development.

The fact that miRNAs such as miR399 and its target *MtPho2* are subjected to an AMS-dependent regulation further suggests a general role of miRNAs in the posttranscriptional gene regulation in the reprogramming of root cortex cells during AMS development. miRNAs became a central aspect in the plant research because of their crucial role in plant development, hormone signalling, nutrient homeostasis and in host-microbe interactions. Hence, the involvement of miRNAs in AMS development and maintenance is of great interest. To identify transcripts that are important for AMS development and specifically degraded by miRNAs a high-throughput sequencing of the *M. truncatula* degradome of colonized and non-colonized roots will be performed. The degradome analysis allows the identification of new miRNA targets where transcript degradation is the mode of repression. This second part of this work will be carried out in cooperation with the Bioinformatics workgroup of Dr. Dirk Walther at the MPI-MP.

2 Material and Methods

2.1 Materials

2.1.1 Chemicals

2.1.1.1 Enzymes

The following enzymes were used in this study:

Advantage [®] 2 DNA Polymerase	Clontech (St-Germain-en-Laye, France)
Anti-DIG-alkaline phosphatase	Roche (Mannheim, Germany)
BP-Clonase	Invitrogen (Darmstadt, Germany)
GoTaq [®] Flexi DNA Polymerase	Promega (Mannheim, Germany)
LR-Clonase	Invitrogen (Darmstadt, Germany)
Lysozym	Carl Roth (Karlsruhe, Germany)
MultiScribe [™] Reverse Transcriptase	Applied Biosystems (Carlsbad, CA, USA)
Proteinase K	Invitrogen (Darmstadt, Germany)
RNase A	Fermentas (St. Leon-Rot, Germany)
Restriction enzymes (Fast Digest [®])	Fermentas (St. Leon-Rot, Germany)
Restriction enzymes	NEB (Frankfurt a.M., Germany)
RiboLock [™] RNase Inhibitor	Fermentas (St. Leon-Rot, Germany)
SuperScript [®] III Reverse Transcriptase	Invitrogen (Darmstadt, Germany)
TURBO DNase [™]	Ambion (Austin, TX, USA)

2.1.1.2 Reaction kits

Advantage [®] 2 DNA Polymerase Kit	Clontech (St-Germain-en-Laye, France)
FirstChoice [®] RLM-RACE Kit	Ambion (Austin, TX, USA)
Gateway [®] BP Clonase [®] II Enzyme Kit	Invitrogen (Darmstadt, Germany)
Gateway [®] LR Clonase [®] II Enzyme Kit	Invitrogen (Darmstadt, Germany)
GoTaq [®] Flexi DNA Polymerase Kit	Promega (Mannheim, Germany)
Maxima [™] SYBR Green/ROX qPCR Master Mix (2x)	Fermentas (St. Leon-Rot, Germany)
pENTR [™] /D-TOPO [®] Cloning Kit	Invitrogen (Darmstadt, Germany)
Phire [®] Plant Direct PCR Kit	Finnzymes (Vantaa, Finland)
SuperScript [®] III Reverse Transcriptase Kit	Invitrogen (Darmstadt, Germany)
TOPO [®] TA Cloning [®] Cloning Kit for subcloning	Invitrogen (Darmstadt, Germany)

MATERIAL AND METHODS

TURBO DNA-free™	Ambion (Austin, TX, USA)
MAXIscript® T7/T3 in vitro transcription kit	Ambion (Austin, TX, USA)

2.1.1.3 Other kits

DNA extraction Kit Plant mini	nexttec™ (Hilgertshausen, Germany)
mirVana™ miRNA Isolation Kit	Ambion (Austin, TX, USA)
Plant RNA Isolation Aid	Ambion (Austin, TX, USA)
Wizard® SV Gel and PCR Clean-up System	Promega (Mannheim, Germany)

2.1.1.4 Antibiotics

Antibiotic	Concentration	Target organism
Gentamycin	20 µg/ml	<i>E. coli</i>
Kanamycin	25 µg/ml	<i>M. truncatula</i>
	50 µg/ml	<i>E. coli</i>
Spectinomycin	50 µg/ml	<i>E. coli</i> , <i>A. rhizogenes</i>
Streptomycin	50 µg/ml	<i>E. coli</i>
	600 µg/ml	<i>A. rhizogenes</i>

2.1.1.5 Buffers and solutions

All buffers and solutions were prepared with bi-distilled H₂O (ddH₂O), if not mentioned otherwise.

Plasmid mini preparation

Solution 1	25 mM	Tris-HCl pH 8
	10 mM	EDTA
	5 mg/ml	Lysozym
Solution 2	0.2 mM	Sodium hydroxide (NaOH)
	1 % [w/v]	Sodium dodecylsulfate (SDS)
Solution 3	2 mM	Potassium acetate pH 4.8

Phosphate measurements

Color reagent	1 vol.	4.2 % [w/v] Ammonium molybdate ([NH ₄] ₆ Mo ₇ O ₂₄ ·H ₂ O) in 5 M HCl
	3 vol.	0.2 % [w/v] Malachite Green in H ₂ O

MATERIAL AND METHODS

Phosphate Standard	0.5 mM	di-Potassium hydrogen phosphate (K ₂ HPO ₄)
--------------------	--------	---

RNA isolation

RNA extraction buffer, pH7	6 M	Guanidinium chloride (GdmCl)
	20 mM	EDTA
	20 mM	MES

Gel electrophoresis

50x TAE buffer	242 g	Tris base
	57.1 ml	glacial acetic acid
	100 ml	0.5 M EDTA (pH 8)
		add ddH ₂ O to 1 l
DEPC-H ₂ O	0.1 % [v/v]	in ddH ₂ O
		stirred over night
		2x autoclaved
Ethidium bromide (EtBr) solution	0.01 % [w/v]	0.01 mg EtBr in 100ml 0.5xTAE
10x MOPS buffer	200 mM	MOPS
	50 mM	sodium acetate
	20 mM	EDTA (pH 7)
RNA sample buffer	100 µl	formamide
	38 µl	formaldehyde
	20 µl	10x MOPS buffer
	42 µl	DEPC-H ₂ O
RNA loading buffer	99 µl	6x loading dye
	1 µl	10 mg/ml EtBr

Staining of fungal structures

Trypan blue solution	0.1 % [w/v]	Trypan blue in lactophenol (25% [w/v] phenol in water/glycerol/ lactic acid in the ratio 1:1:1)
Alexa Fluor 488	1mg/ml	in PBS, pH7.4

MATERIAL AND METHODS

In-situ hybridization

1 M Tris-HCl	121.1 g	Tris-HCl, pH 8 adjust with HCl
Solution B1	0.1 M	Tris-HCl, pH 7.5
	0.15 M	Sodium chloride (NaCl)
Solution B3	0.1 M	Tris-HCl, pH 9.5
	0.1 M	NaCl
1 x PBS	137 mM	Sodium chloride (NaCl)
	2.7 mM	Potassium chloride (KCl)
	12 mM	di-Sodium hydrogen phosphate (Na ₂ HPO ₄) / Potassium di-hydrogen phosphate (KH ₂ PO ₄)
PBST		1 x PBS with 0.1 % [w/v] Tween-20
1 x TBS	50 mM	Tris-HCl
	150 mM	Sodium chloride (NaCl)
		adjust to pH 7.5 with HCl
TBST		1 x TBS with 0.1 % [w/v] Tween-20
Fixative	10 ml	10 % [w/v] para formaldehyde
	2.5 ml	10 x PBS
		add ddH ₂ O to 25 ml, adjust to pH 7
EDC buffer	1.6 ml	130 mM 1-methylimidazol
	130 ml	ddH ₂ O
	450 µl	conc. HCl
	16 ml	3 M sodium chloride
		add ddH ₂ O to 160 ml
EDC solution	10 ml	EDC buffer
	176 µl	EDC
	100 µl	conc. HCl

Other Buffers

1 x TAE	40 mM	Tris-acetate
	1 mM	EDTA, pH 8
TE buffer	10 mM	Tris-HCl, 1 mM EDTA, pH 8

Nicotiana benthamiana infiltration

AS medium for 100ml:

stock solution		stock C	volume added	final C
MgCl ₂	25,4g in 50ml	2,5M	400µl	10mM
MES-KOH buffer (pH 5,6)	19,5g in 100ml	1M	1ml	10mM
AS ¹ (dissolved in DMSO)	0,294g in 10ml	150mM	100µl	150µM

fill up with ddH₂O

2.1.1.6 Synthetic oligonucleotides and genes

5'-DIG-labelled miRCURY LNA probes for *in situ* hybridization (Exiqon, Denmark). All probes were diluted to 2.0 pmol/µl; position of LNA substitution is not indicated.

Scramble probe	5' DIG-GTGTAACACGTCTATACGCCCA
Mtr-miR399b probe	5' DIG-CAGGGCAGCTCTCCTTTGGCA
Mtr-miR399d probe	5' DIG-TAGGGCAGCTCTCCTTTGGCA

5'-DIG-labelled RNA-oligonucleotides for miRNA-mRNA interaction studies (Eurofins mwg operon, Ebersberg)

Scramble probe	5' DIG-GUGU AACACGUCUAUACGCCCA
Mtr-miR399b	5' DIG- UGCCAAAGGAGAGCUGCCCUG
Mtr-miR399d	5' DIG- UGCCAAAGGAGAGCUGCCCUA

Synthetic gene for *in vivo* validation of miR399-mediated cleavage of *MtPt8* (synthesized by Eurofins MWG operon, Eberberg, Germany)

ctcgagTAGGTGTTGCGTTGTGTGGCACCCCTGCAGGGCAACTCTTCTTTGGCTGGCTTCAGGGCAACTCTTCTTTGGCTcac
 gtCAGGGCAACTCTTCTTTGGCTcgcgCAGGGCAACTCTTCTTTGGCTGGCTTCAGGGCAACTCTTCTTTGGCTGGCTGGT
 GACaagcttGGTAGAATCCTATAACAACCAACCAAGCCAGGGCAGATAGCGTTTGGCTGGCTTCAGGGCAGATAGCGTTT
 GGCTctgcgCAGGGCAGATAGCGTTTGGCTacgcgCAGGGCAGATAGCGTTTGGCTGGCTTCAGGGCAGATAGCGTTTGGC
 TGTATATCCAATAAATGTACGTTTCTggatcc

legend for highlights:

underlined	linker region, used as primer binding site for PCR-amplification
bold	miR399 binding site of the <i>MtPt8</i> transcript
bold italic	mutated miR399 binding site of the <i>MtPt8</i> transcript
lowercase	enzyme restriction site

All primers used for standard PCR, qRT-PCR and (stemloop)-cDNA-synthesis were synthesized by Eurofins MWG operon (Ebersberg, Germany) and are listed in the supplementary table 1.

2.1.1.7 Other chemicals

6x DNA Loading Dye	Fermentas (St. Leon-Rot, Germany)
Bacto™ Agar	Becton Dickinson (Heidelberg, Germany)
Bacto™ Trypton	Becton Dickinson (Heidelberg, Germany)
Biozyme LE Agarose	Biozym Scientific (Hess. Oldendorf, Germany)
Blocking Reagent for nucleic acid hybridization and detection	Roche (Mannheim, Germany)
CIP solution	Carl Roth (Karlsruhe, Germany)
DEPC	Carl Roth (Karlsruhe, Germany)
EDC	Sigma-Aldrich (Munich, Germany)
GeneRuler™ 100bp Plus DNA Ladder	Fermentas (St. Leon-Rot, Germany)
GeneRuler™ 1kb DNA Ladder	Fermentas (St. Leon-Rot, Germany)
<i>In situ</i> hybridization buffer	ENZO® life science (Lörrach, Germany)
IPEGAL® CA-630	Sigma-Aldrich (Munich, Germany)
MOPS	Sigma-Aldrich (Munich, Germany)
NBT/BCIP	Roche (Mannheim, Germany)
Nuclease free water (not DEPC-treated)	Ambion (Austin, TX, USA)
Select Agar®	Invitrogen (Darmstadt, Germany)
Yeast extract	Duchefa Biochemie B.V. (Netherlands)

2.1.2 Growth media

2.1.2.1 Bacterial growth media

LB medium	10 g/l Bacto™ Tryptone, 5 g/l Yeast extract, 10 g/l NaCl, pH 7 (NaOH)
TY/Ca medium	5 g/l Bacto™ Tryptone, 3 g/l Yeast extract, pH 7.2 (NaOH), 4.5 mM CaCl ₂ (addition after autoclaving)
YEB medium	5 g/l Bacto™ Beef extract, 5 g/l Bacto™ Peptone, 1 g/l Yeast extract, 5 g/l sucrose, 2 ml of 1 M Mg ₂ SO ₄ added to 1 l medium, pH 7.2 (NaOH)
SOC medium	20 g/l Bacto™ Tryptone, 5 g/l Yeast extract, 0.5 g/l NaCl, 10 ml of 0.25 M KCl per 1 l medium (addition after dissolving the previous compounds), pH 7 (NaOH), addition of 5 ml sterile 2 M MgCl ₂ solution after autoclaving, addition of 20 ml filter-sterilized 1 M glucose

after autoclaving

For solid media 15 g/l Select Agar[®] (or Bacto™ Agar for TY medium) was added before autoclaving.

2.1.2.2 Plant growth substrates, media and solutions

Medium	conc.	compound
Quartz sand/vermiculite mixture (3:1)	2 vol	0.6 – 1.2 mm quartz sand
	1 vol	0.3 – 0.8 mm quartz sand
	1 vol	vermiculite
Modified Fahraeus medium ⁷⁷	0.8 mM	Na ₂ HPO ₄ x H ₂ O
	0.7 mM	KH ₂ PO ₄
	0.5 mM	MgSO ₄ x 7H ₂ O
	0.5 mM	NH ₄ NO ₃
	50 μM	FeSO ₄ x 7H ₂ O
	50 μM	Na ₂ EDTA x 2H ₂ O
	0.1 mg/l	CuSO ₄
	0.1 mg/l	H ₃ BO ₃
	0.1 mg/l	MnSO ₄ x H ₂ O
	0.1 mg/l	Na ₂ MoO ₄ x 2H ₂ O
	0.1 mg/l	ZnSO ₄ x H ₂ O
	15 g/l	Bacto™ Agar
	1 mM	CaCl ₂ (added after autoclaving) pH 6.5 (KOH)
Modified 0.5x Hoagland's solution ⁷⁷	2.5 mM	Ca(NO ₃) ₂ x 4H ₂ O
	2.5 mM	KNO ₃
	1 mM	MgSO ₄ x 7H ₂ O
	50 μM	NaFeEDTA
	20 μM	KH ₂ PO ₄ /K ₂ HPO ₄ pH 6.8
	10 μM	H ₃ BO ₃
	2 μM	MnCl ₂ x 4H ₂ O
	1 μM	ZnSO ₄ x 7H ₂ O
	0.5 μM	CuSO ₄ x 5H ₂ O
	0.2 μM	CoCl ₂ x 6H ₂ O
	0.2 μM	Na ₂ MoO ₄ x 2H ₂ O
	0.2 μM	NiSO ₄ x 6H ₂ O

2.1.3 Biological material

2.1.3.1 Bacterial strains

<i>Escherichia coli</i> DB3.1	Invitrogen (Darmstadt, Germany)
<i>Escherichia coli</i> DH5 α	Invitrogen (Darmstadt, Germany)
<i>Escherichia coli</i> TOP10	Invitrogen (Darmstadt, Germany)
<i>Agrobacterium rhizogenes</i> Arqua-1	Quandt <i>et al.</i> , 1993 ⁷⁸
<i>Agrobacterium tumefaciens</i> GV2260	Schmidt Willmitzer, 1988 ⁷⁹
<i>Sinorhizobium meliloti</i> WT	Dr. Helge Küster (Hannover, Germany)

2.1.3.2 Fungal inoculum

<i>Glomus intraradices</i> BB-E	Agrauxine (Dijon, France)
---------------------------------	---------------------------

2.1.3.3 Plant material

<i>Medicago truncatula</i> cv Jemalong genotype A17
<i>Medicago truncatula</i> R108

2.1.3.4 Plasmids

pCR2.1	Invitrogen (Darmstadt, Germany)
pDONR207	Invitrogen (Darmstadt, Germany)
pENTR/D-TOPO	Invitrogen (Darmstadt, Germany)
pK7GW2D	Karimi <i>et al.</i> , 2005 ⁸⁰
pKDSR(I)	Dr. Igor Kryvoruchko (Ardmore, Oklahoma, USA)
RFP-PT4:: <i>expr.</i>	Franziska Krajinski, unpublished
pCambia2301	
pMDSR163	Dr. Igor Kryvoruchko (Ardmore, Oklahoma, USA)
pGWB454	Nakagawa <i>et al.</i> , 2007 ⁸¹
pGWB443	Nakagawa <i>et al.</i> , 2007 ⁸¹
pGWB433	Nakagawa <i>et al.</i> , 2007 ⁸¹

2.2 Methods

2.2.1 Plant growth and transformation of *Medicago truncatula*

2.2.1.1 Surface sterilization and germination of seeds

Medicago truncatula cv. Jemalong line A17 seeds were incubated with concentrated sulfuric acid followed by repeated washings with distilled water. Afterwards surface sterilization was carried out using 6 % (v/v) sodium hypochlorite for 8 min. After rinsing with sterile water, seeds were germinated on water agar at 4 °C for 48 h followed by a 3-day incubation (if not mentioned otherwise) at room temperature. Seedlings were placed in sand and vermiculite (3:1).

2.2.1.2 Inoculation with *Glomus intraradices*

For inoculation with the AM fungus *G. intraradices*, an inoculum was added to a sand /vermiculite substrate (3:1) at 10% (v/v). For inoculum production *G. intraradices* (strain BB-E, provided by Agrauxine, Dijon, France) was propagated on *Allium porrum* plants, which were fertilized twice a week with half strengths Hoagland's solution containing 20 µM phosphate. After 4 month, the *A. porrum* plants were harvested and the growth substrate was used as inoculum for *M. truncatula* seedlings.

2.2.1.3 Nodulation of *M. truncatula* plants

For nodulation assays of *M. truncatula* plants using *Sinorhizobium meliloti* plants were kept under nitrogen starvation for the whole treatment by equimolar replacement NO₃⁻ with Cl⁻ in the Hoagland's solution. *S. meliloti* WT was grown in liquid culture containing TY media until an optical density of 0.5 (λ = 600 nm) was reached and diluted 1:10 (v/v) with ddH₂O prior to inoculation by watering the plants with the bacterial suspension.

2.2.1.4 Plant growth conditions

Growth conditions greenhouse

Plants were grown at 21 °C during the day and 17 °C during the night. A 16 h light period was used in the greenhouse. Relative humidity was 60 %.

Growth conditions phytotron

Root transformed plants were grown in a phytotron at $200 \mu\text{E m}^{-2} \text{s}^{-1}$ for 16 h, dark period 8 h, 22°C day/night, 65 % humidity.

2.2.1.5 Time course experiment

After a germination period of 4 days *M. truncatula* seedlings were planted in 16 cm pots with 4 plants per pot and grown in the greenhouse in a sand/vermiculite substrate (3:1), either non-inoculated or inoculated with *G. intraradices*. The plants were fertilized twice a week with Hoagland's solution containing $20 \mu\text{M P}_i$. Roots and shoots were harvested after 1, 2, 3, 4, 5, 6 and 8 weeks post-inoculation. For every condition, 4 independent biological replicates each including material of two plants were harvested.

2.2.1.6 P_i -gradient experiment

M. truncatula seedlings were planted as described above and fertilized twice a week with Hoagland's solution with the following P_i concentrations: $0 \mu\text{M}$, $100 \mu\text{M}$, $250 \mu\text{M}$, $500 \mu\text{M}$, $750 \mu\text{M}$, 1 mM and 2 mM P_i . Root and shoot material was harvested 5 weeks post-inoculation in 4 independent biological replicates each including material of two plants.

2.2.1.7 Plant root transformation using *A. rhizogenes*

For the root transformations, seeds were surface sterilized and germinated as mentioned above (2.2.1.1). The following protocol is based on axenic transformation developed by Boisson-Dernier *et al.*⁸².

The complete root from the seedlings was cut off with a sterile razor blade and discarded. The fresh wound from the shoot of the seedling was dipped on a 2 day old culture of *A. rhizogenes* strain Arqua-1 cultivated on YEB-media and containing the appropriate destination vector. For efficient transformation of the roots, the seedlings were afterwards kept in dark at room temperature for two days. The seedlings were then transferred on Fahraeus-media containing $25 \mu\text{g/ml}$ kanamycin for 2-3 weeks. Plants expressing the visible marker in the roots were then transferred onto a quartz sand 0.6-1.2 mm/vermiculite/expanded clay mixture (2:1:1) with or without *G. intraradices* inoculum and grown in the phytotron. The plants were treated according to the experimental condition.

2.2.1.8 Infiltration of transformed *A. tumefaciens* into *Nicotiana benthamiana*

Transformed *A. tumefaciens* were grown at 28 °C for 2 days in selective YEB medium to produce a thick Agrobacteria stock that can be kept at 4 °C for two weeks. 4 ml of selective YEB medium were inoculated with 1 ml of the stock solution and shaken for 4 h at 28 °C. The cultures were pelleted by centrifuging for 15 min at 4000 rpm. The supernatant was discarded and the pellet resuspended in 1 ml freshly prepared AS-medium (acetosyringon-medium, 2.1.1.5). The OD₆₀₀ of the culture was adjusted to 1.0 and the culture was incubated for further 2-3 h at room temperature. 5 weeks old *N. benthamiana* plants were watered well and then infiltrated after 4 h. 500 µl of the bacterial solution was injected into the abaxial side of the tobacco leaf using a syringe without a needle (1 ml). The plants were incubated for 3 days in the phytotron. For interaction studies such as miRNA-target interactions the appropriate constructs were mixed in a 1:1 ratio before infiltration.

2.2.2 Biomolecular methods

2.2.2.1 Cloning strategies and preparation of plasmids

Gateway cloning

Overexpression and RNAi constructs for *MtPhr1* were created via directional TOPO[®] cloning. For the overexpression construct a primer-pair was used to amplify the whole ORF of TC115503. The PCR was performed with Advantage[®] 2 Polymerase (Clontech) and cDNA derived from RNA of *M. truncatula* roots. PCR fragments were cloned into the pENTR[™]/D-TOPO vector and transformed into One Shot[®] TOP 10 *E. coli* cells using the pENTR[™] Directional TOPO[®] Cloning Kit (Invitrogen) according to the manual, resulting in the entry vector pENTR_phr1oex for the ORF of *MtPhr1*. White colonies were picked after a blue-white selection and positive constructs were confirmed via PCR and plasmid restriction. Positive constructs were sequenced by LGC Genomics (Berlin, Germany) using the Donr-F and T7-Promoter sequencing primer. Verified constructs were used for recombination with the destination vector pK7GW2D, using the LR-Recombinase Mix (Invitrogen) according to the manual. The vector pK7GW2D⁸⁰ containing eGFP as a visible marker was used for the overexpression construct resulting in the vector pKphr1oexD.

Using the same cloning and control procedures, a RNAi construct was generated from PCR amplified sequences with a length of 300 bp of the *MtPhr1* 3'-UTR. The generated entry

clone pENTR_phr1RNAi3' was used for LR recombination with the destination vector pKDSR(I).

The Gateway cloning strategy was also used for promoter studies of miR399b and miR399d, and the overexpression of the miR399d primary transcript and *Mt4*. For the promoter studies 1500 bp of the putative promoter region of miR399b and miR399d were amplified from genomic DNA using specific primer pairs and cloned into pGWB443 for promoter-CFP fusion via the entry clones pENTR_miR399b-pro and pENTR_miR399dpro.

Sequences of *Mt4* and pri-miR399d were amplified from cDNA using specific primer pairs containing attB-sites. The PCR fragments were inserted into the entry vector pDONR207 using the BP-Recombinase Mix (Invitrogen). The entry clone was then used to transfer the gene of interest into the destination vector pK7GW2D as described above.

For transient co-expression experiments in *Nicotiana benthamiana* the constructs pKmiR399dPToexD, pGWB_5xMtPt8-miR399bs and pGWB_5xmutMtPt8-miR399bs were generated using the Gateway cloning strategy. The mtr-miR399d primary transcript was PCR amplified from genomic DNA, cloned into the entry vector pDONR207 and subsequently introduced into the overexpression vector pK7GW2D which contains the constitutively expressed visible fluorescent marker eGFP. The gene itself is driven by the constitutive CaMV 35S promoter. The generation of the other two constructs was based on a synthetic DNA synthesized by Eurofins MWG operon (Ebersberg, Germany) containing five sequences of the *MtPt8*_{miR399 bs} or *MtPt8*_{mutated miR399 bs} in series for the positive or negative control, respectively. Both sections were synthesized in a row separated by linker sequences for specific PCR amplification. Each section was separately amplified using specific primer pairs containing CACC-sites in the forward primer for the subsequent cloning into pENTR™-D/TOPO®. Plasmids of the entry clones were checked by PCR and sequencing. Positive clones were used for the following LR reaction to introduce the sequences into the destination vector pGWB455. This vector allows the N-terminal fusion of genes of interest to mRFP. Positive clones were selected after check with PCR and sequencing.

Classic cloning

This type of cloning was used to introduce *Mt4*, pri-miR399d or GUS (as control) into the vector RFP-Pt4::expr (unpublished). This vector was generated to express genes of interest

under the strong arbuscule-specific promoter of *MtPt4*. The gene of interest was PCR amplified with gene specific primer pairs containing sequences of unique restriction sites which are also present in the multiple cloning site of RFP-Pt4::expr. The PCR product was cloned via bidirectional TOPO TA[®] cloning into pCR2.1. At least 5 µg of the entry clone and the empty RFP-Pt4::expr vector were digested using the appropriate restriction enzymes in a reaction volume of 50 µl. This step is critical because for a higher efficiency in the following ligation step the digest should be complete. Using Fast Digest[®] enzymes the reaction was incubated for 2 h and cleaned up afterwards with the Wizard[®] SV Gel and PCR Clean-up System (Promega) according to the user manual. The plasmids were eluted in 25 µl nuclease-free water and the concentration was determined using the Nano Drop – 1000 spectrophotometer. For the ligation reaction the appropriate amounts of insert were calculated as shown in the formula below. The amount of vector was adjusted to 150 ng/µl, therefore 1 µl was applied in every reaction.

$$V_{insert(\mu l)} = \left(\frac{vector(ng) \cdot insert(kb)}{vector(kb)} \cdot \frac{3}{1} \right) \cdot \frac{1}{c_{insert(ng/\mu l)}}$$

In a final volume of 10 µl ligation reaction 1 µl plasmid, 1 µl 10x T4 buffer, 1 µl T4 ligase, the calculated volume of insert and nuclease-free water were mixed and incubated over night at 4 °C. The construct was transformed into competent One Shot[®] TOP 10 *E. coli* cells (Invitrogen) and positive clones were validated by PCR and sequencing.

Plasmid preparation

A liquid bacterial culture (5ml) was grown over night at the according culture condition for the used bacterial species and strain. 4 ml of the culture was centrifuged at 8000 rpm to pellet the bacteria. The supernatant was discarded and the pellet afterwards resuspended in 100 µl mini prep solution 1 and 5 µl RNaseA (10 mg/ml). After the mixture was incubated for 5 min at room temperature, 200 µl of solution 2 and 150 µl of solution 3 were added followed by an incubation time of 5 min on ice after each step. The solutions were mixed very carefully by inverting the tube. The probes were then centrifuged at maximum speed for 10 min and the supernatant (V = 450 µl) transferred into a new tube. 800 µl 96 % [v/v] ethanol and 40 µl 3 M sodium acetate pH 4.8 were added and the samples were incubated for at least 30 min at -20 °C to precipitate the plasmid DNA. The plasmids were afterwards

pelletized by 10 min centrifugation at full speed and the pellet was washed with 70 % [v/v] ethanol prior to drying. The plasmids were resuspended in 40 µl autoclaved ddH₂O or TE-buffer.

Restriction analysis of constructs

Prior sequencing for construct validation a restriction analysis was applied. For digestion usually two enzymes cutting once on the left and right hand of the inserted fragment were used. If appropriate enzymes available the Fast Digest system (Fermentas) was used. For the reaction, 1 µl 10xFast digest buffer, 1 µl Plasmid, 1 µl of each enzyme were mixed and add with ddH₂O up to 10 µl. The reaction was incubated for 1 hour at 37 °C and afterwards analyzed by electrophoresis.

2.2.2.2 Transformation of microorganisms

Transformation of Escherichia coli

50-80 µl chemically competent *E. coli* cells were thawed on ice. Afterwards 1 µl of the appropriate vector was added to the cells and incubated on ice for 20 min. The cells were heat shock transformed by incubating them for 30 s at 42 °C, subsequent chilling on ice for 5 min and addition of 200 µl SOC medium. The transformed cells were incubated for 1 h at 37 °C. Positive clones were selected by plating 50 – 150 µl of the cells on solid LB medium containing an appropriate antibiotic.

Transformation of Agrobacterium strains

50 µl electro-competent *A. rhizogenes* cells were thawed on ice and mixed with the appropriate vector in an electroporation cuvette (1 mm). The cells were incubated on ice for 30 min. After transforming the cells via electroporation (2.5 kV), 500 µl YEB medium was subsequently added. The transformed cells were incubated for 2-3 h at 28 °C and 50-100 µl of the cell suspension were plated on solid YEB medium containing appropriate antibiotics.

2.2.2.3 DNA isolation methods

100 mg of frozen and grinded plant material was mixed with 600 µl 2xCTAB DNA extraction buffer. The samples were incubated for 30 – 45 min at 65 °C. Afterwards, 1 vol (600 µl) chloroform: IAA (24:1) was added and mixed by inverting the tube. To separate the water

phase from the organic phase the samples were centrifuged for 2 min at maximum speed and the upper phase transferred into a new tube. The extraction step was repeated once. To the water phase 600 μ l of 100 % ethanol were added and the DNA precipitated by incubation at -20 °C for at least 60 min. The samples were afterwards centrifuged at maximum speed for 15 min and the pellet washed with 70 % ethanol. The pellet was air dried and resuspended in 50 μ l 1xTAE buffer containing 5 μ l RNaseA (1mg/ml) by incubating the samples at 37 °C for 20 min.

2.2.2.4 RNA isolation methods

For degradome library preparation total RNA was isolated from plant tissue using *mirVana*[™] miRNA Isolation Kit (Ambion) together with the Plant RNA Isolation Aid (Ambion) according to the manufacturers description.

For cDNA synthesis used for (stemloop) qRT-PCR total RNA (>200nt) was isolated from plant tissue using an organic extraction method with GdmCl. Therefore 100 mg grinded tissue was extracted with 400 μ l RNA extraction buffer by vortexing thoroughly. After 10 min centrifugation at full speed (4°C) the supernatant was taken into a new tube and 300 μ l of CIP solution (Roth) was added and vortexed for 1 min. For phase separation the extract was centrifuged at full speed for 10 min (4°C). The upper phase was carefully collected (\approx 1 vol). After addition of 0.1 vol 1 M acetic acid and 0.7 vol 100 % ethanol, the mixture was incubated 30 min at RT. The nucleic acid was pelletized by centrifugation for 30 min at full speed (RT). The pellet was successively washed with 3 M sodium acetate and 70 % [v/v] ethanol, then dried and resuspended in 42 μ l nuclease free water.

2.2.2.5 cDNA synthesis for real-time quantification of mRNAs

Superscript[™] III Reverse transcription kit (Invitrogen) and oligo (dT)₁₈ primer (Fermentas) was used for the cDNA synthesis. First strand synthesis was performed with \sim 1 μ g of total RNA (in a reaction volume of 20 μ l) according to the manufacturers protocols.

2.2.2.6 cDNA synthesis for real-time quantification of small RNAs

Small RNAs were reverse transcribed according to Chen *et al.*⁵⁸ and Pant *et al.*¹⁵ using sequence specific stem-loop primer. The protocol was modified to allow simultaneous relative quantification of mRNAs and subsequent normalization against Housekeeping genes.

An amount of 1 µg total RNA including small RNA fraction (<200 nt) was added to reaction mix of 1 µl of 10 mM dNTPs, 1 µl stem-loop primer mix (maximum of 4 individual primers) with a concentration of 2.5 mM for each primer, 1 µl oligo (dT)₁₈ primer in a total volume of 36.5 µl. The mixture was incubated for 5 min at 65 °C and chilled on ice. 10 µl 5x First strand buffer, 2 µl of 100 mM DTT, 0.5 µl RNase inhibitor and 1 µl MultiScribe™ Reverse Transcriptase were added. cDNA was synthesized using the following program: 30 min at 16 °C, 1 h at 42 °C, 5 min 85 °C, kept on 4 °C until storage at -20 °C

2.2.2.7 Polymerase-chain-reaction (PCR)

Quantitative real-time PCR (qRT-PCR)

QRT-PCRs were performed in reaction volume of 10 µl with 1 µl 1:10 diluted cDNA, 4 µl of 2 mM primer-pair mix and 5 µl Maxima™ SYBR Green/ROX qPCR Master Mix (Fermentas). For the measurement, the qRT-PCR machine ABI Prism 7900 HT' (Applied Biosystems) was used with the following program: one cycle 95 °C for 10 min, 40 cycles 95 °C for 15 sec and 60 °C for 60 sec. An additional dissociation stage for analyzing melting curves was included. The data was analyzed using SDS 2.3 (Applied Biosystems) and MS Excel 2003 (Microsoft). The Ct-threshold was set to 0.2 and an automatic baseline correction was chosen for all experiments. The average from the Ct-values of *MtEF1-α*, *MtPDF2* was used as a housekeeping gene-index (HK-index) to normalize transcript abundance. The formula for calculating the relative expression is given below.

$$\text{Relative expression} = P_{\text{eff}}^{-\Delta C_t}$$

The primer efficiency (P_{eff}) was calculated using LinRegPCR⁸³ and ΔC_t was calculated by subtracting the Ct-value of the HK-index from the Ct-values of the measured transcripts. P_{eff} -values below 1.6 and over 2 were set as 2 in order to minimize distortion of the dataset.

Standard PCR

For standard PCR amplification the Advantage® 2 proofreading polymerase (Clontech) or GoTaq™ DNA polymerase (Promega) was used according to the manufacturers instruction. For each primer pair the specific annealing temperature was determined in a PCR temperature gradient. For efficient DNA amplification 35 cycles were applied.

2.2.2.8 Modified 5'-RLM-RACE to determine miRNA target cleavage

miRNA-mediated cleavage products of target mRNAs were identified using a modified RLM-RACE protocol. Adapter ligation and cDNA synthesis were performed according to the manual, but without prior CIP and TAP treatment. Afterwards the cDNA was amplified using specific nested primers downstream of the predicted target cleavage site. Resulting bands of appropriate size were excised from the agarose gel and cloned into pCR[®]2.1 vector using the TOPO[®] TA cloning[®] Kit (Invitrogen) for subsequent sequencing and cleavage position confirmation.

2.2.2.9 Degradome library preparation

Total RNA of *Medicago truncatula* roots was isolated using the mirVana miRNA isolation kit (Ambion) in combination with the Plant RNA Isolation Aid (Ambion). Poly(A) RNA was isolated from total RNA using the Oligotex mRNA Kit (Qiagen). The degradome libraries from 1 µg poly(A)-enriched RNA were generated according to (German et al., 2009). To perform a quality check prior to sequencing, an aliquot of the blunt ended cDNA was adenylated using dATP and GoTaq (Promega) for 10 min at 72 °C and was cloned using the TOPO TA cloning Kit (Invitrogen) for subsequent sequencing of 24 colonies per library. Illumina-Solexa sequencing of both degradome libraries was performed at FASTERIS (Switzerland).

2.2.3 Biochemistry

2.2.3.1 Determination of soluble phosphate

Soluble phosphate was measured in a modified way according to Itaya *et al.*⁸⁴.

A determined amount (20-30 mg) of frozen and grinded plant material was extracted with 200 µl 0.25 M NaOH and incubated at 96 °C under constant and vigorous shaking. Additional 200 µl of 0.25 M HCl and 100 µl 0.5 M Tris-HCl pH8 in 0.25 % [v/v] IPEGAL CA-630 were then added and the extract was incubated 2 min at 96 °C. After centrifugation for 4 min at 8000 rpm using a bench top centrifuge the supernatant was collected and kept frozen at -20 °C until further analysis. The soluble phosphate concentration was determined calorimetrically at OD 630 nm and an incubation of 30 min (RT, dark) using a 96 well micro titer plate containing 15 µl H₂O + 100 µl 1 M HCl in each well, a determined volume from the extract (2-

20 µl) and 100 µl color reagent. The soluble phosphate concentration was calculated via standard curve using a phosphate standard.

2.2.3.2 In situ hybridization using LNA detection probes

The paraffin-embedded tissue was cut in 10 µm cross sections using the microtome, resulting in approximately 60 sections per sample. Half of the sections were hybridized with the LNA miR399d probe and the other half was used as negative control (scramble probe). For each hybridized probe and its corresponding negative control, subsequent sections were used to ensure that the compared sections derived from the same cell layer. After cutting the root sections were deparaffinized (100% xylene, 50% xylene in Ethanol, 100% EtOH, 50% Ethanol in DEPC-H₂O, DEPC-H₂O; 5 min each step), deproteinated (proteinase K 1 µg/ml in TE buffer, 5 min at 37 °C) and fixed in 4 % PFA (10 min at room temperature). To avoid the loss of miRNA molecules, an additional step for the irreversibly immobilization of miRNAs was included. An EDC fixation using 1-ethyl-3-(3-dimethylaminopropyl) carbodiimide was done as described in Pena *et al.*⁸⁵. Afterwards the sections were acetylated (triethanol amine, conc. HCl, acetic anhydride) and dehydrated by an ethanol series (25%, 50%, 70%, 85%, 90%, 100%; 30 sec each step). The sections were dried at room temperature and subsequently hybridized in ENZO hybridization buffer containing 0.4 pmol/µl of the appropriate 5'DIG-labelled LNA detection probe. As negative control a 5'DIG-labelled scramble probe was used, which is a random 21 nt LNA enhanced DNA oligonucleotide (5'gtgtaacacgtctatacgccca 3') not able to bind any known plant transcript. The scramble probe was directly ordered at Exiqon, Denmark. The whole procedure of hybridization, stringency washes and the immunological detection using NBT/BCIP was carried out according to Nuovo *et al.*⁸⁶. This method is also published in Branscheid *et al.*, 2011⁶⁹.

2.2.3.3 Non-radioactive RNA-RNA Gelshift assay

T7-based in vitro transcription

For the production of specific mRNA of *Mt4* and its homologue *Mt4-H1* an *in vitro* transcription approach was applied. The genes were PCR amplified with Advantage[®] 2 DNA polymerase from cDNA using specific primer pairs. TA-overhangs were produced after addition of GoTaq[™] polymerase and a further incubation at 72 °C for 10 min. The PCR products were cloned into pCR2.1 via bidirectional TOPO TA[™] cloning. For the usage of the

T7 promoter of pCR2.1 the fragments need to be inserted in reverse direction therefore insert direction was checked with PCR afterwards. 5 µg of positive plasmids were then digested with HindIII, an one-cutting restriction enzyme cleaving downstream of the insert. The plasmid was phenol/chloroform-extracted according to the MAXIscript® T7/T3 Kit manual (Ambion). The plasmid was resuspended in 10 µl nuclease-free water and the concentration estimated by agarose-gel analysis. 1 µg of the plasmid was used for the following *in vitro* transcription and subsequent purification of the mRNA, which was also carried out according to the manufacturer's protocol for the unlabelled *in vitro* transcription reaction. After purification the mRNA was stored in 5 µl aliquots.

Gel-shift assay

The protocol used for the mRNA-miRNA gel shift assay was adapted to the DIG application manual for filter hybridization (Roche). For 10 µl hybridization reaction 1 µl First strand buffer (Invitrogen), 5 µl *in vitro* transcript (~ 100 ng), 1 µl DIG-labelled miR399b/ d-RNA oligonucleotide (10 pmol/µl) and 3 µl nuclease-free water were mixed. The reaction was incubated for 5 min at 65 °C, 2 min at 48 °C and stepwise cooled down to 25 °C with 0.1 °C decrease per sec. For control reactions the volume of *in vitro* transcript was substituted by nuclease-free water, or a DIG labelled scramble RNA-oligonucleotide was used instead of the miR399 probe. The interaction was then analyzed by non-denaturing TBE-polyacrylamidgel-electrophoresis (5 % TBE gels). 5 µl of non-denaturing RNA sample buffer were added to the hybridization reaction and the whole volume of 15 µl applied to the gel. The gel was run in 1xTBE buffer with constant voltage (200 V) for 45-60 min at 4 °C (the bromphenolblue has passed 2/3 of the gel). The RNA-RNA complex was subsequently transferred to a nitrocellulose membrane by electroblotting with 3.5 mA/ cm² membrane area and UV cross linked (0.120 Joule/cm²) afterwards. The membrane was washed in 1x TBST buffer and blocked in 5 % blocking solution for 1 h at RT. After repeated washing steps in TBST and TBS the membrane was treated with the anti-DIG fab fragments (1:1000) (Roche) for 2 h at RT and washed with TBST and TBS again. For the visualization of signal, the membrane was equilibrated in Tris-buffered NaCl solution pH 9.5 and stained with NBT/BCIP in Tris-HCl pH 9.5 (200 µl stock solution (Roche) in 10 ml buffer) until a good signal-to-background ratio was achieved. The reaction was stopped with water.

2.2.3.4 Staining of fungal structures in roots

Trypan blue

The trypan blue staining approach is suitable for a wide range of AM fungi and was carried out as described in Phillips and Hayman⁸⁷ (1970). Mycorrhizal roots were submerged in 10 % KOH at 90 °C for 20 min. After decanting the KOH the roots were washed twice with distilled water, placed in trypan blue staining solution (25 ml 2 % trypan blue and 1000 ml lactoglycerol solution) and incubated at 90 °C for 3-5 min. The roots were washed with water and mounted in glycerol afterwards for the light microscopic analysis.

Alexa Fluor 488

Roots were treated with KOH as described above. After washing twice with distilled water the roots were incubated with Alexa Fluor 488 antibody in PBS (1:10000) over night. The roots were washed afterwards and mounted in glycerol for analysis using the epifluorescence microscope.

2.2.4 Bioinformatic methods

2.2.4.1 Processing of Illumina SBS high-throughput sequencing data

The deep sequencing raw data obtained from Fasteris (Switzerland) were computationally processed implementing the CleaveLand pipeline v2.0⁷⁶. To apply the raw data into the pipeline all reads from both libraries were trimmed to 5'-most 20 nts in length. In the first stage all degradome tags deriving from structural RNA (tRNA, rRNA, snRNA, snoRNA) were removed by aligning the tags to all known structural RNAs using Oligo maps short reads aligner⁸⁸. The raw counts of tags were scaled to reads per million (RPM) to enable the comparison of read abundances of different datasets. The tags were mapped to *Medicago truncatula* cDNA databases such as Mtr TIGR genome index v9.0 and IMGAG Mtr 3.0 CDS (coding sequences) and to the *M. truncatula* genome (IMGAG Mtr 3.0) using the RazerS tool for fast read mapping⁸⁹ to find matches with 100 % identity. Based on this dataset the reads were further filtered to identify distinct, means non-redundant, sequences for the nm and myc library, respectively.

Tags with multiple distinct hits on one transcript were repeat normalized and the number of different degradation start sites was calculated. The resulting data were used to create t-

plots (target-plots) for each transcript, which enable to classify and assign the degradation sites to a specific degradation mechanism. For each perfect match to the sense strand of an mRNA transcript, a 35-nt long 'query' mRNA subsequence (t-signature) is generated by extracting 15-nt and 20 nt long sequences upstream and downstream, respectively, of the location of the 5`-end of the matching degradome sequence. Using the RNA hybrid tool (solexa data analysis pipeline)⁹⁰ the t-signatures were aligned to all known and novel small RNAs of *M. truncatula* (miRBase, v16.0; miRDeep predicted small RNAs, Branscheid *et al.*, 2011⁶⁸) and checked for binding and cleavage. All hits were categorized based on the abundance of the diagnostic cleavage tag relative to the overall profile of degradome tags matching the target⁷⁶.

3 Results

3.1 Identification of novel miRNA cleavage targets in *M. truncatula* roots using degradome high-throughput sequencing

The establishment of functional AM symbiosis with arbuscule formation requires a complex reprogramming of root cortical cells involving distinct changes of cell morphology and physiology, with the majority of the changes in the root transcriptome. miRNA-mediated mRNA cleavage is one specific mode of post-transcriptional gene regulation and has a great impact particularly in adaptation to environmental changes. In our previous study we demonstrated that the miR399 gene family, a key regulator in the systemic signalling to maintain plant P_i homeostasis, is involved in AM symbiosis⁴². Several genes of the miR399 family were stronger induced in shoots of mycorrhizal plants as compared to non-mycorrhizal plants, which was accompanied by the accumulation of mature miR399 molecules in mycorrhizal roots. Moreover, as demonstrated by *in situ* hybridizations (3.2.3.1), mature miR399 molecules accumulate in the phloem, although primarily in arbuscule-containing cells. Therefore, a general role of miRNAs in AM symbiosis is assumed. To analyze the impact of miRNA-mediated mRNA cleavage related to the transcriptional reprogramming in roots during AM symbiosis and to identify novel miRNA cleavage targets, an Illumina high-throughput sequencing approach of the root degradome was applied.

3.1.1 Construction and quality control of degradome libraries of *G. intraradices* colonized and non-colonized roots

For the construction of two degradome cDNA libraries, *M. truncatula* seedlings were grown either non-inoculated or inoculated with *G. intraradices* and harvested after 3 weeks post inoculation (wpi). The mRNA was extracted from root tissue from a pool of 15 and 16 non-mycorrhizal (nm) and mycorrhizal (myc) plants respectively. The quality of total RNA extraction was confirmed via Bioanalyzer (RIN = 6 - 7). Degradome libraries were constructed according to German *et al.*⁹¹. Before sending the libraries to high-throughput sequencing by the Illumina SBS (sequencing-by-synthesis) approach, an 0.5 µl aliquot of each library was cloned into a TOPO[®]-TA vector and 24 clones per library were sequenced as a quality check. The distribution of read lengths was as expected (figure 5) with the most abundant molecule

sizes ranged between 21-22 nt as a result of the *MmeI* restriction pattern. Only one clone out of 48 contained self-ligated adapters without insert. The two libraries were sent to FASTERIS (Switzerland) for high throughput sequencing.

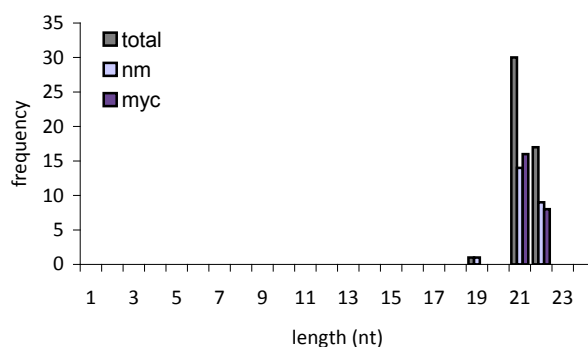


Figure 5. Quality control after sequencing of 48 colonies from each library (myc, nm). The length of the small RNAs is displayed in nucleotides (nt).

3.1.2 Mapping of degradome sequence tags to *Medicago truncatula* genome resources

In total 5,737,931 and 7,907,566 reads for the nm and myc library respectively were obtained (table 1). More than 97% of all reads were of the appropriate sizes, i.e. 20-21 nt with slightly more 20 nt than 21 nt sequences. The obtained sequencing raw data were subjected to the CleaveLand pipeline v2.0⁷⁶ for computational processing (2.2.4.1) in order to identify degradome tags derived from miRNA-mediated mRNA cleavage.

Table 1. Statistics of the Illumina sequencing of two degradome libraries. nm: non-mycorrhizal roots, myc: mycorrhizal roots

	deg-nm	deg-myc
raw reads	5737931	7907566
reads of appropriate size	5620484	7777769
unique reads of appropriate size	2897498	4594450
% total reads mapping to <i>M. truncatula</i> mt3.0 (100% identity)	85.86	75.77
% total reads mapping to <i>G. intraradices</i> (100% identity)	0.05	7.65

Mapping the degradome tags with 100% identity to *M. truncatula* and *G. intraradices* sequences (Mtr TIGR genome index v9.0, IMGAG Mtr3.0 genome, IMGAG Mtr 3.0 CDS, the

Glomus consortium), revealed a match of 86% and 76% of the nm- and the myc-deg sequences to *M. truncatula* genome sequences. Out of these, 2,897,498 and 4,594,450 represent distinct, i.e. non-redundant, sequences for the nm and myc library, respectively. Of the myc-deg sequences, 7.7 % mapped to *G. intraradices* sequences (INRA GlomusDB⁹²). Figure 6 shows a summary of read annotation and the assignment of degradome tags to distinct functional classes. Each single tag was assigned to one functional class only. Comparing both libraries, a similar distribution of reads in each class, with exception of those tags that were assigned to the *G. intraradices* transcriptome, was observed. Just a small fraction of 15 % of all degradome tags could not be mapped to genome sequences of *M. truncatula* or *G. intraradices* and were assigned to the class of not mapped degradome tags.

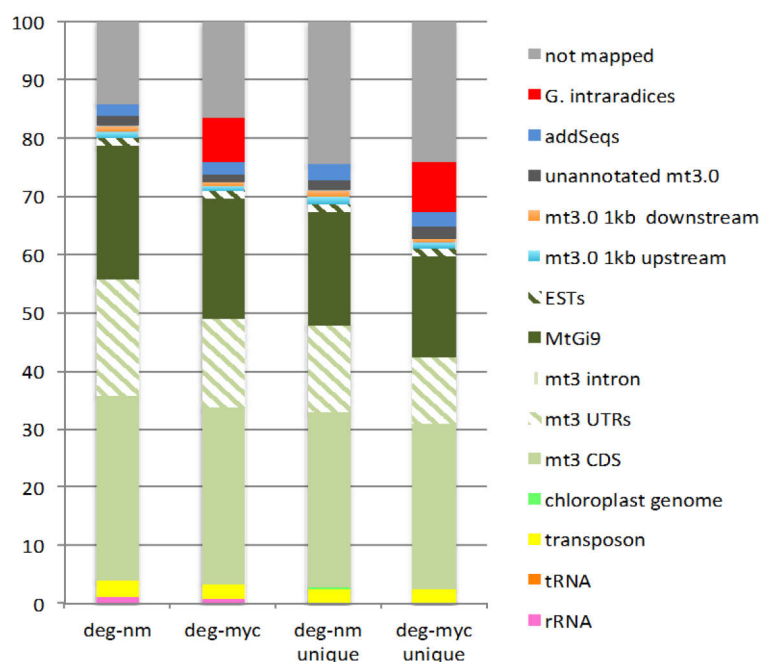


Figure 6. Read annotation of the degradome libraries. Degradome sequence tags were mapped to relevant functional classes, which are distinct from bottom to top. adds: additional mt3 (Illumina) sequences. Figure is published in Branscheid *et al.*, 2011.

3.1.2.1 The degradome sequences are correlated to transcriptome data of mycorrhizal and non-mycorrhizal roots

Recent degradome analyzes in rice and Arabidopsis showed that only a small fraction of these sequence tags represent miRNA-mediated transcript cleavage^{93,94}, the vast majority of these sequence tags represent non-miRNA-mediated, unspecific RNA degradation. Therefore, a correlation of transcript abundance represented by read counts for each transcript between both tissues in the degradome libraries and previous transcriptome studies is expected. The Log₂-fold-changes (LFC) of transcripts identified in both degradome

libraries were calculated and compared to transcriptome data obtained by microarray hybridization of mycorrhizal versus non-mycorrhizal *M. truncatula* roots⁹⁵, resulting in a significant correlation (Pearson correlation coefficient: 0.51, p value > 0.00001) of degradome data to transcriptome data (figure 7). To compensate ratio compression by saturation effects on microarrays, the half minimum normalized abundance for those transcripts was used for strongly specifically expressed genes (i.e. sequence tags in one condition and at least ten tags in the second condition). The degradome sequencing data can then be used to detect miRNA-mediated mRNA cleavage, and in parallel, can also be used to investigate transcriptional changes between the two tissues⁶⁸.

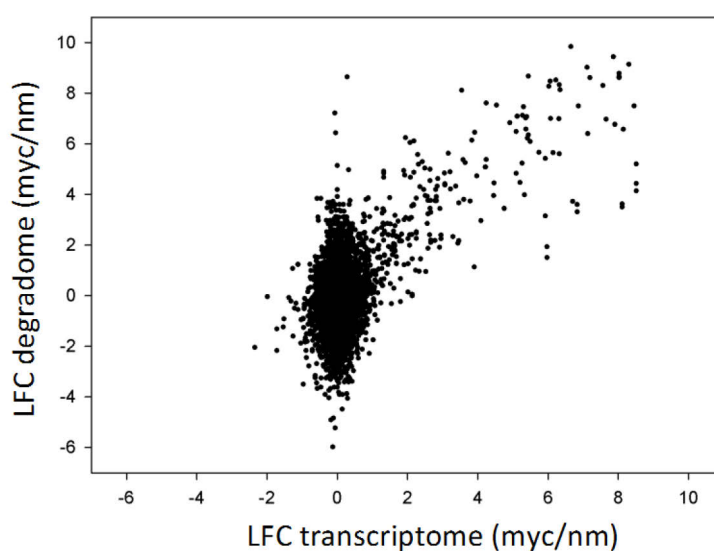


Figure 7. Correlation of log₂-fold changes (LFC) myc versus nm obtained by degradome library sequencing (deg) and Medicago Genome Array Hybridization data deriving from Gomez *et al.*, 2009. Figure is published in Branscheid *et al.*, 2011.

3.1.3 Identification of miRNA/miRNA* cleavage targets

The datasets of degradome deep sequencing and Medicago miRNAs deriving from miRBase v16.0 and miRDeep predictions after small RNA deep sequencing run through to the CleaveLand pipeline 2.0⁷⁶. The hybridization of query sequences to miRNAs (RNAhybrid⁹⁶) resulted in the identification of 371 and 404 cleavage sites for miRBase-annotated miRNAs within the *M. truncatula* genome sequences and the *Medicago truncatula* Gene Index (MtGI) cDNA sequences, respectively⁶⁸. Searching for targets for the 243 novel miRBase annotated miRNAs, 56 cleavage sites in mt3 sequences and 62 cleavage sites in MtGI sequences were found⁶⁸. Surprisingly, the degradome analysis showed 44 targets of both databases which are cleaved by miRNA* (table 2), suggesting that star strands also have an important biological relevance in post-transcriptional gene regulation. Among these transcripts

targeted by miRNA*, 8 cleavage targets, including transcripts encoding for protein kinases and disease resistance proteins, were found to be cleaved by star strands of the miR399 family.

Table 2. miRNA*-mediated mRNA cleavage detected by degradome analysis identified by CleaveLand 2.0⁷⁶

miRBase identifier	cleavage	alignment	Category		accession no.	target gene family
	site	score	nm	myc		
MIR5204*	765	1.5	no tag	2	Medtr8g109760.1	GRAS transcription factor
MIR5204*	72	2.5	no tag	4	TC139113	TC139113
MIR5211*	290	3	no tag	4	CB892526	hypothetical protein
miR172b*	511	6.5	2	2	Medtr7g040960.1	Albumin I S-adenosyl-L-homocysteine
miR172b*	1008	1.5	no tag	3	Medtr4g132640.1	hydrolase
MIR156b*	3663	5.5	1	2	Medtr4g156260.2	Armadillo-like helical protein
MIR156i*	102	4.5	no tag	1	Medtr2g038500.1	hypothetical protein
MIR160*	1648	3.5	4	no tag	Medtr4g130250.1	Poly(A)-binding protein
MIR166e*	834	5.5	no tag	3	Medtr8g133160.3	Sucrose synthase
MIR166h*	1883	3.5	4	2	Medtr8g016500.1	Tyrosine protein kinase
MIR166h*	571	3.5	2	no tag	Medtr8g140110.1	Protein phosphatase 2C
MIR169d*,e.2*,i*, m*	496	5.5	no tag	3	Medtr7g102930.1	Blue (type 1) copper domain
MIR172*	3369	6	2	1	Medtr5g093930.1	Peptidase C19
MIR172*	532	6	0	2	Medtr3g020380.2	Annexin
MIR398a*	1222	6	2	0	Medtr3g102850.1	Short-chain dehydrogenase
MIR398a*	840	6	1	2	TC114776	Deaminase
MIR398a*	458	6	1	no tag	TC137315	hypothetical protein
MIR399c*, k*	356	2	4	no tag	Medtr4g135140.1	hypothetical protein
MIR399c*, k*	134	2	4	no tag	Medtr4g135420.1	hypothetical protein
MIR399d*	572	6.5	1	0	AC225519_18.2	Alpha-helical ferredoxin
MIR399k*	122	6	no tag	1	AW693165	TIR; Disease resistance
MIR399h*	808	6	1	4	Medtr1g121460.2	CD9/CD37/CD63 antigen
MIR399h*	196	5.5	0	no tag	Medtr7g026570.1	Protein kinase
MIR399q*	972	6.5	1	2	Medtr3g080760.1	Nucleotide-binding protein
MIR399q*	665	6	1	4	TC138105	Protein kinase family
miR1510a*	678	4	3	no tag	Medtr4g114680.1	TIR; Disease resistance
miR1510a*	727	4	3	no tag	Medtr6g098900.1	TIR; Disease resistance
miR1510a*	8901	4	3	no tag	Medtr6g099020.1	TIR; Disease resistance
miR1510a*	741	4	3	no tag	Medtr6g099070.1	TIR; Disease resistance
miR1510a*	8902	4	3	no tag	Medtr6g099090.1	TIR; Disease resistance
miR1510a*	699	4	3	no tag	Medtr6g099150.1	TIR; Disease resistance
miR1510a*	685	4	3	no tag	Medtr6g099160.1	TIR; Disease resistance
miR1510b*	284	7	0	2	BE240495	PR10-1 protein
miR1510b*	392	7	0	2	BF649495	PR10-1 protein
miR1510b*	2942	7	2	2	DY615507	PR10-1 protein
miR1510b*	452	7	2	2	TC118500	PR10-1 protein
miR1510b*	519	7	2	2	TC118796	PR10-1 protein
miR1510b*	491	7	2	2	TC118868	PR10-1 protein
miR1510b*	491	7	0	2	TC121811	PR10-1 protein
miR1510b*	567	7	2	2	TC125034	PR10-1 protein
miR1510b*	237	7	2	2	TC128485	PR10-1 protein
miR1510b*	418	7	2	2	TC131880	PR10-1 protein
miR1510b*	244	7	0	2	TC132039	PR10-1 protein
miR1510b*	633	7	2	2	TC141258	Proline-rich cell wall protein

In total, 185 mRNAs (mt3) were identified to be miRNA and miRNA* cleavage targets, of which 157 are targets of novel miRBase annotated miRNAs. In order to estimate the frequency of miRNA-mediated mRNA cleavage in the *M. truncatula* root transcriptome, all degradome sequence tags were mapped to mt3 genes. 27,729 genes could be aligned to degradome tags of which 185 were miRNA cleavage targets as previously described. Therefore, this specific mode of mRNA repression occurs in a proportion of 0.67% of the represented root transcriptome. For a functional characterization of all miRNA targets identified, a MapMan analysis⁹⁷ was carried out.

Interestingly, disease resistance proteins (27 genes) and transcription factors (33 genes) were clearly overrepresented within the identified target genes (figure 8). This indicates that particularly the transcriptional regulation and the defense responses are controlled by miRNA-mediated mRNA cleavage in roots.

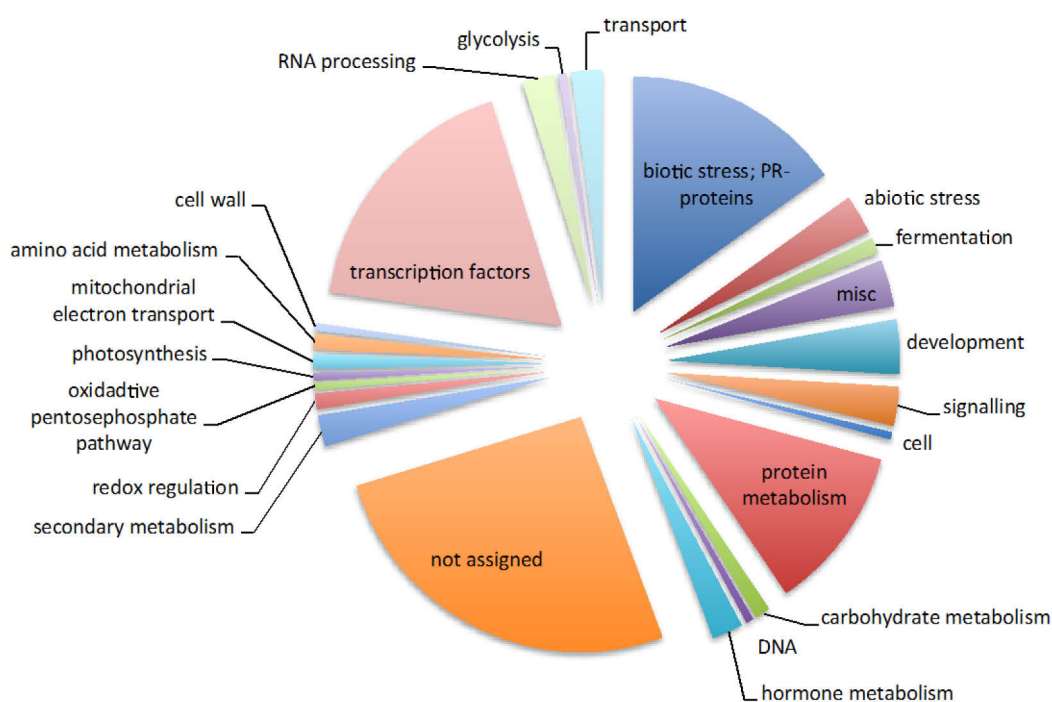


Figure 8. Distribution of functional classes after MapMan analysis of miRNA and microRNA* cleavage targets (mt3.0). Figure is published in Branscheid *et al.*, 2011.

3.1.4 *MiRNA/miRNA*-mediated mRNA cleavage of genes involved in root endosymbioses*

To identify transcripts, which represent miRNA targets and show strongly elevated or decreased transcript levels in mycorrhizal roots as compared to non-mycorrhizal roots, a read count analysis of the degradome sequence tags was carried out. Read count analysis is a method to quantify the abundance of transcripts by determining the absolute normalized number of degradome tags matching to one transcript. The log₂-fold values were calculated based on estimated read counts in both conditions for each of the 27,729 genes detected in the degradome sequences. Using a log₂-fold cutoff of +/-1, we could identify 111 miRNA targets with differential transcription in mycorrhizal versus non-mycorrhizal roots. Table 3 shows all detected miRNA targets with a log₂-fold cutoff of +/- 1.5.

Table 3. miRNA targets with differential transcript accumulation in mycorrhizal roots as compared to non mycorrhizal roots

target ID	target gene family	LFC (miRNA target)	cleavage site	miRNA ID	alignment score	category nm	category myc	LFC (miRNA)
Medtr8g109760.1	GRAS TF Major facilitator superfamily	19.0	765	miR5204*	1.5	no tag	2	2.6 -0.2 -
Medtr5g076920.1	Blue copper-binding Glutathione S-transferase	8.6	496	miR399a-q, r	5	no tag	0	+0.3
Medtr7g102930.1	EGF domain containing	8.6	892	miR169d*/e.2*/l*/m*	5.5	no tag	3	4
Medtr5g084780.1	Heat shock DnaJ kinase family	8.6	72	miR5282	5.5	no tag	3	0
TC139113	Glycogenin-like	5.6	1684	miR5204*	2.5	no tag	4	2.6 -0.1 -
Medtr3g150590.1	MADS-box TF	3.2	665	miR166a-h	5.5	no tag	1	+0.3
TC138105	Hypothetical	2.6	463	miR399q*	6	1	4	-0.6
AW687825	TIR, resistance	2.3	977	miR5253	2.5	no tag	4	0.5 -1.5 - -
Medtr7g014850.1	Glycogenin-like	2.1	161	miR164a- d	6	1	no tag	0.7
AW697209	hypothetical	1.9	187	miR5206	7	no tag	0	4.9
TC134204	hypothetical	1.8	283	miR5213	5	1	0	0.7
TC132098	hypothetical	1.8	47	miR5253	2.5	no tag	4	0.5
TC125161	hypothetical	1.8	531	miR164 a/b/c	5.5	no tag	1	-0.7
Medtr6g015300.1	Biotin-binding site	1.7	531	miR2086	3	no tag	4	0.8
TC120550	Albumin I	1.7	349	miR2643	7	2	2	0.3
TC120550	Albumin I	1.7	511	miR172b	2.5	no tag	4	0.7
AW693165	TIR, disease resistance	1.7	122	miR399k*	6	no tag	1	-0.6
BQ138232	hypothetical	1.7	170	miR1509b	5.5	4	0	2
Medtr3g097800.1	Nsp2	1.6	427	miR171h	3	0	0	1.1 -0.2 -
Medtr4g018250.1	hypothetical	1.5	172	miR399a/c/e/f/g/h/i/l/p	1.5	no tag	4	+0.2
Medtr4g018250.1	hypothetical	1.5	172	miR399r	3.5	no tag	4	0.2 -0.2 -
Medtr4g018250.1	hypothetical	1.5	467	miR399b/d/j/k/m/n/o/q	4	no tag	0	+0.3
Medtr6g028360.1	TIR, disease resistance	-1.5	429	miR5213	4	2	0	0.7
Medtr3g103970.1	SBP	-1.5	1083	miR399b/d/j/k/m/n/o/q	1	no tag	0	0 - +0.7

RESULTS

Medtr3g103970.1	SBP	-1.5	1083	miR156j	2	no tag	0	-0.2
Medtr6g099150.1	TIR; Elongation factor Ts	-1.5	699	miR1510a*	4	3	no tag	-0.6
Medtr2g046350.1	TIR, disease resistance	-1.6	140	miR1510a*	0.5	4	no tag	0
Medtr2g046350.1	TIR, disease resistance	-1.6	131	miR5213	5.5	3	2	0.7 -0.3 -
Medtr7g121710.1	Auxin response factor	-1.6	1406	miR160a- e	1.5	1	1	+2.4
Medtr7g121710.1	Auxin response factor	-1.6	1406	miR160f*	1	1	1	4.8
Medtr7g026570.1	kinase	-1.7	196	miR399h*	5.5	0	no tag	0.4
TC123814	GRF TF	-1.8	573	miR399h*	4	0	0	0 - +0.3 -0.3 -
Medtr7g121610.1	Auxin response factor	-1.8	1406	miR160a-e	1.5	1	1	+2.4
Medtr7g121610.1	Auxin response factor	-1.8	1406	miR160f*	1	1	1	4.1
TC127408	Auxin response factor	-1.8	1407	miR160f*	3.5	no tag	5	4.1
Medtr6g098880.1	TIR, disease resistance	-1.8	203	miR2678	0	4	no tag	0
Medtr6g098880.1	TIR, disease resistance	-1.8	194	miR5213	4	no tag	2	0.7
TC116942	TIR, disease resistance	-1.9	84	miR5213	4	0	no tag	0.7
TC129665	TIR, disease resistance	-1.9	927	miR1507	5.5	1	no tag	0.4
Medtr6g098900.1	TIR, disease resistance	-1.9	727	miR1510a*	4	3	no tag	-0.6
Medtr6g098900.1	TIR, disease resistance	-1.9	139	miR2678	2	4	no tag	0
Medtr4g114680.1	TIR, disease resistance	-2.0	678	miR1510a*	4	3	no tag	-0.6
Medtr4g114680.1	TIR, disease resistance	-2.0	153	miR2678	0.5	2	no tag	0
Medtr6g099020.1	TIR, disease resistance	-2.0	8901	miR1510a*	4	3	no tag	-0.6
Medtr6g099090.1	TIR, disease resistance	-2.0	8902	miR1510a*	4	3	no tag	-0.6
Medtr6g099090.1	TIR, disease resistance	-2.0	8305	miR5213	4	0	no tag	0.7
TC138295	TIR, disease resistance	-2.0	132	miR5213	5	3	3	0.7
Medtr3g125280.3	Alcohol DH superfamily	-2.1	424	miR172b,c	5	3	4	-0.1
Medtr6g099070.1	TIR, disease resistance	-2.1	741	miR1510a*	4	3	no tag	-0.6
Medtr6g099070.1	TIR, disease resistance	-2.1	153	miR2678	0.5	2	no tag	0
Medtr3g125230.2	Alcohol DH superfamily	-2.2	222	miR2119	3.5	2	2	0.9
Medtr3g166270.1	hypothetical	-2.3	55	miR2118	4.5	1	1	-0.4
Medtr4g069410.1	Male sterility	-2.3	347	miR5269b	2	4	no tag	0.4 -0.2 -
Medtr4g133300.1	hypothetical	-2.5	216	miR399a/c/e/f/g/h/i,	1	4	no tag	+0.2 -0.2 -
Medtr4g135410.1	hypothetical	-2.5	89 / 216	miR399a/c/e/f/g/h/i/k/l/p	2 / 1	4	no tag	+0.2 -0.6 - -
Medtr4g135140.1	hypothetical	-2.5	356	miR399c*/k*	2	4	no tag	0.3 -0.6 - -
Medtr4g135420.1	hypothetical	-2.8	134 351/	miR399c*/k*	2	4	no tag	0.3
BE999763	Senescence-associated	-3.3	474	miR5211	5	4	4	0.5

Listed accession numbers of the mt3- and MtGI databases are non-redundant.

TF: transcription factor, SBP: squamosa promoter binding

The most strongly regulated miRNA target (Medtr8g109760.1) encodes a putative GRAS transcription factor, *MtGras8*, which is specifically transcribed in arbuscule-containing cells⁷⁰. Interestingly, transcripts encoding a putative phosphate transporter (Medtr5g076920.1) strongly accumulate in mycorrhizal roots and are a target of the miR399 family. In addition, we identified previously described genes induced during mycorrhizal symbiosis to be miRNA targets, such as *MtBcp1* (Medtr7g102930.1)^{25, 98}, which is cleaved by miR169d*/l*/m*/e.2* (figure 9 e). Additionally, this miRNA itself is induced in mycorrhizal roots, which is shown by the LFC comparing nm and myc roots in table 3. Interestingly, we

found that one mycorrhizal symbiosis-specific transcript, *MtGst1*³⁰, seems to be a target of miR5282 and in addition of the predicted miRNA candidate new_miRc_275 (PhD thesis, Emanuel Devers) (figure 9a). It is further worth mentioning that *MtNsp2* transcripts, which are a target of miR171h (figure 9b), show elevated levels (\log_2 -fold 1.6) in mycorrhizal roots. In addition, target plots of miR160c and miR167 are shown in figure c and 9d. Both miRNAs cleave mRNAs encoding auxin response factors and were induced in mycorrhizal roots. MiR169 targets a CCAAT-binding transcription factor present in mycorrhizal roots (figure 9 f). Notably, within the population of transcripts with decreased levels in mycorrhizal roots, disease resistance genes are highly overrepresented. 16 miRNA cleavage sites were found within disease resistance genes encoding transcripts with decreased levels in mycorrhizal roots.

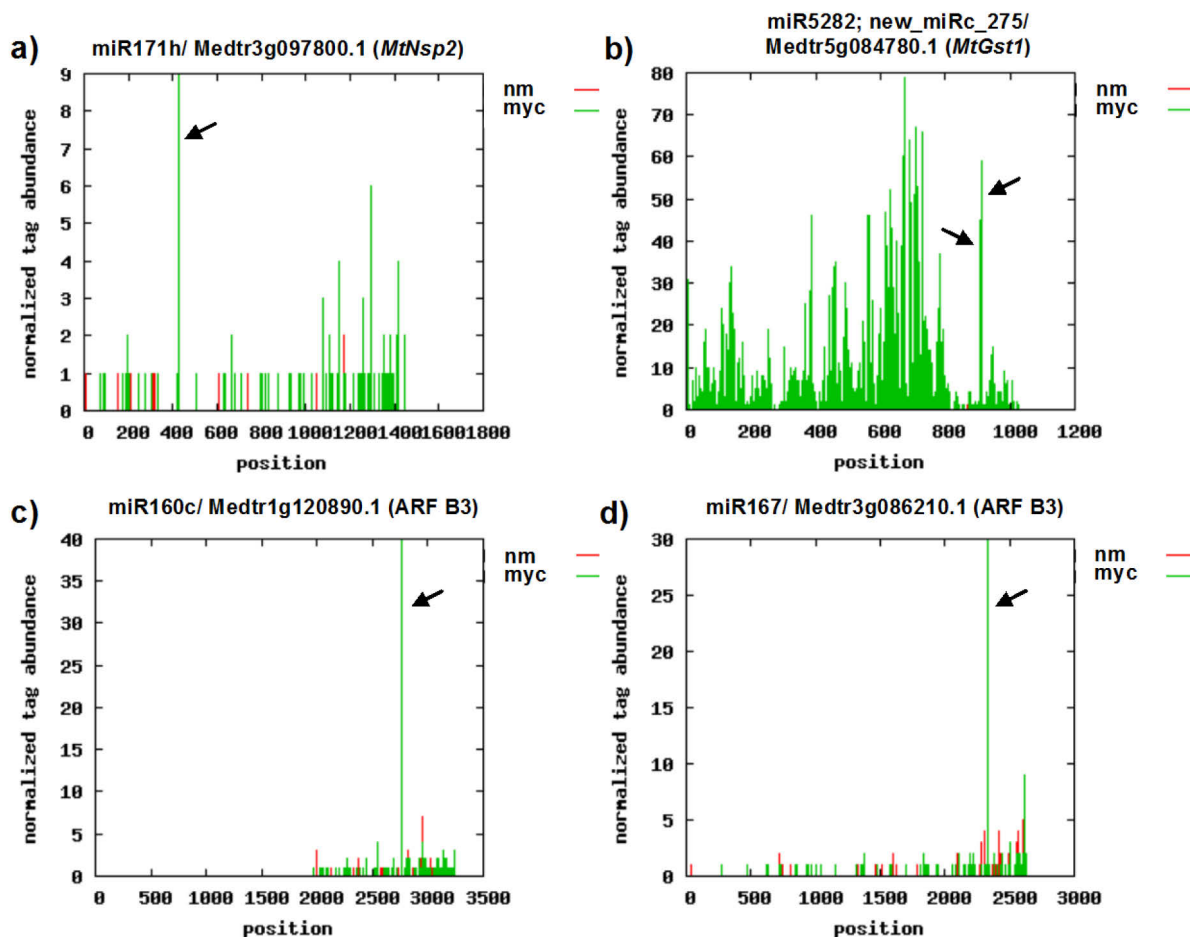


Figure 9. Target plots demonstrating miRNA mediated transcript cleavage. Distribution of 5' ends of the degradome tags within the full-length target mRNA sequence. Tags aligned with cleavage sites of corresponding miRNAs are indicated by black arrows. Target plots of (a) *MtNsp2*, (b) *MtGst1*, (c) auxin response factor (ARF) B3, (d) ARF B3, (e) *MtBcp1* and (f) CCAAT-binding transcription factor. Figure is published in Branscheid *et al.*, 2011.

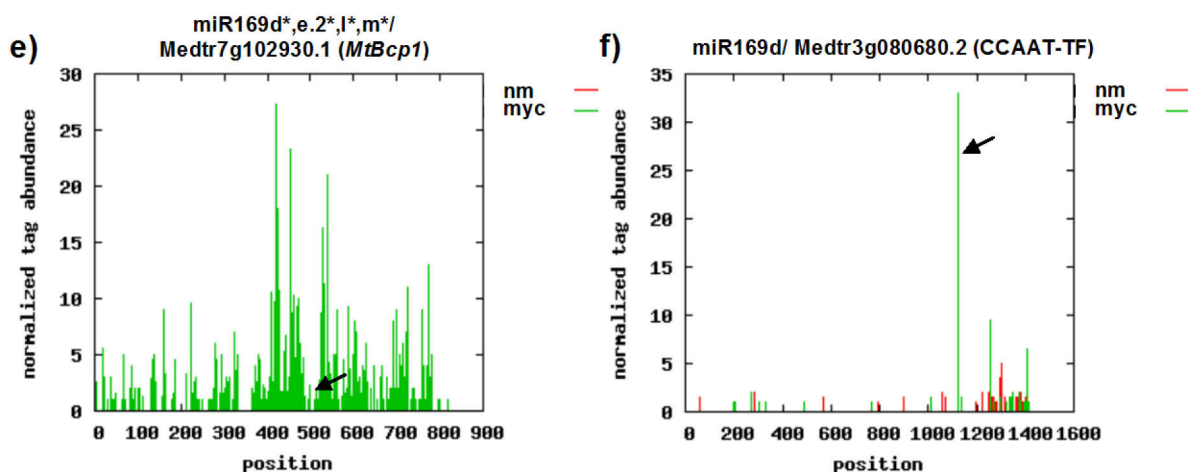


Figure 9. Continued.

3.1.5 The distribution of degradome tags provides information about miRNA precursor processing and regulation of miRNA abundance

Besides the identification of novel miRNA targets, the degradome analysis provides information about the processing of miRNA precursors. During miRNA biogenesis, two sequential cleavages of the long miRNA hairpin structure by DCL1-activity releases a miRNA/miRNA* duplex^{99, 100}. The number of precise DCL1-cleavage sites within a miRNA primary transcript indicates whether the miRNA is processed from base-to-loop or vice versa^{101, 102}. If the precursor is processed from base-to-loop, most of the degradome tags within the precursor are found behind the mature/star sequence at the 3'-end. In the case of loop-to-base processing the majority of tags are arranged at the 5'-end of the mature/star miRNA sequence.

Figure 10 shows the procedure of extracting the appropriate information, using miR399d as an example, degradome and small RNA data provided by the MPI Medicago genome browser (<http://chlamycyc.mpimp-golm.mpg.de/cgi-bin/gbrowse/medicago/>). In the region of the miR399d precursor, 31 degradome tags were found, of which 29 indicate cleavage at the 3'-end of the mature miR399 and only two at the 5'-end of the respective miRNA, suggesting a base-to-loop processing.

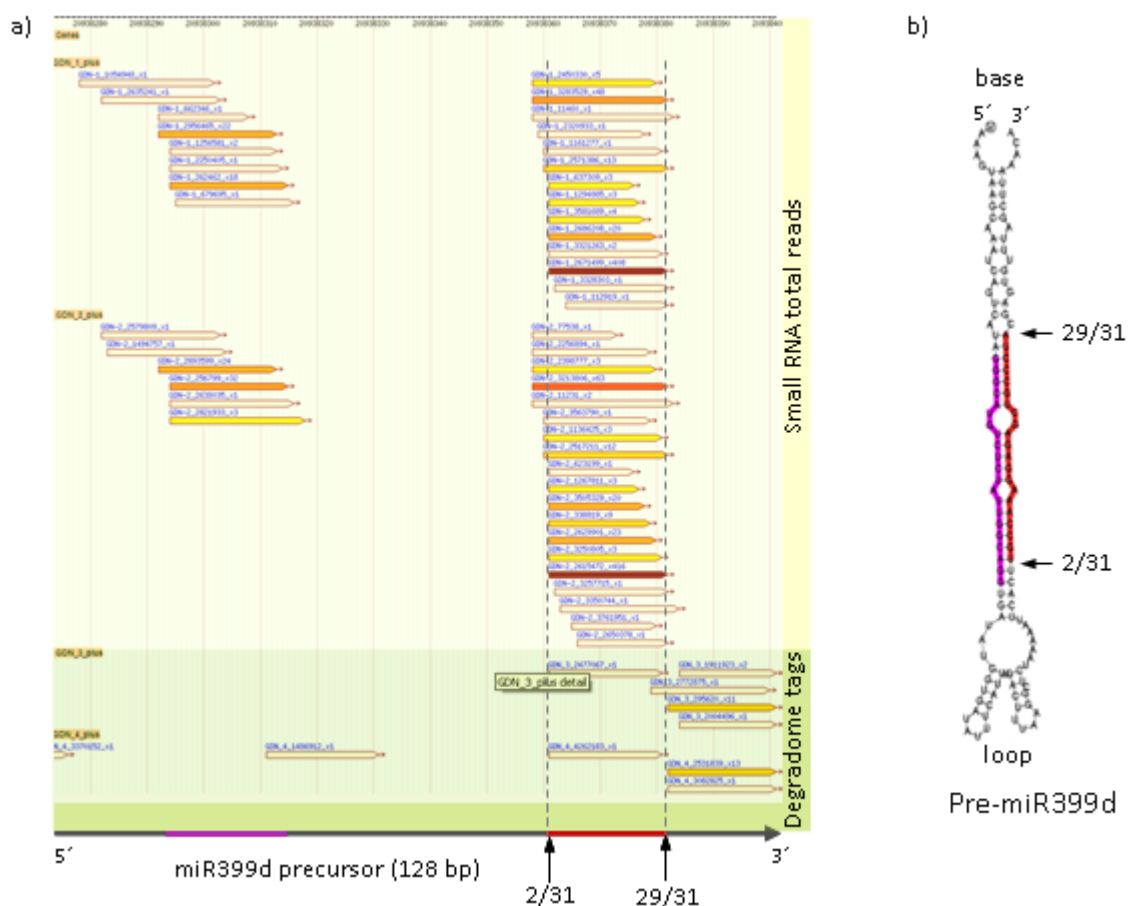


Figure 10. (a) Depiction of the degradome tag distribution within the miR399d precursor sequence as displayed in the Mtr3.0 genome browser of the MPIMP.

In addition, the precursor processing of all members of the miR399 family was analyzed in order to assign the processing type (table 4). For 11 of the 18 miR399 precursors of *M. truncatula* (miRBase v18) are most likely processed via base-to-loop. Only 3 precursors, namely miR399b, c, l, showed a deg tag distribution indicating a loop-to-base processing. Interestingly, for 4 miR399 precursors no tags were detected in either nm, as well as myc roots, although the absolute number of these miRNAs in both tissues was high (Branscheid *et al.*, 2011). There is evidence that some of the miR399 precursors, namely miR399b, f, k, l, m, were subjected to a differential processing in nm and myc roots. For miR399b and miR399f, significantly more deg tags were found in nm roots, whereas miR399k, l, m are more frequently processed in myc roots.

Table 4. Number and distribution of degradome tags in the miR399 precursor sequences the resulting processing type and total read numbers of the appropriate mature/star miR399 sequence in nm and myc roots.

miRNA	genome location (mt3.0)	deg tags on precursor	base- to-loop	loop-to- base	most likely processing type	differential processing (nm/myc)	total reads			
							mature		star	
							nm	myc	nm	myc
miR399a	MtChr4: 31906697-31906830 [-] MtChr4: 32898127-32898260 [+]	no tag	no tag	no tag	-	-	265	297	23	9
miR399b	MtChr6: 20991069-20991180 [+] MtChr6: 21048380-21048491 [-]	9	2	7	loop-to-base	yes (6/3)	236	225	4	2
miR399c	MtChr4: 32754956-32755074 [-] MtChr4: 32924208-32924326 [-]	4	no tag	4	loop-to-base	no	60	53	26	21
miR399d	MtChr6: 20938272-20938400 [+]	31	29	2	base-to-loop	no	416	408	32	18
miR399e	MtChr4: 31918034-31918167 [-] MtChr4: 32722233-32722366 [+] MtChr4: 32886791-32886924 [+] MtChr4: 32955823-32955956 [+]	no tag	no tag	no tag	-	-	265	297	23	9
miR399f	MtChr4: 31909420-31909523 [-] MtChr4: 32730890-32730993 [+] MtChr4: 32895434-32895537 [+] MtChr4: 32964463-32964566 [+] MtChr4: 33034250-33034353 [+]	24	24	no tag	base-to-loop	yes (4/20)	265	297	23	9
miR399g	MtChr4: 31901726-31901829 [-] MtChr4: 32738600-32738703 [+] MtChr4: 32903128-32903231 [+] MtChr4: 32972167-32972270 [+]	no tag	no tag	no tag	-	-	265	297	2	2
miR399h	MtChr4: 31896057-31896146 [+] MtChr4: 32804691-32804780 [+] MtChr4: 32908811-32908900 [-]	18	17	1	base-to-loop	no	60	53	6	8
miR399i	MtChr4: 32913577-32913666 [-]	23	17	no tag	base-to-loop	no	60	53	0	0
miR399j	MtChr4: 32745963-32746053 [+] MtChr4: 32915241-32915331 [+]	2	2	no tag	base-to-loop	no	65	55	30	16
miR399k	MtChr4: 32749020-32749113 [-] MtChr4: 32918295-32918388 [-]	3	3	no tag	base-to-loop	yes (1/2)	116	122	108	71
miR399l	MtChr6: 11362065-11362143 [-] MtChr6: 20977253-20977337 [+]	8	1	7	loop-to-base	yes (2/6)	148	131	0	0
miR399m	MtChr6: 21062223-21062307 [-]	267	265	2	base-to-loop	yes (122/145)	416	408	32	18
miR399n	MtChr6: 20963897-20963996 [+]	31	29	2	base-to-loop	no	416	408	32	18
miR399o	MtChr6: 21004909-21005000 [+]	31	28	3	base-to-loop	no	236	225	32	18
miR399p	unknown	-	-	-	-	-	148	131	0	0
miR399q	MtChr1: 29007565-29007738 [+]	138	137	1	base-to-loop	no	89	110	na	na
miR399r	MtChr4: 32756744-32756845 [+]	no tag	no tag	no tag	-	-	7	8	0	0

3.2 Involvement of plant P_i homeostasis signalling components in AMS development

3.2.1 *PHR1 as transcriptional regulator of the low phosphate response and its putative function during AMS*

PHR1 (phosphate starvation response 1) is a transcription factor involved in the P_i homeostasis signalling in plants¹². PHR1 is activated upon phosphate deprivation and induces a subset of genes regulated during P_i starvation including the miR399 family and *IPS1/At4*. The transcription factor binds to a palindromic DNA sequence, namely P1BS (PHR1 binding site)¹², and enhances the transcription of its target genes. This DNA binding motif was also found in promoter regions of genes specifically induced during AMS, such as *MtPt4*⁴⁴. Therefore, PHR1 might be an important regulator in the link of P_i homeostasis and AMS development in plants.

3.2.1.1 Identification of putative *AtPhr1* homologues in *M. truncatula*

In *Arabidopsis*, the function of PHR1 as transcriptional regulator in the response to P_i deprivation is well described⁹⁻¹². However, in *Medicago truncatula*, homologues of the *AtPhr1* gene are so far not known. Therefore, *Medicago* EST and genome resources (*Medicago truncatula* Gene Index, MtGI 9.0; *Medicago truncatula* HAPMAP project Mt3.0) were analyzed to find putative *AtPhr1* homologues. The tentative consensus sequence TC115503 listed in the MtGI database showed the highest similarity to the *AtPhr1* mRNA (NCBI reference accession number NM_119003.3) with an e-value of 3,7e-55. The sequence corresponds to the *M. truncatula* identifier Medtr7g116700 and is annotated as MYB homeodomain transcription factor.

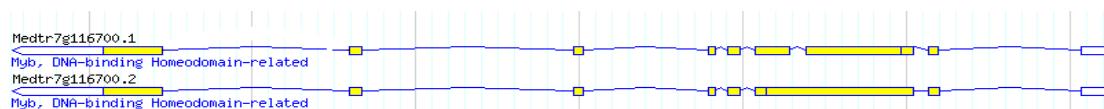


Figure 11. Schematic depiction of the Medtr7g116700 gene structure with a length of 6726 bp. Two different splicing variants resulting in 9 and 8 exons for the first and the second gene model, respectively. Exon are shaded in yellow, 5' and 3' UTR are depicted with blue boxes. Blue lines describe sequences of Introns. Figure was generated using the generic genome browser version 1.7

The 6726 bp gene contained 8 to 9 exons, depending on the splicing variant (figure 11), resulting in a CDS of a length of 678 bp. The translated protein sequence exhibited one Myb homeodomain and 3 sumoylation sites and could therefore be a good candidate for a homologue of *AtPhr1* (Interpro, Sumo sp. 2.0). The putative homologue is subsequently named as *MtPhr1*.

3.2.1.2 Functional characterization of *MtPhr1* during AMS

As previously mentioned, the transcription factor PHR1 induces a subset of Pi starvation responsive genes and is probably sumoylated for activation¹³. To verify the putative *AtPhr1* homologue in *M. truncatula*, a transcriptional analysis using qRT-PCR and reverse genetic approaches were carried out.

qRT-PCR analysis of *MtPhr1*

For the analysis of transcript accumulation in roots, plants were grown under different P_i conditions as described in chapter 2.2.1.6. Interestingly, *MtPhr1* transcripts were detectable in every P_i condition tested. However, no significant changes in transcript levels could be

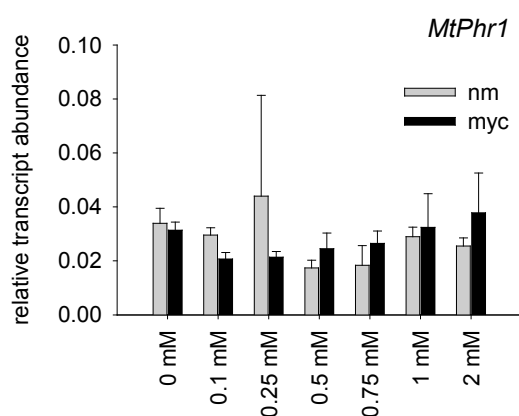


Figure 12. qRT-PCR analysis of *MtPhr1* transcripts in terms of different P_i fertilization treatment. *M. truncatula* were treated with 0-2 mM Pi in Hoagland's solution, either non-inoculated or inoculated with *G. intraradices*, and harvested 5 wpi. The relative transcript abundance was calculated relative to the reference gene *MtEf1a*. (n=5 ± stdev)

detected by comparing the different P_i treatments, which was true for nm as well as myc roots (figure 12). This is in line with previous findings of the homologue *AtPhr1*, where a transcriptional regulation due to changes in the P_i-availability could not be observed (3.2.3.4). A slight drop in transcript abundance of myc roots compared to nm was observed, although there was no evidence for a significant difference in regulation between the both conditions.

Modulation of *MtPhr1* expression and expression analysis

To investigate the role of the putative PHR1 homologue during AMS development, different constructs for a functional knock-down (RNAi) or overexpression were generated (2.2.2.1). Constructs for both, overexpression and RNAi, were driven by the CaMV 35S-promoter to modulate transcript abundance independent from exogenous treatment.

Unfortunately, no RNAi expressing roots were obtained after 2 trials of *A. rhizogenes* mediated root transformation (2.2.1.7).

For overexpression, 35Spro::PHR1(ORF) constructs were introduced into *M. truncatula* roots. By overexpressing *MtPhr1* transcript levels, the influence of increased PHR1 and its target

transcripts on AMS development in P_i -replete plants was analyzed using qRT-PCR.

Root transformed *G. intraradices* inoculated *M. truncatula* plants were fertilized with 20 μ M or 1 mM P_i in Hoagland's solution and harvested at 5 weeks post-inoculation (wpi).

Figure 13 shows the phenotype of the root-transformed plants. *MtPhr1* overexpression positively effects plant growth under low P_i but it leads to reduced growth with a lower number of fully developed and healthy leaves under high P_i .

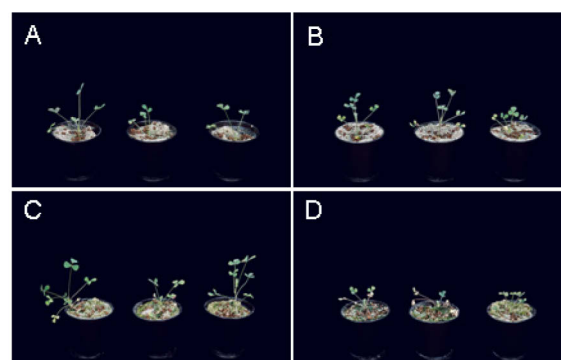


Figure 13. Phenotype of representative empty vector (pK7GW2D) and 35Spro::PHR1(ORF) root-transformed plants 5 weeks after planting. (A, C) Empty vector control (B, D) *MtPhr1* overexpressing plants grown at 20 μ M (upper images) and 1 mM P_i (lower images) in Hoagland's solution.

The plants grown under P_i -replete conditions were analyzed in terms of AMS and P_i -stress marker gene expression (figure 14) using qRT-PCR. To differentiate between exo- and endogenously expressed *MtPhr1*, primer pairs specific for the ORF (exogenous) and the 3'UTR (endogenous) were used to measure *MtPhr1* transcript abundance. A 10-fold increase of *MtPhr1* ORF in the overexpression lines were achieved as compared to the empty vector control (figure 14 a, b). Dependent from the number of transformation events in a root, the impact on gene expression can strongly diverge, therefore, the results of plants with a weaker overexpression (plant 3, 4, 6) were combined as well as those with a strong overexpression (plant 1, 2, 5) and are shown next to the graphs representing single plants. Interestingly, levels of the endogenous *MtPhr1* 3'UTR decrease in the overexpression lines (figure 14 c, d). Although the increased levels of *MtPhr1* did not cause an induction of pri-

miR399d under high P_i (figure 14 i, j), an accumulation of mature miR399 in the overexpression lines was observed (figure 14 k, l). The expression of its target transcript *MtPho2* was very low in all conditions, as well the abundance of *Mt4*, except for a strong induction in two of the three strong overexpression lines. Additionally, the elevated levels of *MtPhr1* ORF seem to positively effect *MtPt4* transcript abundance (figure 14 e, f) and *Gl rRNA* levels (figure 14 g, h). Although there was no statistical significance ($P=0.087$, Bonferroni t-test), the putative PHR1 homologue tend to increase fungal parameters, such as *MtPt4* whose promoter region also contains the P1BS for transcriptional activation and enhancement

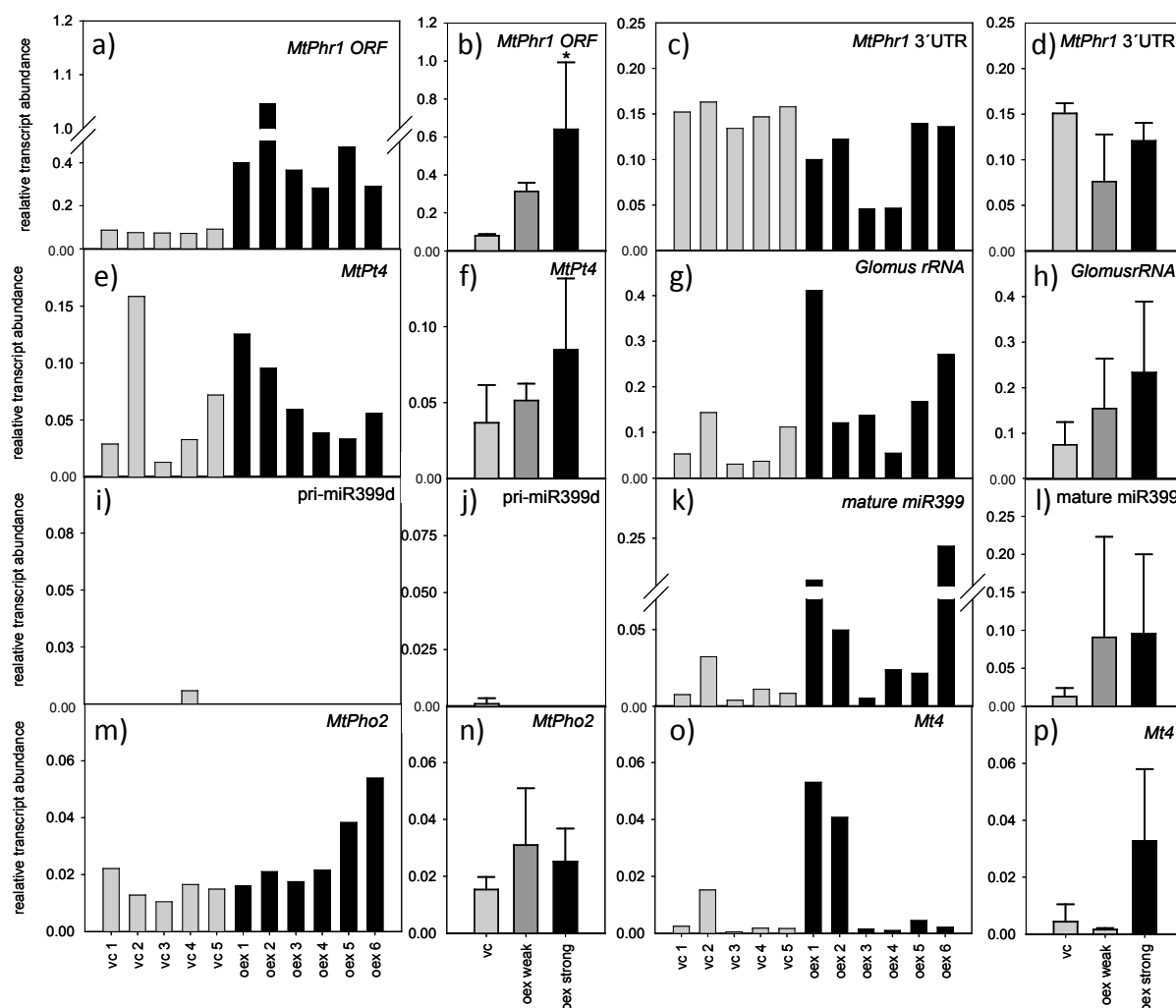


Figure 14. qRT-PCR measurements of (a, b) *MtPhr1* (ORF) and (c, d) *MtPhr1* 3'UTR several P_i -stress and AMS marker genes including *MtPt4* (e, f), *Glomus-rRNA* (g, h), pri-miR399d (i, j), mature miR399 (k, l), *MtPho2* (m, n) and *Mt4* (o, p). All plants were grown under P_i -sufficient conditions (1 mM P_i). Vector controls correspond to roots transformed with *A. rhizogenes* containing the empty vector pK7GW2D. Oex lines were transformed with 35Spro::PHR1(ORF) constructs. The results are shown for each single transgenic line and summarized in dependence of overexpression intensity next to each other. Transcript abundances of plants with a weaker overexpression (plant 3, 4, 6) were combined as well as those with a strong overexpression (plant 1, 2, 5). . The transcript abundance was calculated relative to the reference gene *MtEf1a*.

3.2.2 The role of *Mt4* during AMS – characterization of a functional *Mt4* knock-out mutant

Mt4 is an important component in the systemic regulation of P_i -homeostasis¹⁰³. Besides the fact, that *Mt4* is strongly induced during P_i -deprivation, the colonization of plant roots with AM fungi leads to decreased expression levels as compared to non-colonized roots^{43, 103}. *Mt4* is an orthologue of *IPS1* in *A. thaliana*, which regulates miR399 activity via a target mimicry mechanism¹⁸. The imperfect binding of mature miR399 with the *IPS1/Mt4* conserved region prevents these non-coding RNAs from miRNA-mediated degradation and thus reduce the amount of active mature miR399 molecules. By modulating *Mt4* expression, the miR399 activity can be affected: overexpression reduces the miR399 activity, whereas a knock-down leads to increased levels of active mature miR399. The generation of a stable *Mt4* overexpression line (Diploma thesis, Anja Branscheid) and the analysis of *Tnt1* knock-down mutants from *M. truncatula* will elucidate the specific role of *Mt4* and miR399 during AMS.

3.2.2.1 Identification of a *Mt4 Tnt1* insertional knock-out mutant

Through PCR-based screening of 400.000 *Medicago truncatula Tnt1* retrotransposon insertional mutants¹⁰⁴ (<http://bioinfo4.noble.org>) using specific primer pairs for *Mt4* and the *Tnt1* transposon, a putative *Mt4 Tnt1* insertion line was identified (PhD work of Igor Kryvoruchko; figure 15).

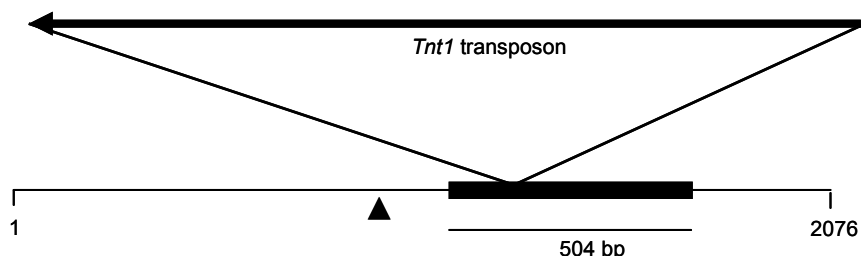


Figure 15. Schematic depiction of the genetic map of the 2076 bp spanning *Mt4* gene, which is composed of 1 single exon (black box). The putative transcription start site (black arrow) is indicated at position 978 bp. The *Tnt1* insertion is located within the exon at position 1291 of the genomic sequence.

Seeds of the T2 generation were grown under standard conditions and screened for homozygous *Tnt1* insertion. Genomic DNA of the appropriate plants was used for PCR amplification of the *Mt4* mRNA sequence (540 bp) using specific primer pairs (Mt4-F/ Mt4-R). In the case of a *Tnt1* insertion, no wild type band is expected. The *Tnt1* transposon insertion was confirmed using a primer combination binding to the *Mt4* gene and the transposon sequence (figure 16). Only 6 of 15 seedlings survived after germination of which all were heterozygous. 180 plants of the following T3 generation were grown under low P_i (20 μM) and analyzed. This resulted in the identification of 10 *Mt4* wild type plants and 10 plants that were homozygous for the *Tnt1* insertion in the *Mt4* gene. Figure 17 shows an example of the resulting PCR amplicons in the wild type and the *mt4-1* mutant.

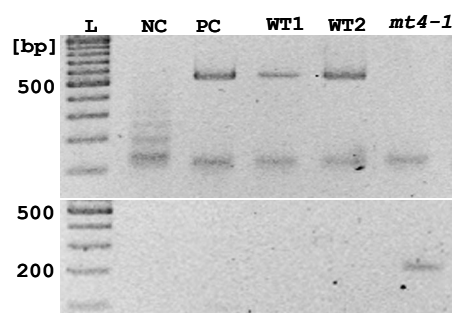


Figure 17. PCR screening of *Tnt1*-insertional mutant plants of the T3 generation concerning the *Tnt1* insertion in the *Mt4* locus. The primers Mt4-F and Mt4-R are flanking the *Mt4* mRNA sequence resulting in a fragment of 540 bp for the wild type (WT). This band is absent in homozygous *Tnt1* insertional line *mt4-1* (upper picture). The *Tnt1*-F2 binds within the transposon and results in the combination with the Mt4-F primer in a *Tnt1*-specific fragment of 220 bp (lower picture). L: 100 bp DNA ladder, NC: negative control with plasmid DNA, PC: positive control (gDNA), WT1/WT2: *M. truncatula* R108 wild type, *mt4-1*: *M. truncatula* R108 homozygous *Tnt1*-insertional mutant.

Five plants of both the wild type and the mutant line were used for seed production. The remaining plants were harvested 12 weeks after planting and used for molecular phenotyping via qRT-PCR. The *Tnt1* insertion measurements resulted in a strong downregulation of the *Mt4* transcript to non-detectable levels (figure 18 a), whereas the wildtype plants showed transcript levels as expected for P_i-depleted plants. Therefore, the *Tnt1* insertion led to a transcriptional knockout of the *Mt4* gene. Although there were no differences in pri-miR399d expression between *Tnt1* and wild type plants, all *Tnt1* plants showed significantly increased levels of mature miR399 (p=0.0007, students t-test, figure 18 b), which is consistent with significant decreased *MtPho2* levels (p=0.03, students t-test, figure 18 c) and weakly increased P_i-levels (figure 18 e). Interestingly, transcript levels of the

AMS marker genes *MtPt4* and *Glomus* rRNA slightly decreased in *Tnt1* plants as compared to the wild type, indicating a lower colonization of these plants 12 weeks post-inoculation.

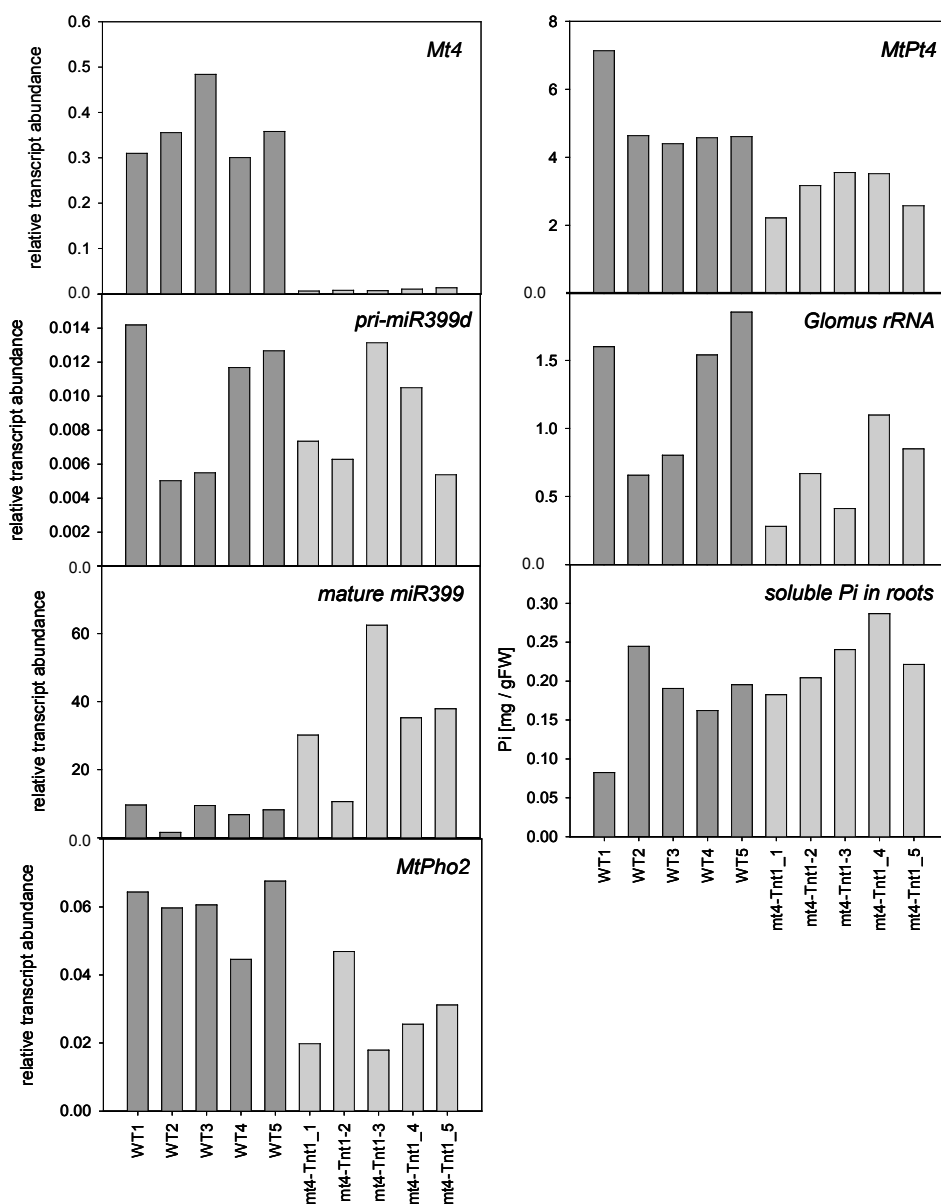


Figure 18. qRT-PCR measurements of (a) *Mt4* transcripts, (b) *pri-miR399d*, (c) *mature miR399* (d) *MtPho2*, *MtPt4* (e) and *Glomus rRNA* (f) in *M. truncatula* wild type and homozygous *mt4_Tnt1* plants. Expression levels were calculated relative to the reference gene *MtEf1α*. Plants were inoculated with *G. intraradices* and grown under P_i -limitation for 3 month (g). Soluble P_i -content of the roots, indicated values given as mg P_i per mg shoot fresh weight.

3.2.2.2 Overexpression of *Mt4* transcripts

During my diploma thesis, one stable plant line was generated through transformation of *M. truncatula* plants with a construct leading to overexpression of *Mt4* (35Spro::*Mt4*). However, the analysis of the stable transformants in several P_i - and time course experiments during my PhD work showed, that the plants did not overaccumulate *Mt4* transcripts to substantial levels in any of the tested conditions compared to the wild type (Suppl. Fig. 1). Thus, the *Mt4* sequence was cloned into the pK7GW2D overexpression vector for *A. rhizogenes* mediated

root transformation. Although transgenic roots were selected through the fluorescent GFP marker and GFP transcripts were detected in qRT-PCR measurements, there was no difference in *Mt4* transcript abundance in the overexpression lines compared to the vector control. The transformation using this construct was repeated twice with the same results. Since mature miR399 accumulate in arbuscule-containing cells of colonized roots, the regulating function of *Mt4* might play an important role in these cells. To investigate the influence of increased *Mt4* transcript abundance in arbuscule-containing cells, the *Mt4* mRNA sequence was fused to the strong and arbuscule specific promoter of *MtPt4* (2.2.2.1). After two independent root transformations and subsequent growth of the chimeric plants on a sand/vermiculite/expanded clay/*G. intraradices* inoculum at low and high P_i for 5 weeks, the root material was harvested and analyzed using qRT-PCR measurements. The transformation efficiency was very high as proven by high transcript levels of the dsRed visible marker. Unfortunately, no significantly elevated *Mt4* expression levels were detected between the vector control and *Mt4* overexpression lines of both P_i-treatments (Suppl. Fig. 2).

3.2.2.3 Identification of a putative *Mt4* homologue in *M. truncatula*

In Arabidopsis, there are at least two *Mt4* homologous genes, namely *IPS1* and *At4*, that are involved in miR399 regulation by a mechanism called target mimicry¹⁸. The DNA sequences of *IPS1* and *At4*, as well as the *Mt4* sequence, are characterized by the presence of a 24 nt conserved motif which is required for the regulation of miR399 activity. Searching for this motif in *M. truncatula* EST databases (Medicago truncatula genome index, MTGI9) revealed an EST with the accession number BQ159268, which showed similarity to the *Mt4* 24 nt conserved motif, although the overall similarity to *Mt4* was very low. The EST could be assigned to the mt3.0 (IMGAs) identifier AC147501_5.1 and the Affymetrix-ID Mtr.40143.1.S1_at. The expression profile of the *Mt4* homologue as obtained from the MtGEA database (<http://mtgea.noble.org/v2>) is shown in figure 20. In addition to the strong induction in leaves after phytohormone treatment, *Mt4-2* transcripts are highly abundant in P_i-starved roots and slightly downregulated after colonization with AMF. Obviously, *Mt4-2* is a P_i-responsive gene up-regulated during P_i-starvation and shows a similar expression pattern as *Mt4* under these conditions.

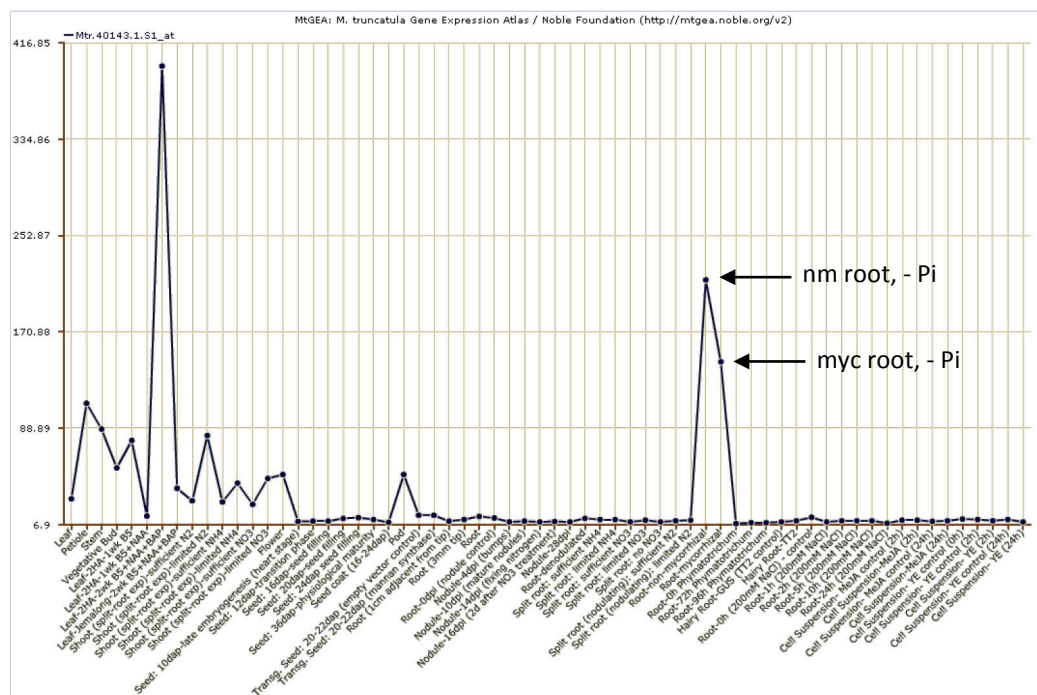


Figure 20. Expression profile of Mtr40143.1S1_at in *M. truncatula* after different treatments. The transcript data were extracted from the MtGEA database. The black arrow indicates the increased transcript abundance in P_i starved roots.

To confirm the presence of *Mt4-2* transcripts in *M. truncatula* P_i -depleted roots, RT-PCR using a gene specific primer pair was carried out, resulting in a specific fragment of an expected size of 606 bp (Suppl. Fig. 3). The amplicon of the expected size showed that *Mt4-2* is transcribed under the condition tested (nm roots, 20 μM P_i).

3.2.2.4 *Mt4-2* interacts with mature miR399

If *Mt4-2* is a functional homologue of *Mt4*, it should be able to bind and sequester mature miR399. The sequence alignment of the 24 nt conserved motifs of *At4-3*, *Mt4* and *Mt4-2* to mature miR399 is shown in figure 21. The insusceptibility for miR399-mediated cleavage of *Mt4* is due to a mismatching loop formed by 4 nucleotides at the miR399 cleavage site. In comparison to the *Mt4* sequence, *Mt4-2* showed a 3 nucleotides substitution and one additional nucleotide. However, these changes are located within the bulb and might not affect the complementary binding of miR399.

```

At4-3      5' TGACCGGGCAACTTCGGAACCTTTGGCAATGT 3'
Mt4       GGAAAGGGCAACTT-CGATCCTTTGGCATTTT
Mt4-2    AGGAAGGGCAACCAATGATCCTTTGGCAATTT
miR399c   GTCCCGTTTAG----AGGAAACCGT
miR399d   ATCCCGTCGAG----AGGAAACCGT
miR399e   GACCCGTTTAG----AGGAAACCGT
miR399j   GC11CCCGTTTAG----AAGAAACCGC
miR399o   GTCCCGTCGAG----AGGAAACCGT
miR399q   3' TTCTCGTCGAG----AGGAAACCGT 5'

```

Figure 21. Sequence alignment of the conserved motif of *Mt4*, *Mt4-2* and *At4-3*. The consensus of the conserved region is highlighted in blue as well as complementary nucleotides of the different mature mtr-miR399 sequences. Nucleotides of mature miR399 sequences complementary to *Mt4* but not *Mt4-2* are underlined.

To study the interaction of *Mt4-2* transcripts with mature miR399, an assay based on RNA-RNA non-radioactive gel-shift assays was developed. The mRNA sequences of *Mt4* and its putative homologue *Mt4-2* were cloned and *in vitro* transcribed to obtain specific mRNA. After purification, both of the mRNAs were subjected to several hybridization reactions using 5' DIG-labelled RNA oligonucleotides of mature miR399d and a scramble probe, a random oligonucleotide sequence not able to bind *Mt4* or *Mt4-2*. The detailed procedure is described in section 2.2.3.3. Figure 22 shows an overview of the different reaction batches covering all possible combinations of RNA detection probes and corresponding mRNAs, the RNA after separation using native polyacrylamide gel electrophoresis (PAGE) (figure 22 a) and the successful validation of a miR399-*Mt4* and miR399-*Mt4-2* interaction after anti-DIG antibody treatment and subsequent alkaline phosphatase reaction (figure 22 b). The different molecule sizes of *Mt4* (504 nt), *Mt4-2* (560 nt) and 5'-DIG-miR399d (21 nt) / random RNA oligonucleotide sequence (21 nt) and the resultant difference in running distances were used to confirm an interaction through a shift of the small RNA oligonucleotides from the lower (unbound RNA detection probe) to the upper part of the membrane (detection probe-mRNA duplex). The shift was observed after hybridization of miR399d with *Mt4* and *Mt4-2* but in no other condition. After hybridization with the random RNA sequence, signals were only detected in the lower part of the membrane indicating that this RNA did not bind to either of the transcripts.

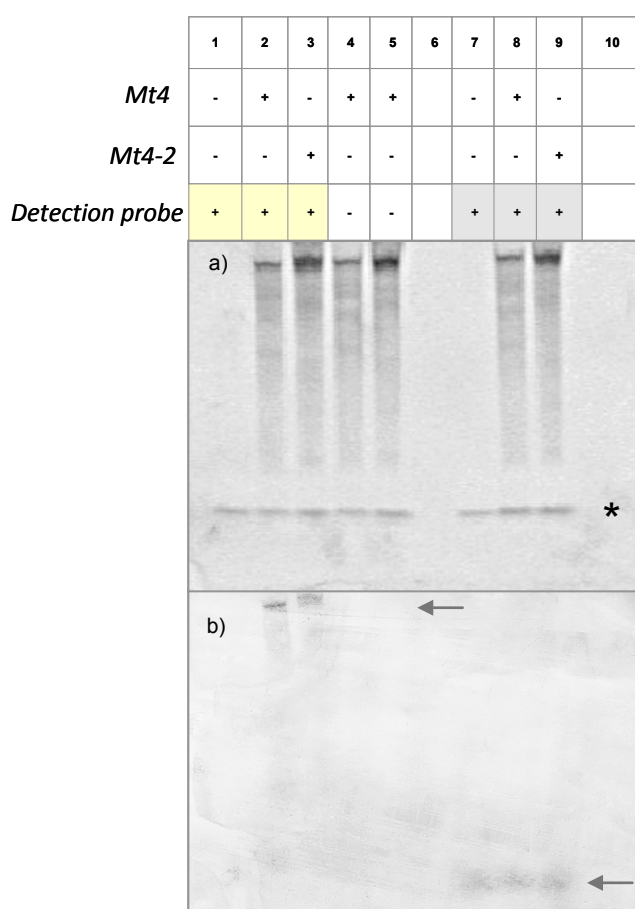


Figure 22. RNA-miRNA gel shift assay to investigate the interaction of mature miR399d and *Mt4-2*. Specific transcripts of *Mt4* and *Mt4-2* were hybridized to 5 DIG labelled RNA nucleotides with a mature miR399d sequence and a random sequence not able to bind either of the transcripts. The hybridized transcripts, non-treated *Mt4* and *Mt4-2* mRNA as well as untreated RNA oligonucleotides were separated through native PAGE (a), electroblotted and treated with an anti-DIG antibody. Signals were visualized after NBT/BCIP alkaline phosphatase reaction (b). Signals were detected in lane 2, 3, 7, 8 and 9 indicated by grey arrows (loading is shown at the top). Whereas the signals of lane 7-8 in the lower area of the membrane derive from the unbound random RNA nucleotide, the signals of lane 2 and 3 confirm an interaction of mature miR399d with *Mt4* and *Mt4-2* indicated by a signal shift towards the transcripts of *Mt4/Mt4-2* to the upper part of the membrane. The star in picture (a) marks the bromphenolblue front after running a 5 % TBE gel.

3.2.3 Involvement of miR399 in AMS regulation

3.2.3.1 Localization of mature miR399 in roots using *in situ* hybridization

Pri-miR399 and mature miR399 levels are positively correlated to AM colonization levels in *M. truncatula* roots. Thus, a role of miR399 in the regulation of the P_i-response in myc roots is assumed.

To localize miR399 accumulation in mycorrhizal roots, a *Locked Nucleic Acid* (LNA)-based *in situ* hybridization (ISH) approach was carried out. LNAs are a class of conformational restricted nucleotide analogs, in which the ribose ring is constrained by a methylene linkage between the 2' oxygen and the 4' carbon resulting in the locked 3' endo formation (figure 23) (Saenger, 1984). LNA nucleotides possess a higher specificity and affinity to its target RNA or DNA due to the increased melting temperature of the duplex. Therefore, LNA-modified

probes are ideal for the analysis of short targets such as miRNAs. In this study, a LNA detection probe for the detection of mature mtr-miR399d was used.

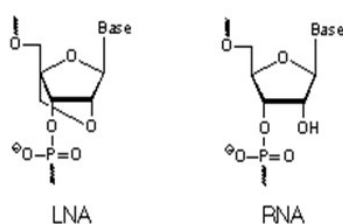


Figure 23. Structural differences between LNA and RNA nucleotides

P_i-depleted *M. truncatula* plants were grown for five weeks, either non-inoculated or inoculated with *G. intraradices*. Root material was harvested and used for paraffin embedding, microtome sectioning and the subsequent ISH (2.2.3.2). 10 µm root cross sections of both conditions were hybridized using either a LNA-miR399d detection probe or the scramble probe as negative control. The latter is a random 21 nt DNA/LNA sequence, unable to bind any known *M. truncatula* miRNA. For signal detection, the Fast Red-substrate system was applied. In the presence of an alkaline phosphatase enzyme, the Fast Red chromogen produces a light red precipitate, which can be detected through light- and fluorescence microscopy.

The microscopic analysis of the sections revealed no signals in the negative control (Figure 24 a-c, g-i) but strong signals after hybridization with the miR399d probe in nm as well as myc roots. In both sample types, mature miR399d signals were detected in the phloem and the surrounding tissue, but not in xylem (figure 24 d-f, j-l). Remarkably, in myc root sections mature miR399 signals appeared outside the phloem, even outside from the central cylinder, and accumulated specifically in arbuscule-containing cells (figure 24 j-l). Interestingly, the vascular tissue-located signals appear like a dense stream, whereas they emerge in cortex cells rather as spot-like structures (figure 25 a). Most of the cortex-located signals were observed close to cell walls, assuming that mature miR399 are cytosolic components. In arbuscule-containing cells, mature miR399 primarily accumulate in direct vicinity to nuclei and mostly degenerating arbuscules (figure 25 d). In addition, a high density of miR399 signals was observed in the region of the endodermis and the cell layer behind, suggesting a symplastic movement of mature miR399 from vascular tissue to the root cortex passing barriers such as plasma membranes, cell walls and even the non-permeable casparian stripe in the endodermis.

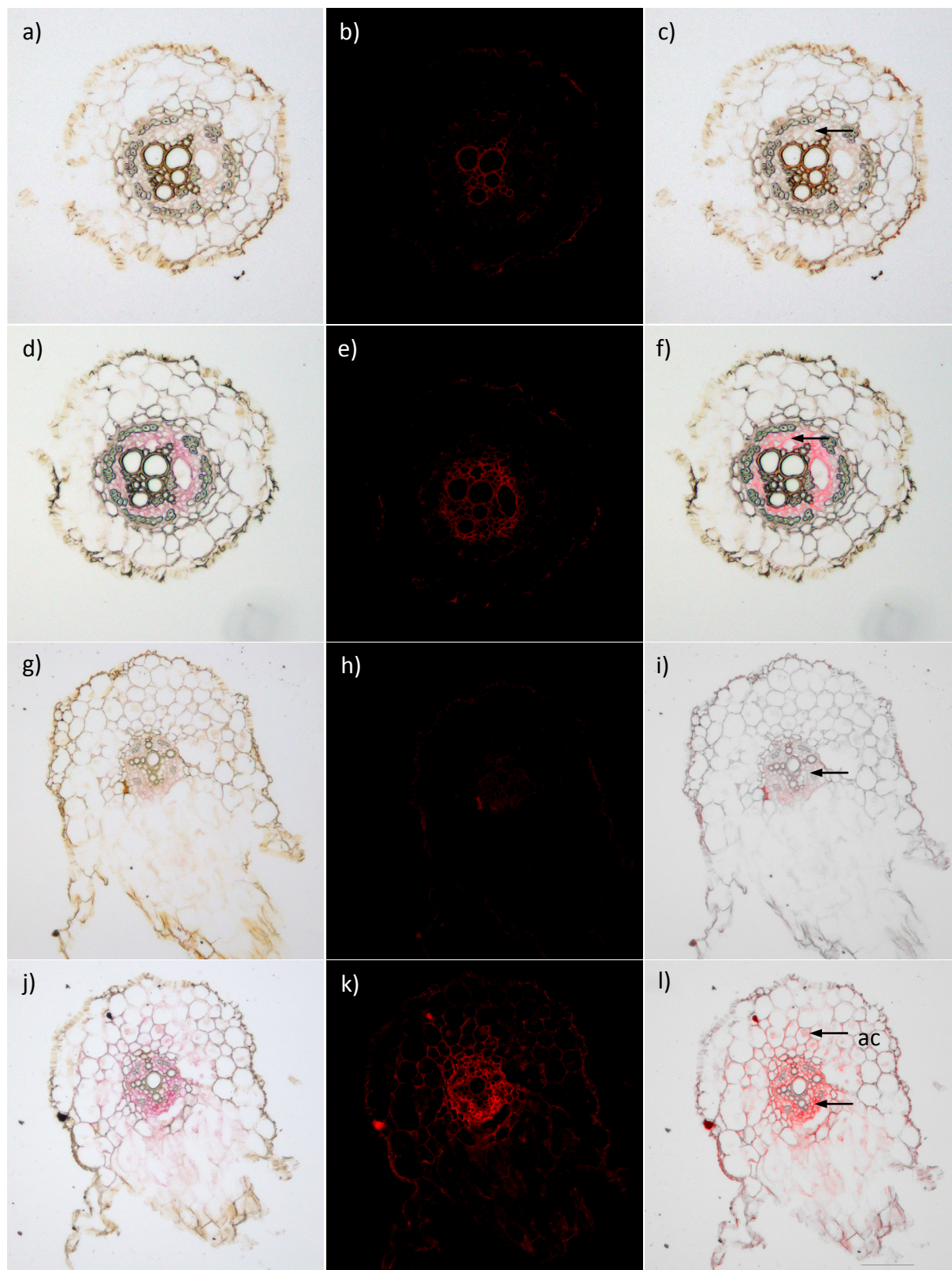


Figure 24. Localization of mature miR399 accumulation in nm and myc roots. Root cross sections were paraffin embedded and hybridized using either LNA-miR399d detection probe or a scramble probe, which is a random LNA containing DNA sequence used as negative control. Signals caused by miRNA accumulation were visualized by Fast Red staining and subsequent epifluorescence microscopy. (a-c) scramble probe, nm root; (d-f) miR399d probe, nm root; (g-i) scramble probe, myc root; (j-l) miR399d probe, myc root. Images in a row illustrate the signal intensity in brightfield, fluorescence and in the overlay of both. (ac) arbuscule-containing cell, black arrows indicate hybridization signals. Scale bars represent 200 μ m.

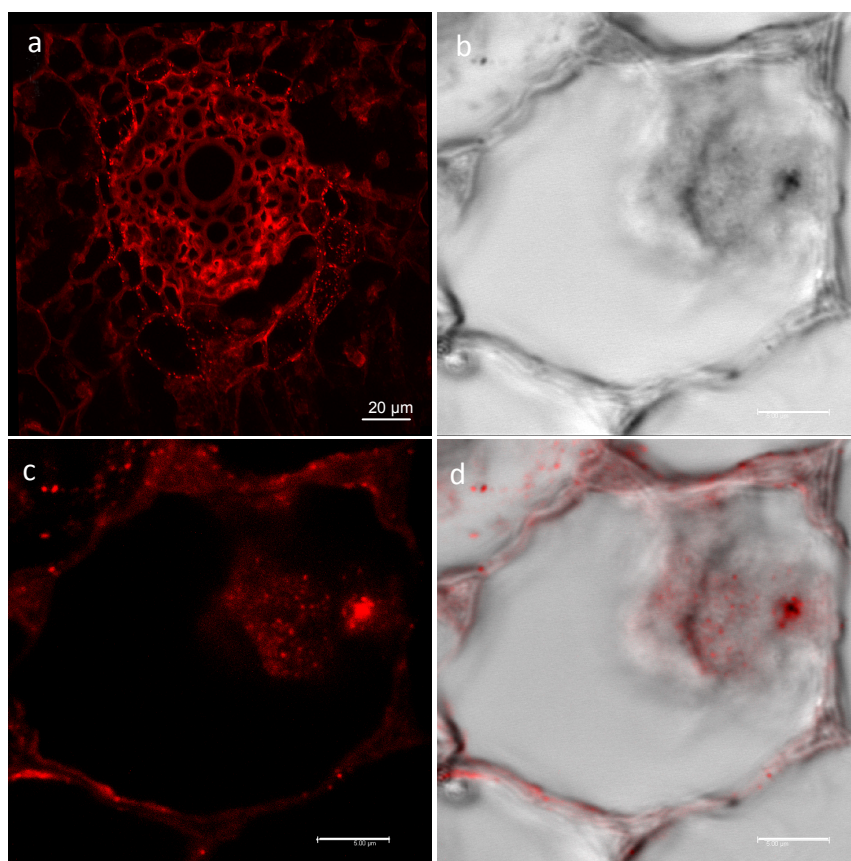


Figure 25. Localization of mature miR399d accumulation in myc roots and arbuscule-containing cells. Root cross sections hybridized using a LNA miR399d detection. Signals caused by miR399 accumulation were visualized by Fast Red staining and subsequent confocal microscopy. (a) Overview of the central cylinder and surrounding tissue. MiR399 accumulates in the phloem demonstrated by the bright red signal within the central cylinder. Outside of the vascular tissue, miR399d signals appear primarily in the cytosol of colonized and non-colonized cortex cells. (b-d) Accumulation of mature miR399d in arbuscule-containing cells, particularly adjacent to arbuscules and the nucleus. Scale bars represent 20 µm (a) and 50 µm (b-d).

3.2.3.2 Localization of miR399 promoter activity

The pri-miR399 expression levels decrease in myc roots as compared to nm roots due to increased P_i -concentrations as demonstrated in a previous study⁴². To investigate whether miR399 transcription is regulated in mycorrhizal roots potentially in distinct cells, promoter-reporter studies were applied. A cell-specific regulation of miR399 transcription would underline the hypothesis that miR399 play an important role to maintain arbuscules in roots under P_i -limitation.

1.5 kb of the putative promoter region of miR399d was used to generate promoter::CFP (cyan fluorescent protein) fusions. As control, a 35Spro::CFP fusion was generated. After *A. rhizogenes* mediated root transformation, chimeric *M. truncatula* plants were grown non-inoculated or inoculated with *G. intraradices* under high or low P_i .

Signals of the 35S-promoter driven control were found in transformed roots of both P_i -treatments evenly distributed and not restricted to a certain area (figure 26 a, b). The MIR399dpro::CFP derived promoter signals were only detected in P_i -depleted roots and appeared predominantly in cortical cells in vicinity to the vascular tissue, in the root tips and

in the meristematic tissue of lateral root primordia (figure 26 c-f).). The spatial accumulation of miR399d-promoter signals in distinct regions such as the root tips and the leaf primordia indicate a further interesting role of miR399 for root growth during P_i -limitation.

In the inoculated transformed roots, promoter signals additionally appear more distributed in the cortex, stronger signals were detected in distinct cells surrounding the central cylinder indicating a localization of miR399d transcription in distinct cells (figure 26 g, h).

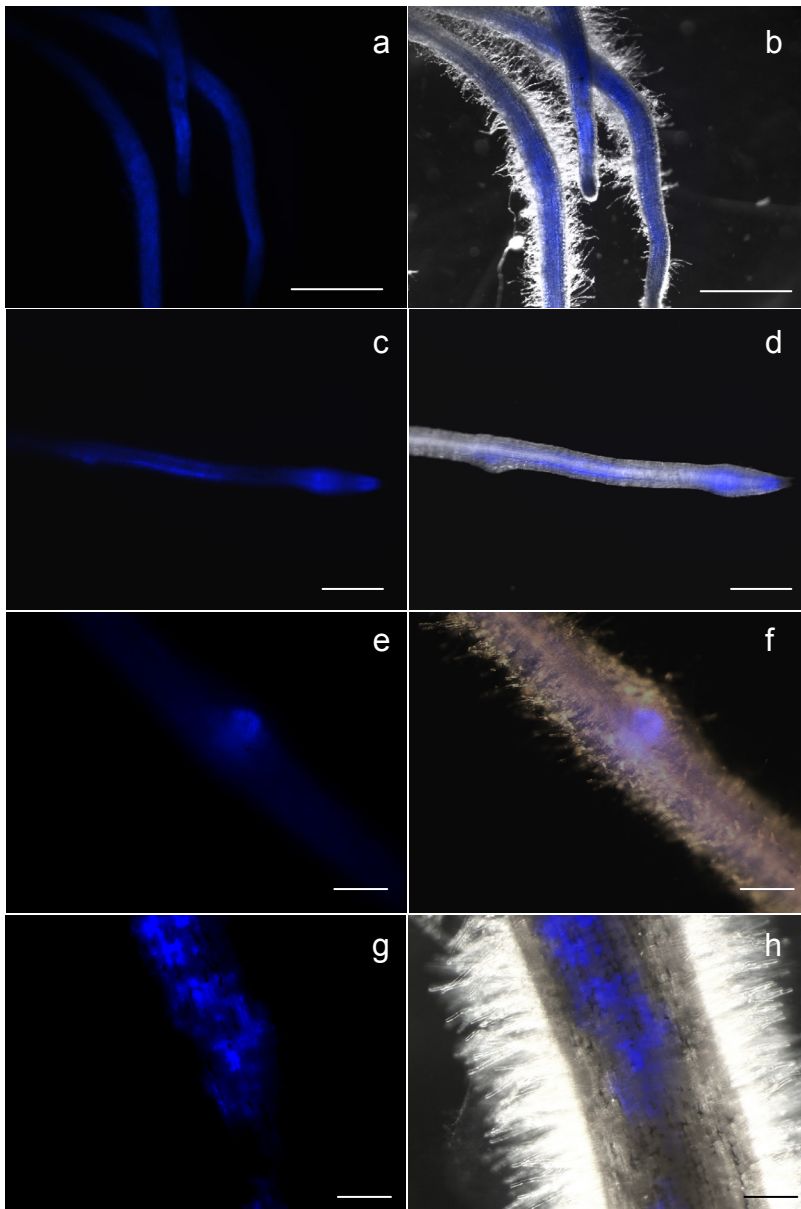


Figure 26. Localization of promoter::reporter fusions in transformed *M. truncatula* nm and myc roots. 35Spro::CFP (control) and miR399dpro::CFP signals were visualized using a stereo fluorescence microscope. Images of (a, c, e, g) show detected CFP fluorescence signals and (b, d, f, g) the corresponding brightfield/fluorescence overlay. (a-b) Roots transformed with the 35Spro::CFP construct; (c-h) miR399dpro::CFP transformed roots. Plants were grown non-inoculated (a-f) or inoculated with *G. intraradices* (g, h) at 20 μ M P_i and harvested 5 weeks post inoculation. Scale bars represent 500 μ m (a, b), 200 μ m (c, d), 50 μ m (e-h).

3.2.3.3 Regulation of miR399 transcription at different stages of AMS development

Several genes of the miR399 family showed elevated expression levels in shoots of myc plants as compared to shoots of nm plants. The observed accumulation of mature miR399 in myc roots at 5 wpi was suggested to be a result of the stronger transcriptional induction and processing of miR399 in the shoots and subsequent phloem transport to the roots⁴².

To obtain more insight on miR399 expression and accumulation during AMS development, a time course experiment was carried out. *M. truncatula* wild type plants were grown under P_i-deficient conditions (20 μM P_i), either non-inoculated (nm) or inoculated with *G. intraradices* (myc). The roots and shoots were harvested once a week in period of 1 to 8 wpi, the soluble P_i-content and the expression of diagnostic markers for AMS and P_i-stress was determined

Soluble P_i-content

In general, shoots showed up to 5 times higher P_i-concentrations as compared to the roots (figure 27). Similar P_i-concentrations of nm and myc plants were also observed. At 1 wpi, the shoots as well as the roots showed elevated P_i-concentrations due to remaining P_i from the seedling stage, but the P_i-concentration of myc plants was significantly decreased compared to nm plants. After 2 weeks, plants of both conditions exhibited similar P_i-concentrations, whereas from the 3rd week the shoots and the roots of the myc plants accumulated higher concentrations of soluble P_i compared to nm plants. Higher P_i-concentrations in myc plants most likely resulted from the symbiotic P_i-uptake after the establishment of a functional symbiosis.

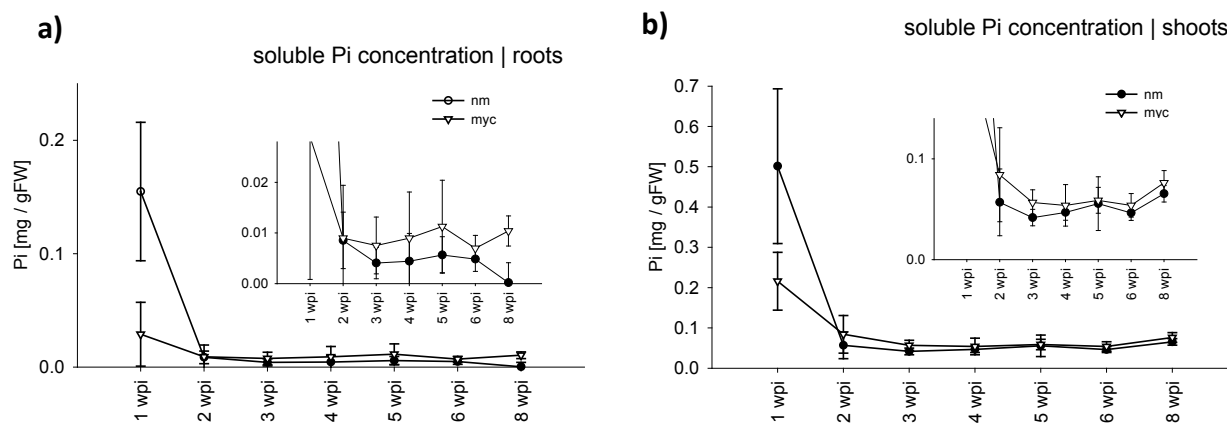


Figure 27. Soluble P_i-concentration in roots (a) and shoots (b) of non-mycorrhizal (nm) and mycorrhizal *M. truncatula* plants harvested 1-8 weeks post inoculation with *Glomus intraradices*. All plants were fertilized with half strength Hoagland's solution containing 20 μM P_i. Concentration of soluble P_i is given in mg P_i per g fresh-weight. Smaller diagrams within the graphs of a and b represent the values between 2 and 8 wpi in a higher magnification. (n = 4, ± stdv)

Transcriptional changes of genes involved in P_i-homeostasis signalling

To investigate the molecular response to the P_i-status, transcript abundances of the P_i-homeostasis involved genes as mature miR399, *MtPho2*, *Mt4*^{10, 43} and the PHO2 independent P_i-stress marker *MtPID* were determined. Further, the expression of the mycorrhizal specific Pi-transporter *MtPt4*²⁸ and the fungal gene *GiαTubulin*¹⁰⁵ were analyzed (figure 28).

MtPID transcript levels reflect the local P_i-status in the roots as previously described (figure 28 a). At 1 wpi, roots of both the nm and the myc plants did not express detectable amounts of *MtPID* because of remaining P_i-resources from the seeds. However, the P_i-deficient growth conditions led to a significant decline of internal P_i-concentrations after 2 weeks and a simultaneous significant induction of *MtPID*. At 3 wpi, the functional AMS was fully established, which is accompanied by increased P_i-concentrations (figure 27 a) and the significant decrease of *MtPID* transcripts in mycorrhizal roots as compared to nm roots. Up to the last harvesting time-point at week 8, *MtPID* levels are constant, with lower levels in myc roots compared to nm roots. In contrast, transcripts of genes involved in the miR399-related P_i-homeostasis pathway showed a different pattern (figure 28 b). Despite the improved P_i-supply caused by the symbiotic P_i-uptake, the mature miR399 showed elevated levels in myc roots compared to nm roots. However, this effect was observed predominantly at later stages of AM development. Related to that, the relative transcript abundance of the miR399 target *MtPho2*, as well as *Mt4*, decrease to lower levels in myc roots as compared to nm roots between 4 wpi and 8 wpi (figure 28 c, d).

As expected, *MtPt4* was only detected in myc roots (figure 28 e). Interestingly, the *MtPt4* expression strongly increases up to 4 wpi, followed by a significant drop to 50 % after the fourth week and a relative constant expression between week five and eight. This expression pattern indicates a peak of arbuscule abundance at 4 weeks followed by a steady state of developing and degenerating arbuscules in the later stages of AMS. The overall fungal presence, which is represented by *GiαTubulin* (figure 28 f), also decreases around 25 % after 4 weeks and confirms the lower abundance of fungal structures within the plant root after an initial peak.

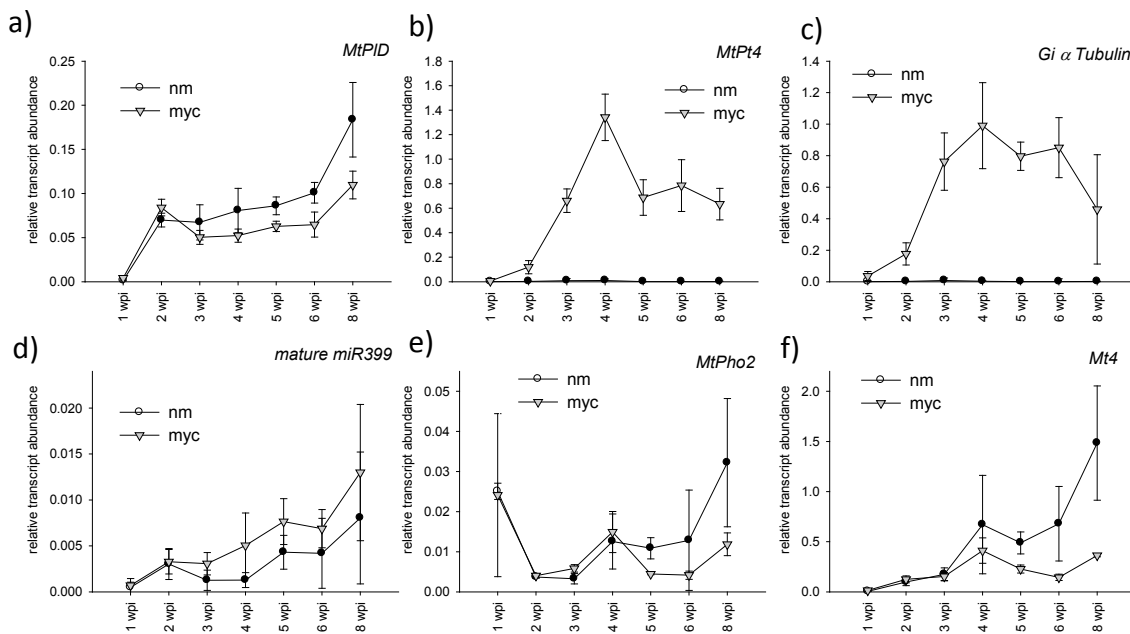


Figure 28. Relative expression levels of (a) *MtPID*, (b) *MtPt4*, *Glomus* α *Tubulin*, (d) mature miR399, (e) *MtPho2*, (f) *Mt4* relative to the reference gene *MtEf1* α . Each data point represents the average of 4 independent biological replicates \pm stdev. Black and grey triangles represent the values of non-mycorrhizal and mycorrhizal roots, respectively.

3.2.3.4 P_i -gradient experiment - effects of the symbiotic P_i -uptake on plant P_i -homeostasis

I was further interested in the influence of varying P_i -concentrations in the plant on the symbiotic P_i -uptake and the AMS development. For this purpose, a P_i -gradient experiment was set up. *M. truncatula* plants were grown either non-inoculated or inoculated with *G. intraradices* and fertilized twice a week with Hoagland's solution¹⁰⁶ containing one of the following P_i -concentrations: 0 μ M, 100 μ M, 250 μ M, 500 μ M, 750 μ M, 1 mM and 2 mM P_i .

Soluble P_i -content

Results of the P_i -measurement are shown in figure 29. The soluble P_i -concentration in both roots and shoots reflected the different P_i -treatments (figure 29 a, b). Both tissues of mycorrhizal plants exhibited higher P_i -concentrations as compared to non-mycorrhizal plants. As expected and confirming by previous results⁴², the symbiosis efficiency increases with declining internal P_i -concentrations. Remarkably, the maximum of the beneficial capacity of the AMS with regard to the symbiotic P_i -uptake is achieved at P_i -concentrations up to 500 μ M P_i in the shoots. Additionally, the symbiotic P_i -uptake seems to be limited at very low and very high P_i -concentrations.

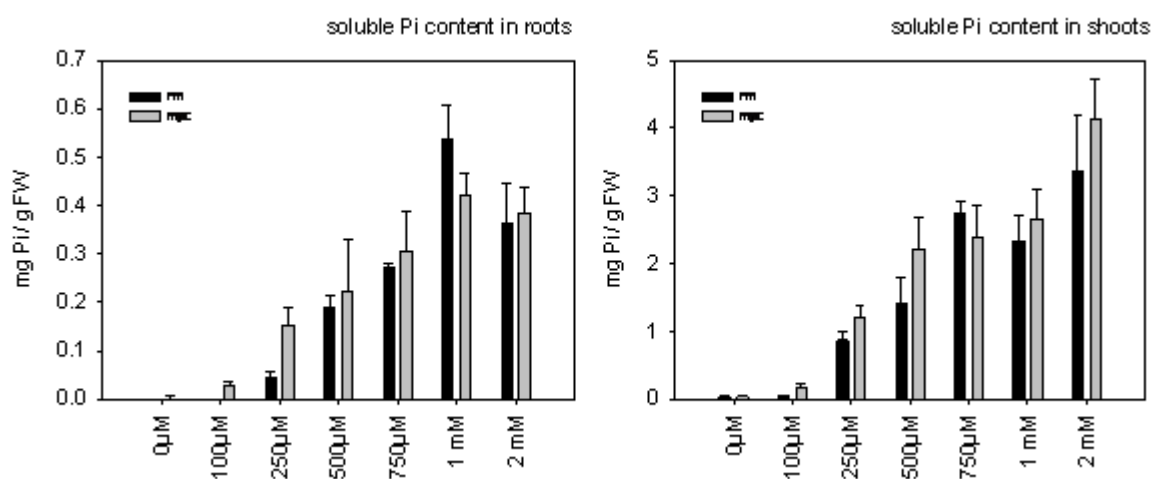


Figure 29. Soluble P_i -concentrations in roots and shoots of plants grown under increasing P_i -conditions (from 0 μM P_i to 2 mM P_i in Hoagland's solution), either non-inoculated or inoculated with *G. intraradices* and harvested 5 wpi. (n=4; \pm stdev)

qRT-PCR measurements

Transcript levels for *MtPID*, *MtPho2*, *Mt4*, *pri-MIR399d* and mature miR399 were determined in *M. truncatula* roots using qRT-PCR. Additionally, transcripts describing the AMS developmental status like *MtPt4*²⁸, *MtGst1*³⁰ and *Glomus α Tubulin*¹⁰⁵ were analyzed. The results are shown in figure 30. Although the AMS marker gene expression, represented by *MtPt4*, *MtGst1* and *Glomus α Tubulin* (figure 30 a-c), was relatively low, the symbiosis had a substantial effect to the local P_i -availability in the root (figure 29). Primarily at low P_i -concentrations, the P_i -stress marker *MtPID* (figure 30 d) showed decreased expression levels in myc roots as compared to nm roots, reflecting the symbiotic P_i -uptake. The 250 μM P_i -treatment was sufficient to repress *MtPID* transcript levels below the detection threshold in both the nm and myc roots.

The *pri-miR399d* and mature miR399 (figure 30 e, f) were highly abundant up to and including 100 μM P_i , with slightly decreased levels of the primary transcript in myc roots. Remarkably, a P_i -concentration of 250 μM completely suppressed the transcription of *pri-miR399d* to non-detectable levels. A similar pattern to *pri-miR399d* was shown by *Mt4* (figure 30 h), a negative regulator of the miR399 activity¹⁸. The mature miR399 showed a higher abundance in myc roots as compared to nm roots especially in the 0 μM P_i -treatment, confirming results from a previous study⁴². However, this effect disappeared at higher P_i -concentrations suggesting that it is highly P_i -dependent. Notably, a basal level of mature

miR399 was also detected in myc roots between 500 μ M and 2 mM P_i resulting in an interesting expression patterns for the target transcript *MtPho2* (figure 30 g). While *MtPho2* showed continuously increasing levels with increasing P_i -concentrations in nm roots, the expression in myc roots seems to be independent from the P_i -treatment and is kept on similar and low levels in each condition.

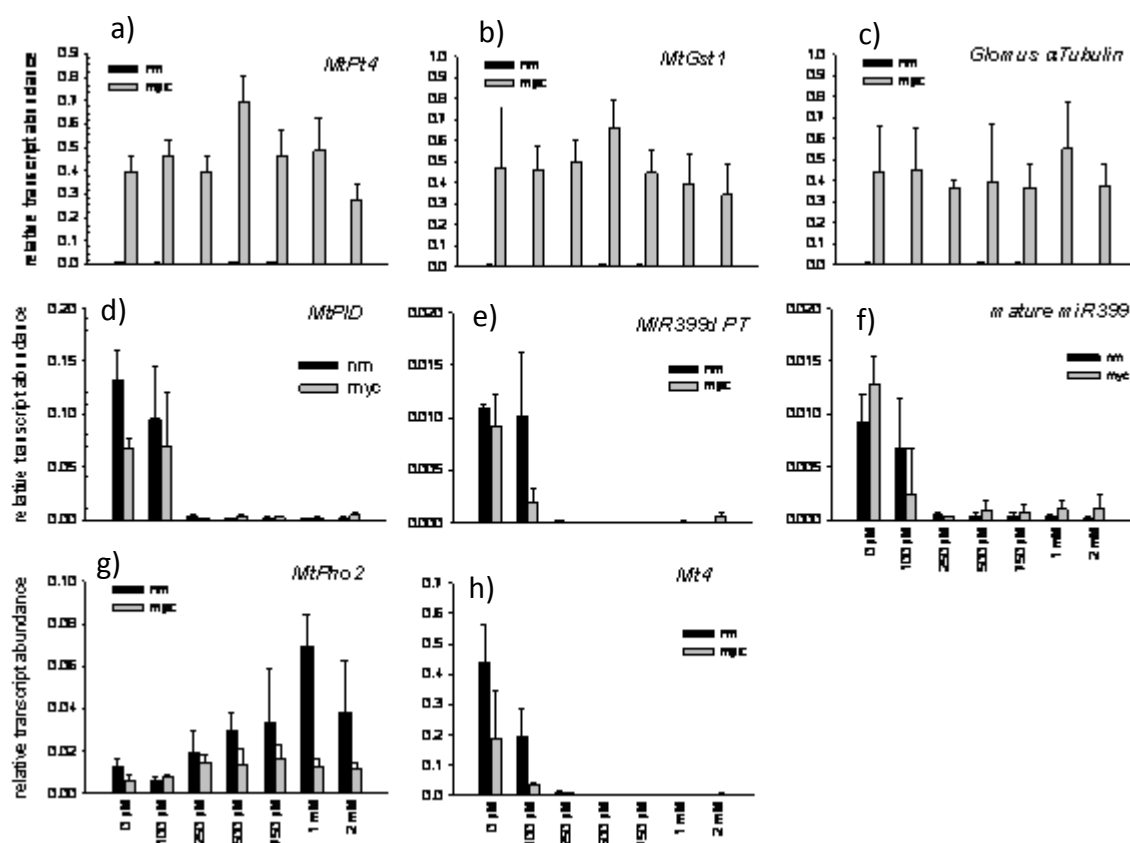


Figure 30. Relative expression levels of (a) *MtPID*, (b) *MtPhr1*, (c) *MIR399d PT*, (d) mature miR399, (e) *Mt4*, (f) *MtPho2*, (g) *MtPt8*, (h) *MtPt4*, (i) *MtGst1* and (j) *Glomus α Tubulin* relative to the reference gene *MtEf1 α* in *M. truncatula* roots treated with gradient P_i -concentrations in Hoagland's solution (0mM – 2 mM P_i). Each column represents the average of 4 independent biological replicates \pm stdev. Black and grey coloured columns represent the values of nm and myc roots, respectively.

3.2.3.5 Crosstalk of P_i -homeostasis, AMS development and photosynthates

The improved P_i -availability and acquisition is substantial benefit for the plants in the interaction with AM fungi and a direct link between phosphorous nutrition and AM colonization levels is indicated. In addition to P_i , also photosynthesis-derived sucrose is an important key player in the regulation of AMS development. P_i and sugar metabolism are directly linked, the induction of many P_i -starvation inducible and PHR1 regulated genes are dependent on the sugar status of the plant¹⁰⁷. The investigation of a correlation of the sugar and P_i -dependent induction of miR399 and the influence to AMS development is of great interest. To investigate the interrelation of these parameters a dark shoot experiment was applied. *M. truncatula* plants were inoculated with *G. intraradices* and grown under high P_i (1 mM) in a sand / vermiculite substrate. After a period of 14 days, the fertilization was altered to low P_i (20 μ M) for further 14 days. At the same time, the several plants had either the entirety or half of their shoot (splitshoot) covered, while the other plants remained in standard light conditions (control). The shoots and roots of the plants were analyzed in terms of P_i -stress marker gene (*pri-miR399d*, *mature miR399*, *MtPho2*, *Mt4*, *MtPID*) and AMS marker gene expression (*MtPt4*, *GirRNA*) using qRT-PCR (figure 31). The relative transcript abundances in the splitshoot roots and the roots of covered plants were normalized to the control condition (see

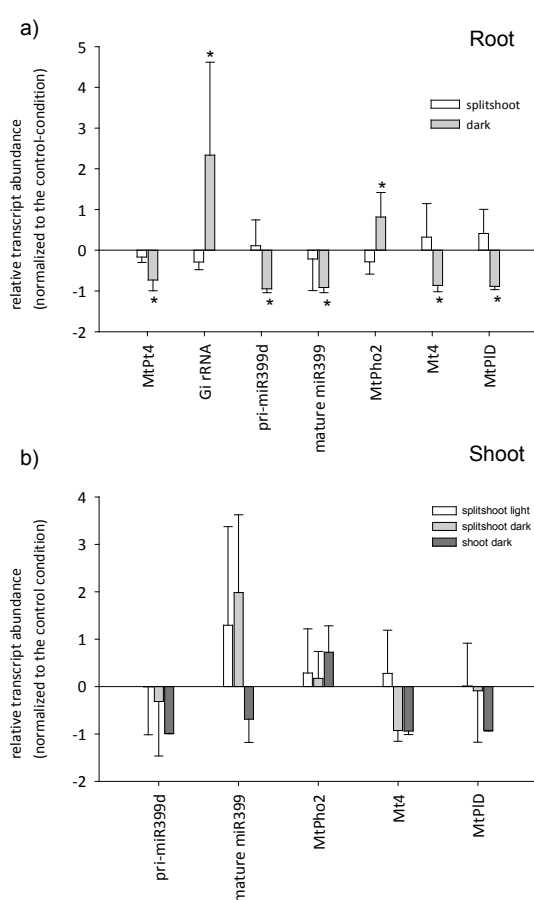


Figure 31. Relative transcript abundance of *MtPt4*, *GirRNA*, *pri-miR399d*, *mature miR399*, *MtPho2*, *Mt4* and *MtPID* in roots (a) and shoots (b) of plants with reduced photosynthesis. Plants were grown either with split shoots (Splitshoot light/dark) or completely darkened shoots for 2 weeks under limiting P_i conditions. The transcript abundances for each single gene was calculated relative to the reference gene *MtEf1a*. The ratio shown here was calculated from transcriptional changes comparing the relative expression of both the treated and untreated plants (control, grown under standard light conditions).

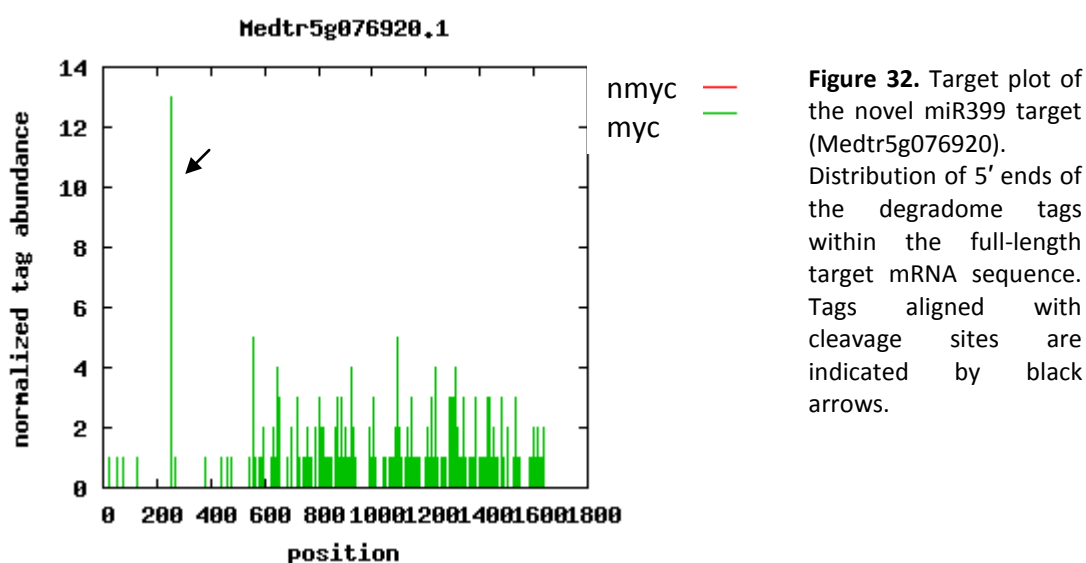
above) in order to detect changes depending upon the treatment (figure 31). The components of the PHR1-PHO2-miR399 signalling pathway showed a similar expression in roots of the splitshoot system as compared to the non-treated control. Interestingly, the darkening of the shoots and the inhibition of photosynthesis had strong effects on the expression of these genes. The abundance of pri-miR399d and *Mt4* transcripts decreased as well as the abundance of mature miR399. This is consistent with increasing levels of the miR399 target *MtPho2*. Additionally, the independent P_i-stress marker gene *MtPID* exhibited lower levels in dark roots as compared to the control roots. The expression patterns of the measured P_i-dependent genes indicate a decline of P_i-stress in these roots, despite low P_i-fertilization. This might be the reason for the decrease of *MtPt4* transcripts, a marker gene for active arbuscules in the roots. However, the overall fungal mass seems to be increased, as shown by elevated levels of *GirRNA* in roots of darkened plants. The analysis of P_i-stress marker genes in the shoots of entirely darkened plants and shoots from the splitshoot system either darkened or exposed to light had similar results (figure 31 b). Genes of the P_i-starvation response were downregulated in the darkened shoots of both conditions whereas the expression in the light exposed part of the shoot was similar to the control shoot. The suppression of photosynthetic carbohydrate production massively affects the transcriptional response to P_i-deprivation. The downregulation of the P_i-starvation response led to lower *MtPt4* expression levels in the root but to extensive fungal growth within the root.

3.2.4 Identification of a novel miR399 target by degradome analysis

Mature miR399 molecules are mobile signals in the systemic regulation of plant P_i-homeostasis^{9-11, 15}. Moreover, expression patterns suggest a role of mature miR399 in the systemic regulation of P_i-dependent AMS establishment and development⁴². However, the only target known so far is the E2 ubiquitin conjugase enzyme (PHO2), which is degraded under P_i-limiting conditions and negatively regulates several phosphate starvation induced genes. Although seedlings of *pho2* mutants showed a slightly faster symbiosis development 7-14 days post inoculation with *G. intraradices* (Emanuel Devers, unpublished), there was no further evidence for a direct link between *MtPho2* transcript abundance and AM development. By degradome analysis, a novel target of the miR399 family with homology to P_i-transporters from *M. truncatula* was identified, which might indicate a P_i-dependent

regulation of AMS by miR399 independent of *MtPho2*. The novel target is subsequently named as *MtPt8*.

The read count analysis of the degradome data showed that one transcript, encoding a major facilitator (Medtr5g076920) strongly regulated in mycorrhizal roots (LFC 18.7), has one of the highest values of all regulated transcripts. Moreover, the data implied this transcript is cleaved by members of the miR399 family. The target-plot of Medtr5g076920, with a clear peak at position 255/256 of the transcript, is shown in figure 32.



3.2.4.1 In vivo validation of miR399-mediated cleavage of *MtPt8* transcripts

Modified 5' RLM-RACE of *M. truncatula* inoculated and non-inoculated roots

In addition to the degradome analysis, the modified RLM-5'RACE is a further possibility to validate miRNA-mediated cleavage of mRNAs. For this purpose, the decapped and 5'phosphate residue-containing mRNA from the same root material used for degradome library construction was ligated to 5'RNA-adapters, cDNA was synthesized and the cDNA libraries were afterwards PCR amplified using adapter- and gene-specific outer and inner primer pairs. The expected sizes of the amplicons were 549 bp and 371 bp for the outer and the inner PCR products, respectively. The obtained band of 371 bp resulting from the nested PCR (figure 33) was only present in the myc library, excised and subcloned. The plasmids of 10 clones were sequenced with all analyzed clones exhibiting inserts confirming the cleavage of the *MtPt8* transcript at position 255/256 relative to the translation start site.

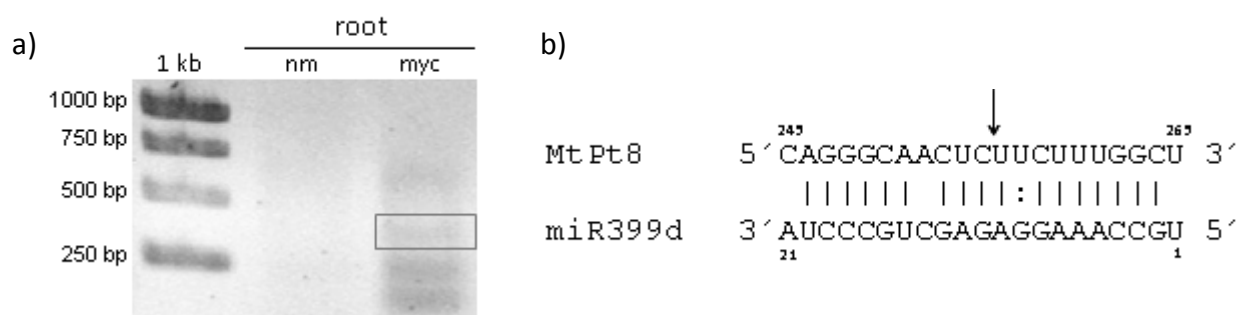


Figure 33. a) PCR products of the nested PCR after modified 5'RACE to confirm the miR399 mediated cleavage of Medtr5g076920. Lane 1: 1 kb DNA ladder; lane 2: Nested PCR of the nm-library; lane 3: Nested PCR of the myc-library. The expected PCR fragment of 371 bp is enframed. b) Alignment of the MtPt8 mRNA sequence (position 245 – 265) and mature miR399d. The confirmed cleavage site at position 255/256 is indicated with a black arrow.

Transient co-expression of pri-miR399d and MtPt8_{miR399bs} in *Nicotiana benthamiana* to validate MtPt8 cleavage in planta

To confirm the *MtPt8* transcript cleavage *in planta* a transient co-expression of the miR399d primary transcript and a transcriptional fusion of the miR399 binding site of *MtPt8* to mRFP driven by the 35S promoter (*MtPt8*_{miR399 binding site (bs)}) in *N. benthamiana* was carried out. Three different constructs were generated (2.2.2.1), an overview of the t-DNA vector constructs is shown in figure 34 a, b.

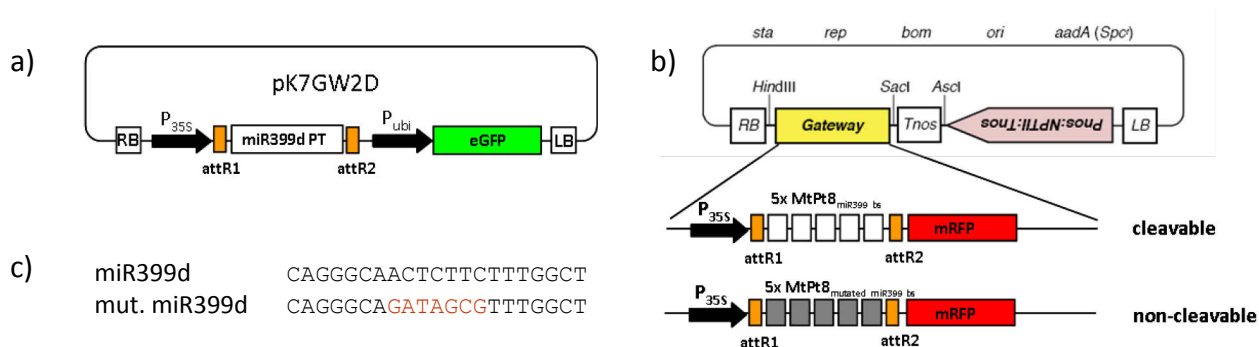


Figure 34. Constructs used for the transient expression of a) mtr-miR399d primary transcript and b) MtPt8_{miR399bs}/ MtPt8_{mut miR399bs} in *Nicotiana benthamiana* leaves. c) Comparison of mature miR399d sequence (3' → 5') and the mutated version of miR399d with 7 nucleotide substitutions at position 8-14 (3' → 5').

The pri-miR399d is driven by the constitutive 35S promoter. For the control of transformation efficiency, the vector contains a constitutive fluorescent marker (eGFP). To confirm the cleavage of the *MtPt8* mRNA, five serial sequences of the miR399 binding site of *MtPt8* were fused to mRFP. If the resulting mRFP-*MtPt8*_{miR399bs} transcript is cleaved by miR399, no mRFP fluorescence would appear. As a control, a mutated non-cleavable version of the miR399 binding site was fused to mRFP (figure 34 c). Here, 7 nucleotides of the critical region were substituted to eliminate the complementary binding of miR399 to the target binding site. A mRFP fluorescence signal after co-infiltration with pri-miR399d is expected. The constructs were transformed into *A. tumefaciens* strain GV2260 and infiltrated either as single construct or as a 1:1 mixture of both constructs. After a 3-day incubation the appropriate leaves were analyzed concerning fluorescent gene expression (figure 35).

Leaves infiltrated with the pri-miR399d only (figure 35 a-c) exhibited no mRFP signal but a strong GFP2 signal deriving from the constitutive expression of eGFP. After infiltration with the mRFP-*MtPt8*_{miR399bs} constructs, a strong mRFP signal but no GFP2 signal was observed (figure 35 d-f). The co-expression of the miR399d PT and *MtPt8*_{miR399bs} resulted in the loss of mRFP signal due to the degradation of the transcript, the success of the transformation and t-DNA insertion was confirmed by the strong GFP signal deriving from the constitutive eGFP expression (figure 35 g-i).

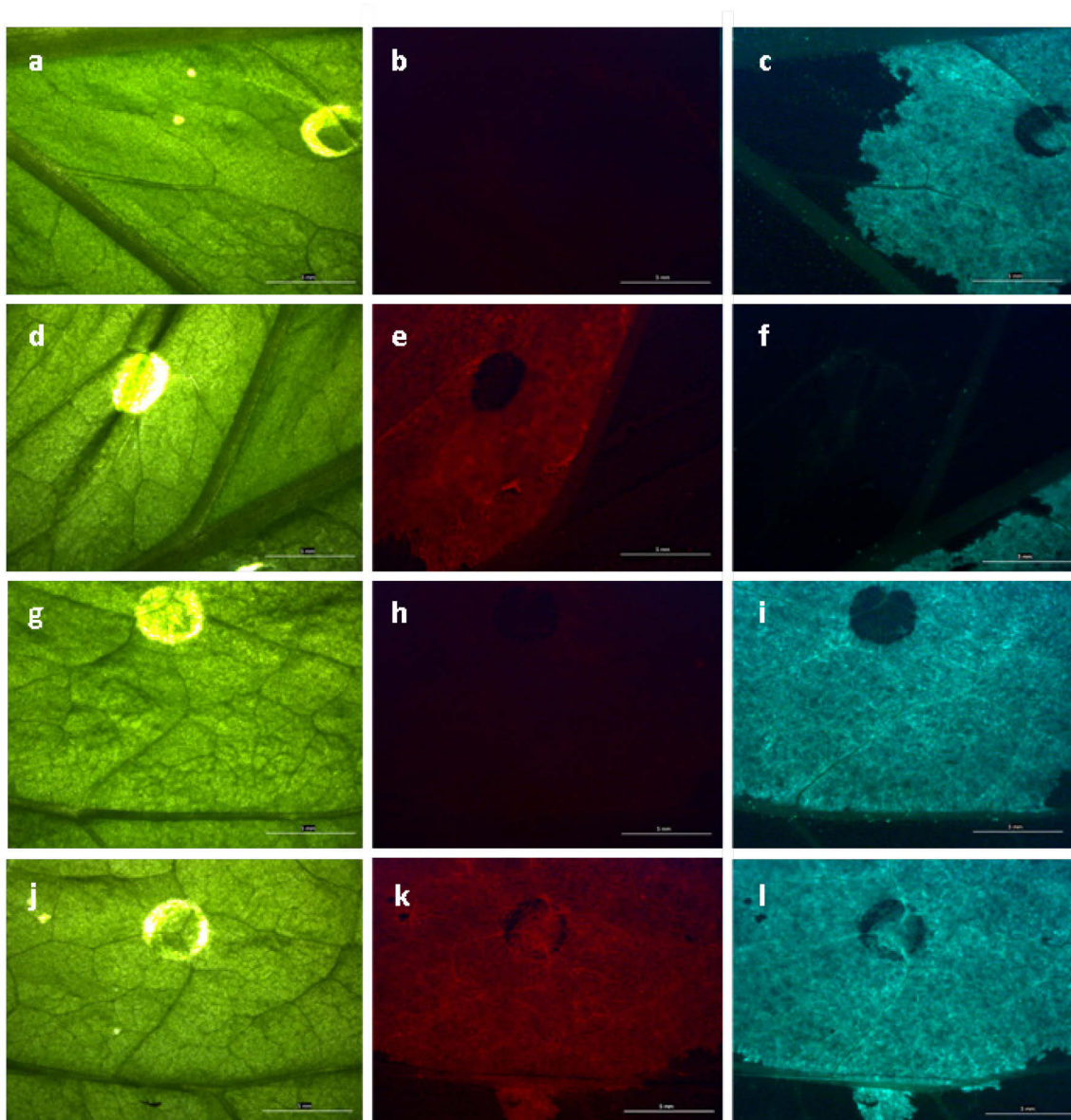


Figure 35. Validation of miR399 mediated *MtPt8* transcript cleavage by transient co-expression of pri-miR399d and *MtPt8*_{miR399bs} in *N. benthamiana*. Leaves were infiltrated with *A. tumefaciens* containing constructs of pri-miR399d (a-c), *MtPt8*_{miR399bs} (d-f), 1:1 mixture of miR399d PT and *MtPt8*_{miR399bs} (g-i), pri-miR399d and *MtPt8*_{mut miR399bs} (j-l) and analyzed using stereo fluorescence microscopy. Pictures of the corresponding infiltration sites (spots and surrounding tissue) were taken in bright field (a, d, g, j), with a RFP filter (b, e, h, k) and a GFP2 filter (c, f, i, l). Scale bars indicate 5 mm.

3.2.4.2 Conservation of miR399 binding sites in the *P_i*-transporter family in *M. truncatula*

The miR399 family plays a key role in the systemic regulation of *P_i*-homeostasis. Due to its annotation as member of the major facilitator superfamily, the novel miR399 target might encode a protein with transport function potentially involved *P_i*-dependent processes. The comparison to known *M. truncatula* *P_i*-transporter sequences could give more information about the putative function of the novel target.

The sequence alignment of *M. truncatula* P_i-transporters including *MtPt7* and *MtPt9* (Maria J. Harrison, personal communication) and the new miR399 target *MtPt8* revealed a sequence similarity of 60 % to 66.2% to the analyzed transporters (figure 36 a). Interestingly, the new target showed the highest similarity to the mycorrhizal induced P_i-transporter *MtPt4*. Further analysis revealed that both the sequences of *MtPt4* and *Medtr5g076920* are clustering and seem to be more distant from all other Medicago P_i-transporters known so far (Clustal W, figure 36 b). Investigations of the research group of Maria J. Harrison confirmed this transcript encoding for a new member of the P_i-transporter family in *M. truncatula*.

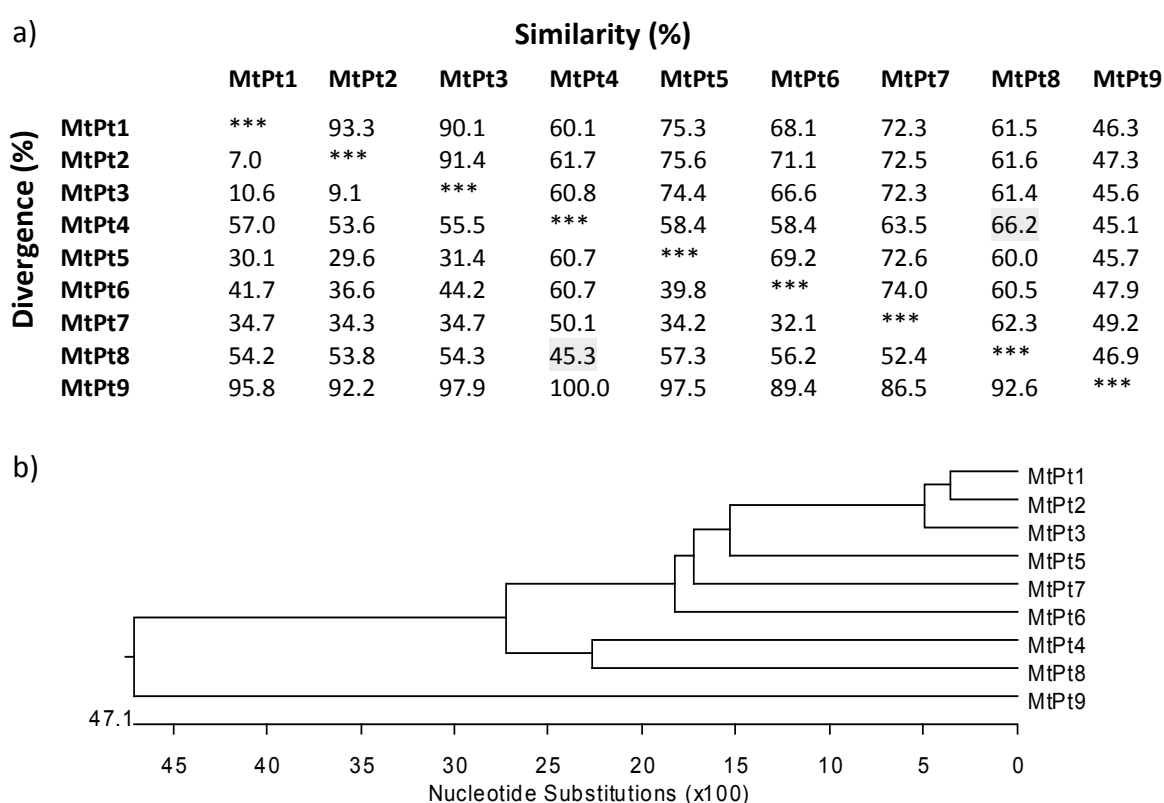


Figure 36. Sequence similarity analysis of known *M. truncatula* P_i-transporter genes (Clustal W Method). (a) Overview of the percent similarity (upper triangle) and divergence (lower triangle) between the coding sequences of the P_i-transporters. Boxes representing similarity and divergence of *MtPt8* to *MtPt4* are shaded in grey. (b) Sequence tree, the number of nucleotide substitutions times 100 is given at the x-axis.

The sequence analysis revealed another interesting aspect concerning the conservation of the miR399 cleavage site within the *M. truncatula* P_i-transporter genes. In general, miRNA mediated degradation of mRNA occurs between the 10th and 11th nucleotide of the corresponding miRNA (5' → 3') and requires the complementary binding of miRNA and mRNA in the seed region¹⁰⁸. Therefore, the critical regions need to be strongly conserved in

the miRNA as well as in the target transcript. The *MtPt8* transcript is the only one that perfectly matches both the seed region and the cleavage site and degradome sequencing confirmed the cleavage (figure 37). Allowing non-Watson-Crick base pairing (G-U), which compensates nucleotide substitutions especially at position 2 and 11, the transcripts of *MtPt6* and *MtPt7* are predicted to be cleaved by miR399. 13 of 17 members of the miR399 family match with a cleavage expectation ranging from 3.5 to 5 (psRNAtarget prediction), where 5 is very low. Additionally, 5 of 17 miR399 were predicted to cleave the transcripts of *MtPt1*, *MtPt2*, and *MtPt3*, the expectation for the cleavage ranges from 4.5 to 5. However, under the conditions tested there was no evidence found for the cleavage of those transcripts by degradome analysis. For transcripts of *MtPt4*, *MtPt5* and *MtPt9*, no miR399 cleavage was predicted. It is not clear at this time, whether *MtPt8* gained the miR399 binding site or all other transporters lost the ability of being targeted by miR399.



Figure 37. Alignment of the putative miR399 binding sites of all known *M. truncatula* P_i-transporters including the new miR399 target *MtPt8* (5'→3') to the 4 subclasses of mature miR399 (3'→5'). Green boxes indicate a perfect match between the putative miR399 cleavage site in the transcript and position 10 and 11 of mature miR399. Nucleotides differing from the *MtPt8* sequence leading to a reduced ability to be cleaved by miR399 are indicated in grey.

3.2.4.3 Conservation of miR399-mediated regulation of P_i-transporters in the Viridiplantae kingdom

The previous results suggest that miR399 not only indirectly affect genes of the P_i-starvation response via PHO2, but also directly influence the transcript abundance of at least one P_i-transporter in *M. truncatula*. To test whether the miR399-mediated P_i-transporter transcript cleavage is conserved among other plant species and families, further analysis was expanded to the Viridiplantae kingdom. Using the Phytozome database (www.Phytozome.net, Joint Genome Institute and Centre for Integrative Genomics, University of California, USA) which

covers genome information of 25 plant species belonging to the groups of green algae and land plants, at least 262 members of the inorganic P_i -transporter family with similarity to *MtPt8* could be identified (figure 38), including the genes encoding for PT1-9 in *M. truncatula*.

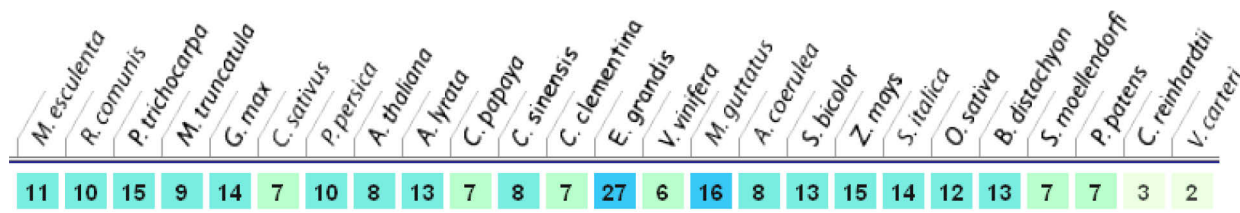


Figure 38. Number of homologues within the inorganic P_i -transporter family of 25 different plant species of the viridiplantae kingdom. Analyzed species from left to right: *Manihut esculenta*, *Ricinus communis*, *Populus trichocarpa*, *Medicago truncatula*, *Glycine max*, *Cucumis sativus*, *Prunus persica*, *Arabidopsis thaliana*, *Arabidopsis lyrata*, *Carica papaya*, *Citrus sinensis*, *Citrus clementina*, *Eucalyptus grandis*, *Vitis vinifera*, *Mimulus guttatus*, *Aequilegia coerulea*, *Sorghum bicolor*, *Zea mays*, *Setaria italica*, *Oryza sativa*, *Brachypodium distachyon*, *Selaginella moellendorffii*, *Physcomitrella patens*, *Clamydomonas reinhardtii*, *Volvox carteri*.

Sequences of all genes were extracted and studied according to putative miR399 cleavage sites using psRNAtarget. This analysis was restricted to members of the *Medicago* miR399 family due to the fact that the miR399 family is highly conserved within the plant kingdom and miR399 members were not yet identified in all plant species studied here. For at least 32 P_i -transporter genes from 12 different species, a miR399-mediated cleavage was predicted (Suppl. Fig. 4). Interestingly, no chlorophytes or grasses were among these species, but 6 of the 12 species can be phylogenetically classified into the group of Fabideae (rosids I), whereof 4 belong to the nitrogen-fixing clade of Fabales. Several genes of the P_i -transporter family in the class of Fabidae even exhibit identical or nearly identical miR399 binding sites as compared to *MtPt8*, for example in genes of *Glycine max* (Glyma10g04230.1), *Populus trichocarpa* (POPTR0019s08990.1) and *Manihut esculenta* (cassava4.1_005221m), and are suggested to be homologues of this novel miR399 target. Possibly, the mechanism of miR399-mediated regulation of P_i -transporters is highly conserved primarily within the group of higher land plants and might be associated with a symbiosis capability of these plants. Also for the non-AM capable modelplant *A. thaliana* a P_i -transporter expressed in roots and floral tissue, namely Pht1;7, was predicted to be a target of miR399¹⁰⁹. However, a mRNA cleavage of these transporters could not be confirmed so far.

3.2.5 MiR399 - MtPt8 interaction links P_i-homeostasis and AMS

3.2.5.1 Expression analysis of MtPt8 transcripts

RT-PCR confirms exclusive transcription in mycorrhizal roots

The degradome read count analysis revealed the *MtPt8* transcript one of the strongest regulated transcripts between myc and nm roots (table 3), suggesting that this new miR399 target might have a specific role during AMS.

To prove this assumption, the influence of the interaction with different symbionts (*Sinorhizobium meliloti*, *Glomus intraradices*) and P_i- and N-limitation on the *MtPt8* transcript abundance was analyzed. *M. truncatula* plants were either inoculated with *S. meliloti* or *G. intraradices* and grown under limiting P_i (20 μM) and/or N (0 mM) conditions, or under full nutrition (1mM P_i, 5 mM N). Shoot and root tissue was harvested 3 wpi and subsequently analyzed via semi-quantitative RT-PCR (figure 39). The expected amplicon size using gene specific primer pair was 199 bp. *MtPt8* transcripts were found in P_i-starved mycorrhizal roots, but not in shoots and roots of plants of any other condition tested. Hence, *MtPt8* is most likely a mycorrhizal root specific transcript and is apparently not expressed during nodule symbiosis, at least under the analyzed conditions. Moreover, the mRNA cleavage of the *MtPt8* transcript by the P_i-responsive miR399 indicates a regulation by P_i in mycorrhizal roots.

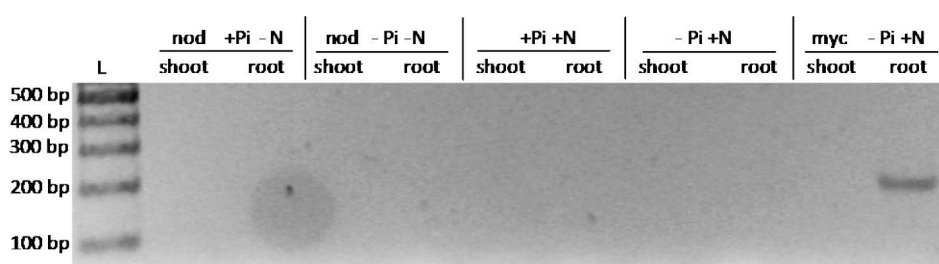


Figure 39. Gel electrophoresis of semi-quantitative RT-PCR products to analyze *MtPt8* transcript abundance in shoot and root tissue of plants grown under different nutrient and symbiotic conditions. Loading of lanes is indicated at the top of the figure. (nod) plants inoculated with *Sinorhizobium meliloti*, (myc) plants inoculated with *Glomus intraradices*, (+Pi) 1 mM Pi, (-Pi) 20 μM Pi, (+N) 5 mM N, (-N) 0 mM N in Hoagland's solution For size description, a 100 bp DNA ladder was used.

MtPt8 expression reversely correlates to mature miR399 abundance

The previous results confirmed *MtPt8* as a mycorrhizal-specific member of the inorganic phosphate transporter family and a cleavage target of miR399. To gain more insight into the

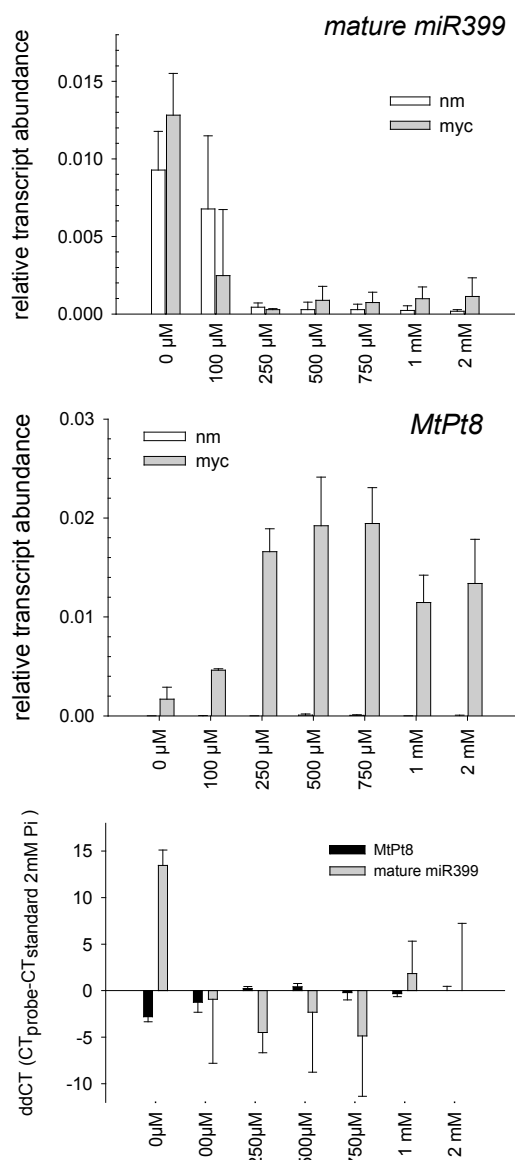


Figure 40. Relative abundance of (a) *MtPt8* transcripts, (b) mature miR399. (c) Correlation of *MtPt8* and mature miR399 in dependence of the P_i-treatment. The following conditions were applied and roots were harvested after 5 wpi: 0 mM, 0.1 mM, 0.25 mM, 0.5 mM, 0.75 mM, 1 mM and 2 mM phosphate. Normalization was carried out against the reference gene MtEf1 (SD; n = 5). Correlation of transcript abundances in mycorrhizal roots (c) is given by ddCT values. All values were calculated based on the standard condition 2 mM Pi.

P_i-dependent regulation of *MtPt8*, the influence of changing external P_i-concentrations on *MtPt8* transcript abundance in terms of miR399 induction was investigated. Plants were grown as described in the methods section (2.2.1.6.). The abundance of *MtPt8* transcripts and mature miR399 was determined using qRT-PCR and stemloop qRT-PCR, respectively. The results are shown in figure 40. *MtPt8* transcripts (figure 40 a) were not detectable in non-inoculated roots but showed a notable expression pattern in mycorrhizal roots. The *MtPt8* transcript abundance significantly decreases (p<0.05, Bonferroni t-test) from higher to lower P_i-fertilization. Whereas the lowest expression was determined at 0 μM P_i, the relative transcript abundance reaches its maximum with 10-fold higher values at 750 μM P_i. For the treatments with P_i-concentrations between 1 mM and 2 mM P_i, an additional drop in *MtPt8* expression was detected, which is

likely a result of the reduction of AM colonization by high P_i . The abundance of mature miR399 reversely correlates to *MtPt8*, with a significant increase ($p < 0.05$, Bonferroni t-test) from high to low P_i -treatment being observed. The lowest mature miR399 level was already achieved at 250 μM P_i , suggesting an efficient repression of the P_i -starvation response at this P_i -concentration. Further, the results from this experiment confirm the results from previous studies, where mature miR399 accumulated to higher levels in P_i -deficient mycorrhizal roots⁴². However, this effect turned out to be strongly P_i -dependent based on the fact that a P_i -concentration of 100 μM is sufficient to reduce the mature miR399 abundance in colonized roots as compared to non-colonized roots (figure 40 b).

3.2.5.2 Localization of *MtPt8* promoter activity

Promoter studies provide insights into the site of gene transcription and putative regulatory elements. The analysis of the 1 kb promoter region of *MtPt8* with regard to putative P_i - and /or AMS-dependent binding sites revealed, that the promoter lacks a PHR1 binding site (P1BS, GnATATnC)¹² but shows the AMS responsive MYCS motif (CTTCTTGTTCT)⁴⁴ starting at position -55 relative to the putative transcription start site (Suppl. Fig.7).

To analyze the transcription site of the *MtPt8* gene, the 1 kb region of the *MtPt8* promoter was fused to the *gusA* gene using the pCambia 2301 binary vector¹¹⁰ (construct provided from M.J. Harrison, Cornell University Ithaca, USA). The construct was inserted into the *M. truncatula* roots via *A. rhizogenes*-mediated transformation. After an *in vitro* phase of 3 weeks, the transformed chimeric plants were grown on a sand/vermiculite/expanded clay substrate (2:1:1) containing 10 % *G. intraradices* inoculum. The promoter activity was visualized using GUS staining and fungal structures were visualized by co-staining with Alexa Fluor® 488 (figure 41). Whole root fragments and 80 μM longitudinal vibratome sections were analyzed using epifluorescence microscopy. Macroscopically, the strongest promoter signals were observed in the cell layer surrounding the central cylinder (figure 41 b), although some diffuse GUS signals could be observed in the root cortex and at branches of lateral roots and root tips. Higher magnification revealed the promoter signal localizing in distinct cells (figure 41 d), which were recognized as arbuscule-containing cells after Alexa Fluor® staining (figure 41 e). Overlay of these images (figure 41 f) confirmed the co-localization of *MtPt8* promoter activity and arbuscule containing cells, implying that *MtPt8*

transcription takes place predominantly in these cells and is strongly regulated at the cell specific level.

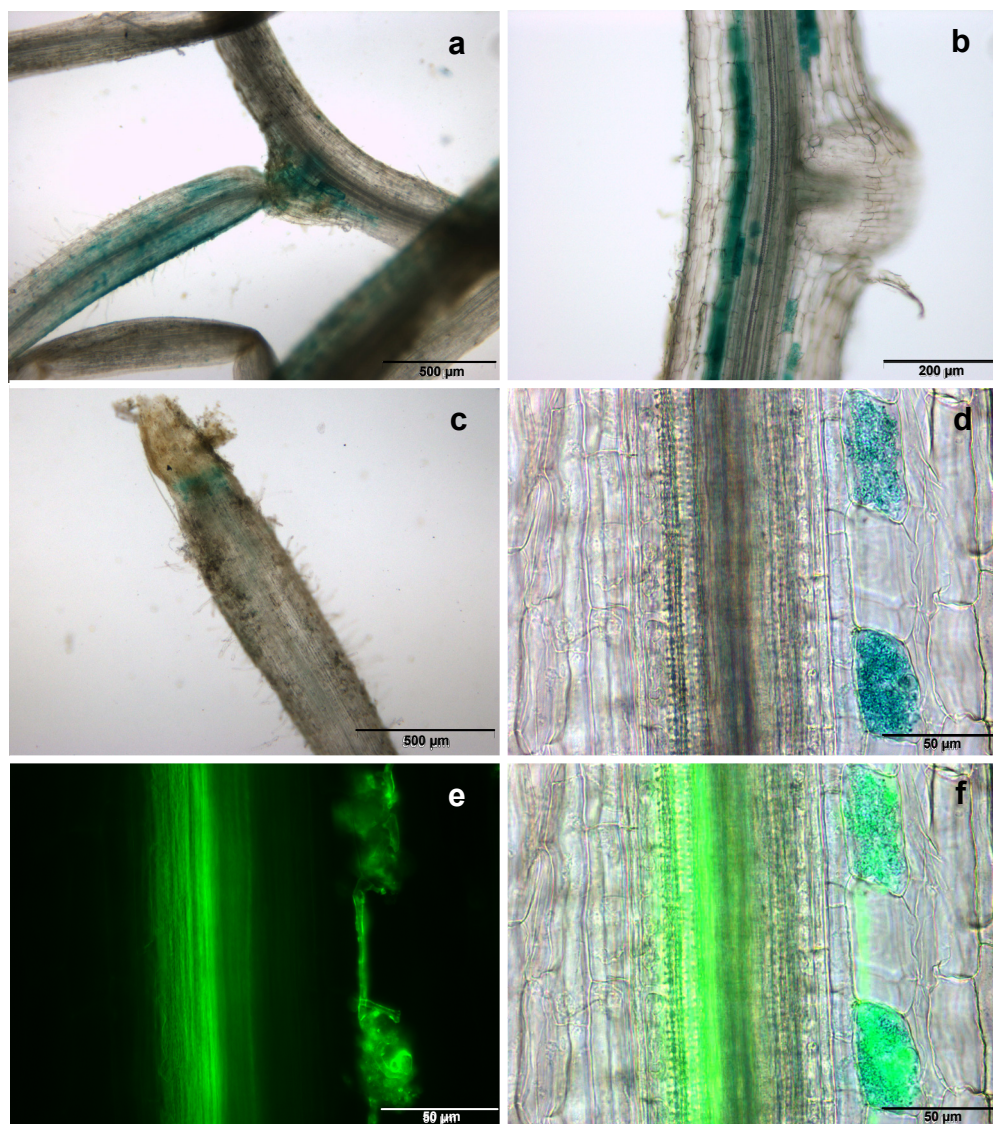


Figure 41. Visualization of GUS and Alexa WGA488 signals in whole root (a, c) and vibratome sectioned (80μm) fragments (b, d-f) from *Medicago truncatula* after transformation with *A. rhizogenes* containing the *MtPt8* promoter::*gusA* construct using an epifluorescence stereomicroscope. Magnification: a, c: 10x; b: 20x; d-f: 40x. Scale bars represent 500 μm (a, c), 200 μm (b) and 50 μm (d-f).

4 Discussion

4.1 Degradome deep sequencing provides information about regulation of mRNA abundance, miRNA cleavage targets and miRNA precursor processing

The aim of degradome deep sequencing was to identify miRNA targets related to arbuscular mycorrhizal symbiosis in *M. truncatula* roots. It has been demonstrated that a high number of novel and annotated miRNAs are expressed in *M. truncatula* roots, indicating the crucial role of miRNAs in the cellular regulation in plant roots⁴². Current *in silico* miRNA target prediction tools in plants generally depend on complementary searches, based on perfect or near perfect base pairing between a mature miRNA and its target mRNA¹¹¹. The high-throughput sequencing of the degradome is one possibility for the experimental identification of miRNA-mediated transcript cleavage^{74, 112}. Here, 185 mRNAs were identified to be cleaved by miRNAs or miRNA*s in *M. truncatula* roots.

4.1.1 mRNA abundance is regulated through general and specific degradation mechanisms

The alignment of the degradome tags with 100 % identity to *M. truncatula* and *G. intraradices* genome recourses resulted in the mapping of 85 % and 76 % to mt3 sequences for the non-mycorrhizal and the mycorrhizal library, respectively. More than 27.000 transcripts were identified to be degraded, of which a minority (0.6 %) were specifically cleaved by miRNAs. This phenomenon was also found in previous degradome studies in *Arabidopsis thaliana*, *Vitis vinifera* and *Oryza sativa*¹¹³⁻¹¹⁵. In these studies, less than 1 % of mapped transcripts were specifically regulated by miRNAs, which might be a hint for the necessity of a tight and controlled regulation of distinct gene sets. Indeed, there is evidence of miRNA- mediated transcript regulation being essential, particularly at the tissue- and cell-specific level, to ensure a highly specific pattern of the target gene expression. miR172 in *Arabidopsis* is highly abundant in the floral tissue and targets the AP2 transcription factor, which is present in the same domain¹¹⁶. Members of the miR165/miR166 family regulate the shoot apical meristematic (SAM) growth by targeting specific HD-ZIP III transcription factors present in the undifferentiated cells of the SAM¹¹⁷. The role of miRNAs at the tissue-

and cell specific level is not restricted to developmental processes but has also great impact on processes related to plant-microbe-interactions. The expression of the *MtHap2* transcription factor is strongly induced during nodule symbiosis and restricted to the meristematic zone of nodules by the action of miR169⁶⁵. Components of the auxin signalling pathway were downregulated by miR167 and miR393 in tumors induced by infection with *A. tumefaciens*, resulting in the indirect promotion of tumor growth⁶⁴.

However, as shown by the degradome, the majority of transcripts were subjected to a general mRNA turnover involving other mechanisms of mRNA degradation such as decapping, storage in P-bodies and the 3'mRNA decay by exonucleases¹¹⁸. Although the type of general degradation mechanisms cannot be verified by degradome analysis, the information value in terms of mRNA expression and turnover rates is high. Changes in degradome tag abundances comparing different conditions give valuable clues to changes in the transcript abundance shown by their correlation to log₂-fold changes (LFC) of the *M. truncatula* transcriptome¹¹⁹. Nevertheless, several transcripts clearly were subjected to an increased degradation compared to their transcription, which can be extracted from the vertical extension of the correlation cloud (figure 7). No changes were detected in the transcriptome (LFC = 0), whereas the number of degradome tags was highly increased in mycorrhizal roots as compared to non-mycorrhizal roots suggesting a higher turnover and relevance of these transcripts during AMS. Presumably, the enhanced promoter activity of specific genes at certain conditions might be compensated at the post-transcriptional level by higher turnover rates of the transcript. This indicates a need for a transcript regulation alternative to miRNA activity.

4.1.2 miRNA*-mediated target cleavage

This degradome analysis provides evidence for miRNA*-mediated mRNA cleavage in *M. truncatula* roots. 44 transcripts were identified to be cleaved by star strands of 11 miRNA families. It is the current understanding that one strand of the miRNA/miRNA* duplex preferably accumulates and is then referred as mature miRNA whereas the opposite strand is called miRNA*^{120, 121}. Nevertheless it was recognized that many miRNA* species such as miR160* and miR169* also accumulate to substantial levels in phloem sap^{16, 122}, and are able to downregulate target mRNAs in animal and plant cells^{123, 124}. Interestingly, *in situ* hybridizations confirmed the accumulation of miR169d*/e.2*/l*/m*, and miR160f* in the

intracellular space and phloem of the roots (Branscheid *et al.*, 2011). In *Solanum lycopersicum*, miR169g* was found to be upregulated in leaves of mycorrhizal or high phosphate treated plants ¹²⁵. The regulatory role of miRNA* sequences has also been observed in animals ¹²⁶ and humans, where miR-155* and miR-155 adjust the type I interferon production in an opposite manner through different targets ¹²⁷.

The degradome analysis unraveled miRNA*-mediated mRNA cleavage of transcripts, which were distinct from transcripts targeted by the corresponding mature strand. One example is miR169, which targets a CCAAT transcription factor important for root nodule development ⁶⁵, whereas the star strand, which is more abundant than the mature miR169 in mycorrhizal roots, mediates the cleavage of the arbuscule-specific protein *MtBcp1*. Therefore, it might be anticipated that the dominant form of this miRNA switches during the two endosymbioses and restricts the expression of different targets to distinct cell types. In addition, a transcript encoding a mycorrhizal-specific GRAS transcription factor, MtGRAS8 ⁷⁰, was found to be cleaved by miR5204*.

Interestingly, the majority of miRNA* cleavage targets identified by degradome analysis are members of the TIR disease resistance gene family and pathogenesis-related (PR) proteins, which are exclusively cleaved by miR1510a*, b* and miR399k*. This indicates the involvement of miRNA* strands in the regulation of plant immunity. A recent study provided evidence that miR393b* participates in the regulation of plant innate immunity by the cleavage of the MEMB12 transcript, a regulator of exocytosis of PR proteins ¹²⁸.

In addition, several targets were found for the star strands of miR399c, d, h, k, q (table 4). The highly conserved mature miR399 was proven to be phloem-transported from shoot to root ¹⁵, which is also true for miR399* ¹²⁹. The putative function of miR399*-mediated regulation of miR399 primary transcripts is discussed below.

In summary, these results imply a biological function of miRNA* which is often unrelated to the function of their corresponding mature strand. Most of the conserved plant miRNAs are involved in developmental processes and in the response to abiotic stress ^{130, 131}. However, a specific role of the star strands in the basal plant immune response is indicated and needs to be further investigated.

4.1.3 miRNAs modulate the defence response upon mycorrhizal infection

Within the group of miRNA-mediated cleaved transcripts, transcription factors and disease resistance genes were clearly overrepresented in the group of downregulated transcripts. Most of the transcription factors are targeted by conserved miRNAs, which agrees with previous findings¹³¹. This study indicates that four primarily moderately conserved miRNAs, namely miR1510a*, miR1507, miR2678^{67, 132} and miR5213, regulate disease resistance genes. Plants have evolved a general defense response to biotic interactions involving TIR/NB-LRR disease resistance genes (R-genes) and PR-proteins^{133, 134}. Although the basal defense mechanisms, which includes the accumulation of phenolic compounds and PR-proteins, are activated upon the interaction with AM fungi^{135, 136}, mRNA levels of many of the miRNA targeted disease resistance genes are decreased in mycorrhizal roots. This might support the fungal growth within mycorrhizal roots. A similar phenomenon was described for a parasitic fungus-plant interaction; it is suggested that miRNA biogenesis and function is compromised in specific tissues in order to promote the activation of disease resistance genes to restrict the growth of biotrophic fungi¹³⁷. The degradome data demonstrate that a subset of defense response genes (Medtr6g098880.1, Medtr2g046350.1, TC138295) is suppressed by miR5213 in mycorrhizal roots, and no specific miRNA cleavage was observed for these genes in non-mycorrhizal roots by this particular miRNA. Moreover, in non-mycorrhizal roots, the same subset of defense genes is regulated by miR2678, indicating a complex regulatory network of defense responses genes involving a combinatorial regulation by different miRNAs. This implies that specific miRNAs restrict target expression to distinct tissues or cells in a certain condition. Notably, miR5213, which mediates the cleavage of defense response transcripts, was conserved only in AM symbiosis-capable plants, such as *Glycine max*, *Lotus japonicus* and *Populus trichocarpa* but not in *Arabidopsis*.

4.1.4 Regulation of symbiosis relevant transcripts by miRNAs

The transcriptome wide degradome analysis gives the unique opportunity to identify mRNAs, which undergo miRNA-mediated cleavage. The analysis revealed 45 miRNA cleavage targets that were differentially regulated between non-mycorrhizal and mycorrhizal conditions. Out of these targets, 26 transcripts were found to be decreased in mycorrhizal roots as compared to non-mycorrhizal roots, of which the most belong to the TIR-disease

resistance gene family. In addition, 19 cleavage targets were found to be upregulated up to LFC of 19 for the 2 highest upregulated genes, including *MtGras8* transcription factor⁷⁰ and *MtPt8*, which was identified as a novel mycorrhizal-specific miR399 target. It is noteworthy, that beside PHO2^{10,17} MtPT8 is the second miR399-target confirmed so far, and two further targets of the miR399 were identified by degradome analysis including a *MtPho2* homologue (Medtr4g018250, Emanuel Devers, unpublished) and a squamosa promoter-binding protein (Medtr3g103970). The strong transcriptional induction of *MtPt8* and its regulation by miR399 further supports the role of miR399 during the cellular phosphate homeostasis regulation in mycorrhizal roots⁴².

Remarkably, four of the highly regulated transcripts, namely *MtNsp2*¹³⁸, *MtGst1*¹³⁹, *MtBcp1*⁹⁸ and *MtGras8*⁷⁰, are known to be involved in root endosymbiosis. *MtNsp2* is a GRAS transcription factor essential for root nodule development¹⁴⁰ and is cleaved by miR171h. Recently, *nsp2-2* mutants were shown to be less colonized by AM fungi, which implies a role in mycorrhizal signalling¹⁴¹. MtNSP2 is involved in early nodule signalling and promotes the transcription of the nodulin *MtEnod11* through heterodimerization with MtNSP1¹⁴². Surprisingly, *MtNsp2* transcript levels were significantly increased in mycorrhizal roots indicated by a LFC of 1.6, which is consistent with previous microarray results (PhD thesis, Emanuel Devers). Therefore, AMS and miR171h, respectively regulate *MtNsp2* transcript abundance at the transcriptional and the post-transcriptional level. Clearly, there is a need for a tight regulation of *MtNsp2* transcript levels and the physiological function of this regulation during AMS remains to be elucidated.

MtGst1 is a transcript strongly induced in mycorrhizal roots, and is also a miRNA cleavage target (table 3). The *MtGst1* transcript encodes a mycorrhizal symbiosis-specific glutathione-S-transferase¹³⁹ and is one example for transcripts being regulated by a pair of miRNAs, namely miR5282 and the candidate new_miR_c_275 (Emanuel Devers, PhD thesis). This regulation by two miRNAs indicates that *MtGst1* levels need to be severely controlled by the host plant to assure a functional symbiosis. A similar phenomenon of a combinatorial regulation was previously described in *Vitis vinifera*¹¹³. Here, both miR156 and miR535 regulate each three squamosa promoter binding transcription factor genes. The analysis of the degradome data revealed at least 8 additional differentially expressed transcripts being cleaved in a combinatorial mode of regulation (table 3).

Another AMS-specific gene, *MtBcp1*, is targeted by star strands of the miR169 family. *MtBcp1* encodes a protein specifically accumulating in the periarbuscular membrane²⁵, and it is speculated that the miR169* sequences accumulating in mycorrhizal roots are involved in restricting *MtBcp1* expression to arbuscule-containing cells.

The strongest regulated transcript is a member of the GRAS transcription factor family, *MtGras8*⁷⁰. Interestingly, this transcription factor is cleaved by miR5204*, whose corresponding mature strand itself is highly upregulated in mycorrhizal roots⁶⁸.

Besides the discussed targets, which were already known as symbiosis related genes additional 14 transcripts were significantly upregulated during AMS and miRNA cleavage targets. Interestingly, only 3 of these genes encode for transcription factors, whereas the others have either very diverse or unknown functions. However, their induction during AMS implies a role during symbiosis relevant processes, which would be worthy to investigate in the future.

4.1.5 Combined analysis of degradome and small RNA data for insight into miRNA precursor processing and regulation

During miRNA biogenesis, miRNA primary transcripts and precursor sequences are processed through two sequential cleavages of the RNA-specific RNase III like enzyme DCL1 (dicer-like 1) in order to release the miRNA/miRNA* duplex^{99,100}. The first of the two DCL1 cleavages can occur from two directions, from either the stem or the loop of the hairpin, which is assigned base-to-loop or loop-to-base processing, respectively. To investigate the precursor processing, the degradome data can be used to analyze the distribution pattern of degradome tags on the miRNA precursors^{101,102}. Different patterns were expected including degradome tags mapping to either the 3' or the 5' end of the miRNA or miRNA*, suggesting base-to-loop or the loop-to-base processing, respectively. For miR171h, two patterns were expected, with 337 of 399 degradome sequence tags mapping precisely to one position in the miR171h primary transcript indicating one DCL1-cleavage at this position and a base-to-loop processing of this miRNA¹⁴³. In addition, the miR399 precursor sequences were systematically analyzed in order to identify DCL1 cleavage sites (table 4). The systematic analysis of the miR399 precursor sequences revealed base-to-loop processing as the dominant processing type. However, in some cases, a clear classification was not possible because tags were found supporting both processing variants in one precursor, although the

number of tags mapping to the 3' end was usually much higher than those mapping to the 5' end. Taking into account that the intermediates of loop-to-base processing (tags mapping to the 5' end of the miRNA) are likely to be immediately processed after genesis and are therefore hardly detectable, a definite statement based on degradome data cannot be done. In such cases, the intermediates of the processing steps have to be further analyzed and verified separately as shown by Bologna *et al.*, 2009.

In addition, degradome tag mapping positions were found within the mature or star sequences of miRNAs. In those cases, a precise cleavage of the respective primary transcript by either the star or the mature strand of the miRNA and a feedback-circuit to their own biogenesis is suggested. Some miRNAs, like miR162 and miR168, can auto-regulate their biogenesis through the targeting of DCL1 and AGO1, respectively^{144, 145}. Moreover, it has been shown that in *Arabidopsis*, miR167 regulates the auxin response factor6 (ARF6) transcription factor by a negative feedback circuit. Several ARF-binding motifs were found in the miR167 promoter region, indicating that miR167 itself is regulated by this transcription factor¹⁴⁶. This study also provides evidence for miRNA self-regulation phenomena, such as the miR399*-mediated cleavage of miR399 primary transcripts¹³. The detailed analysis of the miR399c*, k* targets (Medtr4g135140, Medtr4g135420) revealed these genes to be duplicated genomic loci for primary transcripts of miR399j and k. Both primary transcripts are inversely oriented and have a short overlap at the end of the putative transcript. Interestingly, this overlap appears to be the cleavage site for miR399c*, k*, which might be a mechanism of self-regulation of the miR399 genes. The miR171 family is a further example of miRNA self-regulation in *M. truncatula*, where the miR171h* is cleaved between the 10th and 11th nucleotide¹⁴³. Cleavage of primary miRNA transcripts has been already observed in *Arabidopsis*⁷⁴, but does not seem to occur very frequently in *Oryza sativa*¹¹⁵. Self-regulation through a feedback-circuit between primary miRNA transcripts and corresponding miRNA/miRNA* has been postulated by Meng *et al.*¹⁰¹. It was proposed that the overproduction of miRNA precursors result in an accumulation of miRNAs or miRNA*, which could in turn recognize their host precursors as the downstream targets. Hence, the ratio between mature and star strands might be involved in self-regulation.

In conclusion, degradome analysis is a powerful tool to investigate miRNA gene structure, processing and regulation.

4.2 Phosphate homeostasis signalling is directly linked to AMS and is subjected to a complex regulation in response to the symbiotic interaction

4.2.1 Overexpression of *MtPhr1* positively influences colonization with AMF

In this study a putative *AtPhr1* homologue in *M. truncatula* was identified. The transcriptional analysis of *MtPhr1* revealed that the transcript was not significantly regulated in response to changing P_i -concentrations. This goes in line with previous findings that this transcription factor is post-transcriptionally or post-translationally regulated¹³. The overexpression of the coding sequence led up to 10 times increased transcript levels under P_i -sufficient growth conditions. However, increased levels of the *MtPhr1* CODING SEQUENCE did not result in elevated levels of pri-miR399d, but to an accumulation of mature miR399 in roots. The local miR399 transcription is not induced, which might be caused by a limited activation of PHR1 by SIZ1¹³. On the other hand, it could not be shown, whether elevated transcript levels resulted in higher PHR1 protein levels. Ultimate evidence would be given by the determination of PHR1 protein levels using a specific antibody. However, there is currently no antibody for MtPHR1 available and the production of a specific antibody was beyond the time frame of this work.

Possibly, the accumulation of mature miR399 in roots of *MtPhr1* overexpressing lines despite the high P_i -treatment is a systemic effect resulting from phloem transport of miR399 from shoots to roots^{16, 122}. This raises the question whether *Phr1* transcripts could mediate as direct or indirect signals for the induction of miR399 transcription in shoots. The potential of transcripts and proteins being transported in the phloem was previously demonstrated^{147, 148} and, in addition, identified proteins of the Myb transcription factor family were present in the phloem¹⁴⁹. However, to prove this hypothesis further investigations of the shoot of overexpressing plants in terms of pri-miR399 are required.

Interestingly, the overexpression of *MtPhr1* resulted in elevated transcript levels of *MtPt4* and *GirRNA*, suggesting a positive influence of increased *MtPhr1* transcript abundance to AMF colonization. This is further supported by the fact that *MtPt4*, as well as *Gi rRNA*, transcript abundances were greater in respect to greater strength of *MtPhr1* overexpression. Unfortunately, statistical significance could not be proven, which is mainly due to the

variable expression strength of *MtPhr1*, resulting from the high number of transformation events during *A. rhizogenes* mediated root transformation and a variable colonization levels after inoculation with *G. intraradices*.

Whether the stimulating effect of *MtPhr1* overexpression to AMS is caused rather directly by PHR1, or by mature miR399 or other downstream targets, could not be ruled out at this time and needs to be further investigated.

4.2.2 *Mt4* transcript abundance cannot be modulated through overexpression

In this study, several attempts to downregulate mature miR399 activity through *Mt4* overexpression by stable and transient transformation of *M. truncatula* plants. Unexpectedly, independent of the promoter used, none of the transformants showed significantly elevated *Mt4* transcript levels (Suppl. Fig. 2), to some extent the *Mt4* expression was even decreased in overexpression lines as compared to the wild type. The results imply that the amount of *Mt4* transcripts is highly controlled even under P_i -limiting conditions, which is further supported by the degradome target plots of *Mt4* transcripts (Suppl. Fig. 5), showing a high turnover rate in both non-mycorrhizal and mycorrhizal roots. Obviously, *Mt4* is subjected to a strong regulation presumably by negative feedback regulators. In *O. sativa*, *IPS1* is negatively regulated by the downstream effector OsSPX1¹⁵⁰. In addition, the results of the molecular phenotyping of *mtpho2 Tnt1* mutants indicate a negative regulation of *Mt4* by PHO2 (PhD thesis, Emanuel Devers) in analogy to *At4/IPS1* in *Arabidopsis*¹⁰. The constitutive downregulation of PHO2 led to elevated *Mt4* transcript levels in the mutant as compared to the wild type, indicating a feedback-circuit between PHO2 and *Mt4* to adjust mature miR399 activity. The overexpression of *Mt4* mimics a low activity of mature miR399 causing an increase of its target, *MtPho2*. Taking the previously discussed feedback regulation into account, higher PHO2 levels apparently affect *Mt4* abundance. This might be a possible explanation for the difficulty of modulating *Mt4* abundance through overexpression. The results suggest even more that the maintenance of P_i -homeostasis is a complex system of cross-talking components, where interventions on one side cause responses on the other side. The importance of the maintenance of essential processes is also indicated by the redundancy of genes or presence of functional homologues. As shown in *Arabidopsis*, *At4* and *IPS1* belong to a small family of non-coding RNAs characterized by a 24 nt conserved motif¹⁵¹. In this study, a further *Mt4* homologue could be identified, and

was shown to bind and sequester mature miR399, implying that the fine-tuning of miR399 in the response to P_i-deprivation is crucial for plant growth and development. To investigate the effect of downregulated miR399 activity independent of *Mt4*, an alternative approach would be the knockout of miRNA families through efficient miRNA silencing by artificial miRNAs, as demonstrated in a recent study of Eamens *et al.*¹⁵².

4.2.3 Identification of a *Mt4 Tnt1* knockout mutant

It has been suggested that *Mt4* expression is regulated by two pathways, of which one is dependent on P_i-fertilization and the other one dependent on AMS¹⁰³. Since one function of *Mt4* is the regulation of miR399 activity through target mimicry¹⁸, it has a clear involvement in the plant P_i-homeostasis signalling pathway. In this study, a *Mt4 Tnt1* insertion mutant was identified to further investigate the role of *Mt4* and the impact on the regulation of miR399 in AMS development.

The molecular phenotyping of *mt4-1* mutant plants revealed no changes in pri-miR399d transcription in the mutants as compared to the wild type. But unexpectedly, the *mt4-1* mutants showed a significant accumulation of mature miR399 in the roots, which was consistent with a significant decline of *MtPho2* expression levels, although no substantial differences in the P_i-concentrations between wild type and mutant plants were measured. This opens the question as to why mature miR399 would accumulate in the mutants. One possible explanation is that mature miR399 accumulation originate from technical reasons. The verification of mature miRNAs in this study was carried out using the stemloop-qRT-PCR method⁵⁸, which is based on the hybridization of mature miRNA molecules to long hairpin-forming stemloop primer sequences and the subsequent synthesis of cDNA. During the synthesis reaction, which is carried out at temperatures between 16 °C and 42 °C, the miR399 stemloop primer might compete with *Mt4* transcripts for complementary binding of the mature miR399 leading to the detection of generally lower amounts of mature miR399 compared to the actual miR399 abundance. It is noteworthy to mention, that the mRNA-miRNA-gelshift assay developed in this study is based on hybridization of mRNA and miRNA using a similar temperature profile as for the stemloop-cDNA synthesis, which resulted in detectable amounts of duplexes via blot analysis. The northern blot analysis would be an alternative approach to detect true amounts of miRNAs in the different conditions.

In conclusion, the results of the expression analysis demonstrated an increased activity of mature miR399 in *mt4-1* mutants gathering from significant lower *MtPho2* levels, emphasizing the power of *Mt4* in regulating miR399 activity.

Unexpectedly, *Mt4* knockout led to slightly decreased *MtPt4* and Glomus rRNA transcript abundance, which is in contrast to the hypothesis of a positive effect. It is commonly accepted that a low P_i -status in the plant positively influences arbuscule development and fungal colonization¹⁵³. However, zero P_i -growth conditions reduce AMS development as compared to low P_i -treatment¹⁵⁴. The *Mt4* knockout potentially causes a strong imbalance and intensification of the P_i -starvation response through miR399 imitating a zero P_i -situation, although all plants were fertilized at 20 μ M P_i , leading to a suppression of the fungus after long-term inoculation of 12 weeks. Further experiments are essential to elucidate the role of *Mt4*-miR399-PHO2 in AMS. A time series experiment will reveal insights into effects and causes of a *Mt4* transcriptional knockout, primarily in early stages of symbiosis development. Since *Mt4* is systemically regulated and plays a role in the allocation of P_i within the plant^{103, 151}, it is without question that the shoot should be included for further analysis. However, it has to be considered that *Mt4* is regulated by different P_i -dependent and AMS-dependent signalling pathways¹⁰³, and its transcriptional modulation might have pleiotropic effects, which are not necessarily caused by the miR399-PHO2 pathway.

4.2.4 Dynamics of AMS development and components of the P_i -homeostasis signalling pathway

The molecular dynamics of AMS development and P_i -homeostasis signalling in a period of 8 weeks was analyzed by a time course experiment carried out in this work. A high soluble P_i -content at 1 week post-inoculation indicates remaining P_i -resources of the seedling stage, but with significant lower levels in mycorrhizal roots as compared to non-mycorrhizal roots. It is likely, that for the increased synthesis of phospholipids, which are required for periarbuscular membrane formation¹⁵⁵, a large amount of P_i was recruited from the plant P_i -pool of inoculated roots. However, after a dramatic decline of soluble P_i in both conditions 2 weeks post-inoculation, the levels remained relatively constant over the time. The P_i -concentrations in mycorrhizal roots were slightly increased due to symbiotically improved P_i -availability.

The colonization progress over the time was as similar as described in literature^{156, 157}. In an *Allium porrum* nurse system, Rosewarne *et al.*¹⁵⁷ carried out a time course experiment to study characteristics of fungal colonization. The microscopic analysis of colonized roots revealed a very fast colonization with a maximal arbuscule abundance after 12 days post inoculation followed by a drop and a steady state beginning from 18 days post inoculation¹⁵⁷. Interestingly, the molecular arbuscule marker *MtPt4* measured in the experiment of this study (figure 28b) indicated the same characteristics of colonization progress. The maximum *MtPt4* transcript abundance was detected at 4 weeks post inoculation followed by a drop and relatively constant expression afterwards, indicating a steady state of developing and degenerating arbuscules. This was also true for the molecular marker *G.i. α -tubulin*¹⁰⁵ used in this study (figure 28c), which perfectly correlates with the abundance of internal hyphae¹⁵⁷. Thus, the use of molecular AMS markers in qRT-PCR measurements perfectly coincides with microscopic phenotyping, which is important for valuable statements in connection with expression levels of P_i-homeostasis genes. At 2 weeks post inoculation, no changes in mature miR399, *MtPho2* and *Mt4* transcript abundances were measured comparing non-mycorrhizal and mycorrhizal roots, since a functional symbiosis was not established yet, as indicated by *MtPt4* transcript levels. However, with progressive AMS development and establishment, an increasing divergence in P_i-homeostasis related gene expression between non-mycorrhizal and mycorrhizal roots was detected. Despite elevated P_i-concentrations, mature miR399 accumulate to substantial levels in mycorrhizal roots, and even more in later stages of AMS development, which is accompanied with a decline of *MtPho2* transcripts. This further supports the hypothesis of a previous work that a putative mycorrhizal signal might be responsible for mature miR399 accumulation⁴². Interestingly, the time-dependent expression of *Mt4* is opposite to mature miR399 abundance and decreases in mycorrhizal roots confirming the dependence on the P_i-status and / or AMS¹⁰³. Moreover, the divergence of *Mt4* expression and mature miR399 under mycorrhizal conditions indicates an increased activity of miR399, which is consistent with decreased *MtPho2* transcripts in mycorrhizal roots as compared to non-mycorrhizal roots.

Remarkably, during the analyzed period of 8 weeks approximately every 3 weeks repeating highs and lows in the P_i-homeostasis related gene expression, except for the P_i-dependent, but PHO2-independent *MtPID*, were observed. Diurnal dependent effects were excluded, because harvesting was carried out at the same time of day at each time point.

Therefore, this long-term progression of P_i -homeostasis signalling components is reminiscent of an oscillating system with precise control of transcription by a negative feedback loop of the oscillating components. *Mt4*, *MtPho2* and miR399 may be the central components of such an oscillating system (Figure 42) and part of tightly linked network of genes to regulate P_i -homeostasis. That circadian rhythms are not only important for the regulation of daily cycles but also may have long-term effects on gene regulation was shown in a recent study where long-term vascular tissue modelling, injury and angiogenesis in humans was affected by

defects in short-term circadian clock¹⁵⁸. The reasons for a long-term oscillating regulation of the P_i -homeostasis signalling pathway and its adaptation to AMS development might be diverse: (1) adjustment to changes caused by fundamentally changes in development, e.g. florescence (2) adjustment to symbiotically increased P_i -concentrations and (3) necessity of regulation to sustain AMS primarily in later stages of AM development. To test either of these

assumptions, mutants for P_i -homeostasis relevant genes are required. For example, a

mtpho2 Tnt1 mutant line showed a faster AM colonization after 2 weeks compared to wild type plants (Emanuel Devers, PhD thesis), confirming the impact of genes involved in P_i -homeostasis on AMS development.

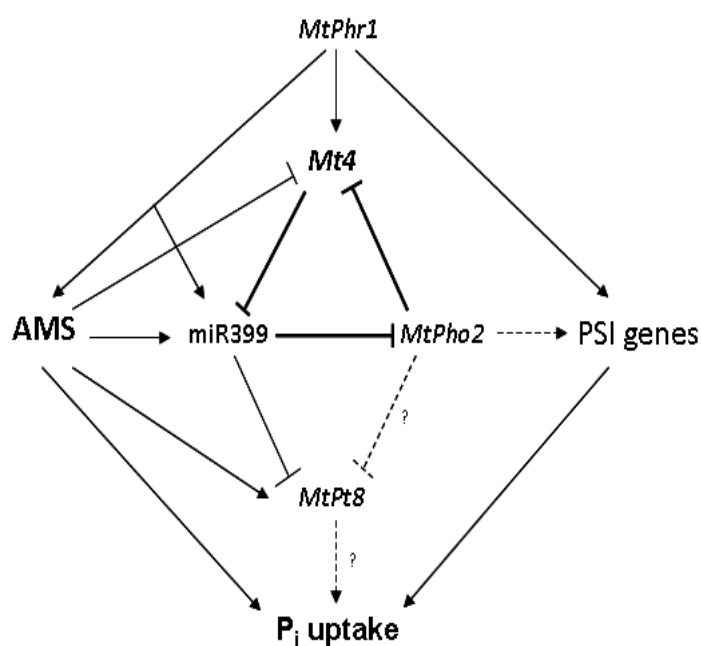


Figure 42. Proposed model of involved components in the regulatory network of plant P_i homeostasis and its linkage to AMS based on the results of this study. *Mt4*, miR399 and *MtPho2* are suggested to form the core in regulatory network and are interconnected by a negative feedback loop. P_i limitation induces *MtPhr1*, which enhances transcription of *Mt4*, miR399 and genes specifically transcribed in mycorrhizal roots (e.g. *MtPt4*). miR399 abundance is further stimulated by AMS derived signals, whereas the negative regulator of miR399, *Mt4*, is repressed through AMS. miR399, as long-distance signalling component, downregulates *MtPho2* transcripts and transcripts of the novel mycorrhizal-specific target *MtPt8* circumstantiating the complexity of regulatory mechanisms of plant and symbiotic P_i uptake and ensure a well-balanced P_i homeostasis within the plant.

4.2.5 Interplay of photosynthetic carbon, P_i-homeostasis and AMS development

miR399s are crucial players in the systemic regulation of the P_i-homeostasis in plants. Their induction is strongly P_i-dependent and interconnected with sugar signalling^{107, 159, 160}. Indeed, the induction of most of the P_i-starvation responsive genes is dependent on sucrose that is usually provided by photosynthates in higher plants¹⁶¹. In a recent study, Liu *et al.*¹⁶² demonstrated in *Phaseolus vulgaris* by dark splitshoot and stem-girdling experiments, the systemic repressive effect of reduced photosynthetic sucrose supply and interrupted phloem transport, respectively, to miR399 transcription.

There are several lines of evidence that there is a crosstalk between phosphate fertilization and carbon (C) allocation during AMS. AMS colonization increases photosynthesis rates in shoots¹⁶³. The constitutive overexpression of *SoSUT1*, a sucrose transporter for phloem loading in several *Solanum* species, showed significantly enhanced AM fungal colonization. However, this effect was strongly P_i-dependent and only observed at high external P_i-fertilization¹⁶⁴. The authors pointed out, that it is still unclear whether improved carbon allocation or other factors caused this effect. In contrast, mutants impaired in phloem loading, which is equivalent to reduced C flux from source to sink tissue, were not affected in the extent of fungal colonization at low external P_i-availability¹⁶⁴. This goes in line with another study, where shading induced C-limitation did not reduce the retained carbon in the mycorrhizal mycelium¹⁶⁵. The authors concluded, that plants can control C-allocation to their associated fungus when soil is enriched with P_i, but not when light is limited.

However, the results of the splitshoot and shading experiment in this study revealed a significant downregulation of genes involved in P_i-homeostasis signalling and *MtPID*, a P_i-stress marker gene, which independently regulated from the PHO2¹⁰. In addition, also *MtPt4* transcripts were substantially reduced in roots of 14 days shaded and P_i-starved plants as compared to control roots indicating a strongly affected arbuscule abundance. This is contrary to the intraradicular overall fungal biomass measured by the marker *Gi rRNA*, which strongly increases upon shading. Roots of splitshoot plants did not show significantly altered expression of these genes, which might be explained by the more extensive growth of the light-exposed part of the shoot as compared to the shaded part. Therefore, the effects observed in the completely shaded plants were dampened in the splitshoot system. In conclusion, the C-limitation through light-dependent reduction of photosynthesis led to a

repression of the P_i-starvation response and a decreased functional AMS, but with an extensive intraradicular hyphae growth instead. However, based on this experiment I assume that the plant probably actively regulates C-allocation and C-costs to support the fungus under low P_i, particularly with regard to different C-costs of different *Glomus* species^{166, 167}. Potentially, the observed phenomenon might be a mechanism of plants to protect themselves from switching the symbiosis into parasitism by the fungus. However, further experiments are required, particularly with mutants of the P_i-homeostasis pathway, to distinguish between C-mediated and P_i-mediated influences on AMS.

4.2.6 Cell-specific accumulation of mature miR399 in arbuscule-containing cells – pros and cons of miR399 movement

Mature miR399 are mobile signals involved in the maintenance of plant P_i-homeostasis¹⁵. *In situ* hybridizations in this study demonstrated the accumulation of mature miR399 in phloem tissue of non-mycorrhizal and mycorrhizal roots, which is consistent with previous studies where a number of miRNAs including miR399 were detected in phloem sap of several plant species^{16, 122, 168-170}. In addition, this study provides evidence, that mature miR399 accumulate outside the central cylinder in root cortex cells, primarily in arbuscule-containing cells of mycorrhizal roots. These results raise the question whether miR399 can move between different tissues to act in specific cells and which signals might trigger the movement.

The current knowledge about miRNA transport mechanisms and causing signals is limited and controversial. It has been proposed that several miRNAs are transcribed in the phloem and, similar to siRNAs, move from cell to cell through plasmodesmata (PD), up to 15 cell layers^{169,171}. Plasmodesmata mediate the local for cell-to-cell exchange of non-cell-autonomous proteins and ribonucleoprotein complexes, including transcription factors and RNA involved in developmental programs¹⁶⁹.

In contrast, the specific transport of synthetic miR164a and miR167b in phloem companion cells through the cell-specific SUT2 promoter showed that although efficiently processed, their action was restricted to the area of their domain of expression¹⁷². Similar results were observed after tissue-specific expression of endogenous and synthetic miRNAs in tomato and tobacco¹⁷³, which suggests cell autonomy without long-distance signalling of miRNAs. However, no phloem transport of miR164 and miR167 was reported so far in contrast to

miR399, where phloem transport and long distance signalling was proven through grafting experiments¹⁵. Obviously, there are differences in the mobility between different miRNA families and the information being transported might be deposited in the promoters or in the miRNA transcript itself. Evidence suggests the differential processing of miR399 precursor in mycorrhizal roots as compared to non-mycorrhizal roots (table 4). For sequences of miR399b, f, k, l, m more degradome tags were found for the mycorrhizal condition indicating an increased processing of these miRNAs in mycorrhizal roots. In addition, for miR399a, e, g, no tags were detected neither in mycorrhizal nor in non-mycorrhizal roots, although their abundance was relatively high (table 4). These findings imply different transcriptional activity and processing of each miR399 member in shoots and roots, which is additionally influenced by putative mycorrhizal signals⁴².

In addition, the fact that mature miR399d molecules appeared close to cell walls and plasmodesmata-like structures indicate a symplastic transport between cells to reach the place of activity. The possibility of directional cell-to cell trafficking of small single-stranded RNAs (ssRNA) through plasmodesmata was demonstrated in *Curcubita maxima*¹⁶⁸. The small RNA binding protein 1 (CmSBPR1) selectively binds ssRNAs with a size up to 25 nucleotides and transport was observed in phloem and surrounding tissue¹⁷⁰. Another study provided further evidence of miRNA movement. Another study using *Zea mays* showed that miR166 was spread in leaves and phloem during development, suggesting a phloem transport and subsequent distribution of miR166 in leaves¹⁷⁴. But it was emphasized, that a non-directional movement of miRNAs between cells and tissues by diffusion through plasmodesmata is very unlikely¹⁶⁸. If miR399 were transported from phloem tissue to arbuscule-containing cells, it is probably done through specific proteins.

However, an increased transcription of miR399 in distinct cortex cells leading to the cell-specific accumulation cannot be excluded. Although a significant downregulation of all miR399 transcripts in mycorrhizal roots was observed⁴², the localization of miR399dpro::reporter signals suggests a transcriptional activity of miR399d in cortex cells of mycorrhizal roots (figure 26). The promoter signal could not be clearly co-localized to arbuscule-containing cells, but the dispersed pattern indicates an increased promoter activity in distinct cells. In conclusion, a final statement on a putative transport of mature miR399 to arbuscule-containing cells based on the results of this study is not possible and further experiments are necessary. Stable miR399 overexpression lines grown under

moderate P_i -conditions, means 250-500 μM P_i to ensure valuable AM colonization with repressed endogenous miR399 transcription, and the subsequent analysis via *in situ* hybridization might confirm a putative translocation of mature miR399 from vascular tissue to distinct cortical cells. Alternatively, the localization of all miR399 promoters in roots and the co-localization to fungal structure might give insights.

4.2.7 The novel miR399 target MtPt8 directly links P_i -homeostasis signalling and AMS

Through degradome sequencing, a novel target of the miR399 family has been identified. Investigations revealed that the new target, named as *MtPt8*, is most likely an inorganic P_i -transporter of the major facilitator superfamily (MFS), and is exclusively expressed in mycorrhizal roots. The miR399-mediated cleavage was confirmed *in planta* in independent experiments (3.2.4.1). Systematic analysis of the *M. truncatula* P_i -transporter family in terms of miR399-mediated transcript cleavage showed that 6 of 9 currently known P_i -transporters^{28, 175, 176} (Maria J. Harrison, personal communication), of which one is *MtPt8*, were predicted to be miR399 cleavage targets. Interestingly, the high-affinity transporters *MtPt1-3*, three of the predicted transporters, are assigned to the direct P_i -uptake pathway (DPU)¹⁷⁶. Moreover, there are several lines of evidence, that these transporters are downregulated by AM colonization²⁷, and the mycorrhizal P_i -uptake pathway can dominate P_i -uptake irrespective of improved growth and total P_i -uptake¹⁷⁷. It is noteworthy to mention that transporters of the *Pht1* family possess PHR1 binding motifs (P1BS) in their promoter region^{12, 44}, indicating the regulation through components of the P_i -homeostasis signalling pathway. Although degradome sequencing did not provide evidence for the miR399 mediated cleavage of *MtPt1-3*, it is speculated whether miR399 are involved in their regulation during AMS under different conditions or through translational inhibition. A recent study showed, that the promoter region of AM-specific P_i -transporters of several species, in addition to a P1BS, exhibit a MYCS binding motif (TTTCTTGTCT), implying that the AM-specific transcription is regulated through this motif⁴⁴. Interestingly, the 1 kb promoter region that the AM-specific *MtPt8* possess MYCS binding motif but lacks a P1BS, indicating a AM-dependent but PHR1-independent regulation. The significant decline of *MtPt8* transcripts at low P_i -concentrations argues for a P_i -independent regulation (Suppl. Fig. 6). In addition, *MtPt8* transcript abundance reversely correlates with P_i -starvation induced

miR399. The relative expression levels of *MtPt8* and mature miR399 were plotted against the symbiotic P_i -uptake efficiency in relation to gradient external P_i -concentrations ranging from 0 μM to 2 mM P_i to clarify the interrelation of these components (figure 43). It is striking that the maximum symbiotic P_i -uptake capacity is achieved at an external P_i -concentration of 250 μM P_i with a parallel slope of *MtPt8* transcript abundance, due to decreasing mature miR399 levels. The data suggest a strong interrelation between *MtPt8* abundance and P_i -uptake efficiency. One might speculate, whether increased symbiotic P_i -uptake is caused by

the establishment of MtPT8 as an additional P_i -transporter in the periarbuscular membrane (Maria J. Harrison, personal communication) or through increased affinity of the AM-specific P_i -transporter MtPT4. The latter might be realized by an interaction of

MtPT4 and MtPT8 to ensure a well-balanced ratio between efficiency and costs of AMS with regard to plant P_i -metabolism. Further experiments are required, e.g. Biomolecular fluorescence complementation (BIFC) experiments and reverse genetic approaches, to elucidate the physiological function of the new AM-specific P_i -transporter MtPT8.

In conclusion, this study provides evidence for a direct link of the regulatory mechanisms of plant P_i -homeostasis and AMS at the cell-specific level.

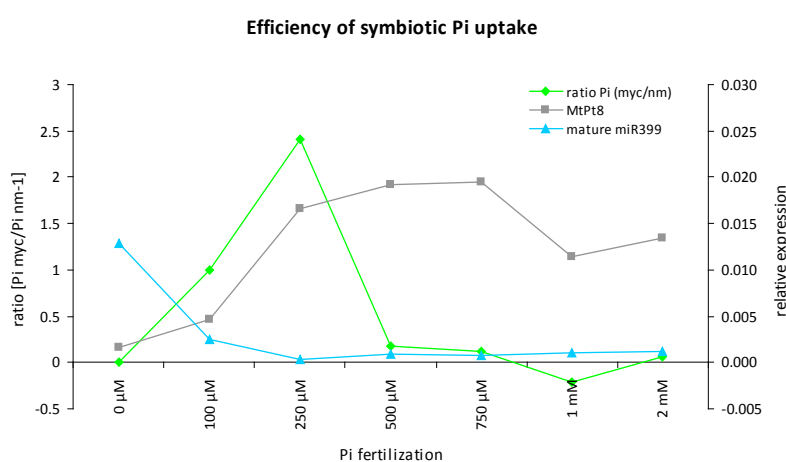


Figure 43. Correlation of symbiotic P_i -uptake efficiency (primary axis) and relative expression levels of *MtPt8* and miR399 (secondary axis). Values for P_i -uptake efficiency were calculated from values of the P_i -gradient (3.2.3.4): P_i myc/ P_i nm⁻¹. For measured P_i -concentrations around 0 mg/gFW, the half-minimum P_i -value obtained in the measurement was used for calculation.

5 Summary

Since available phosphate (P_i) resources in soil are limited, symbiotic interactions between plant roots and arbuscular mycorrhizal (AM) fungi are a widespread strategy to improve plant phosphate nutrition. The repression of AM symbiosis by a high plant P_i -status indicates a link between P_i -homeostasis signalling and AM symbiosis development. This assumption is supported by the systemic induction of several microRNA399 (miR399) primary transcripts in shoots and a simultaneous accumulation of mature miR399 in roots of mycorrhizal plants. However, the physiological role of this miR399 expression pattern is still elusive and offers the question whether other miRNAs are also involved in the regulation of AM symbiosis.

Therefore, a deep sequencing approach was applied to investigate miRNA-mediated posttranscriptional gene regulation in *M. truncatula* mycorrhizal roots. Degradome analysis revealed that 185 transcripts were cleaved by miRNAs, of which the majority encoded transcription factors and disease resistance genes, suggesting a tight control of transcriptional reprogramming and a downregulation of defence responses by several miRNAs in mycorrhizal roots. Interestingly, 45 of the miRNA-cleaved transcripts showed a significant differentially regulated between mycorrhizal and non-mycorrhizal roots.

In addition, key components of the P_i -homeostasis signalling pathway were analyzed concerning their expression during AM symbiosis development. *MtPhr1* overexpression and time course expression data suggested a strong interrelation between the components of the PHR1-miR399-PHO2 signalling pathway and AM symbiosis, predominantly during later stages of symbiosis. *In situ* hybridizations confirmed accumulation of mature miR399 in the phloem and in arbuscule-containing cortex cells of mycorrhizal roots. Moreover, a novel target of the miR399 family, named as *MtPt8*, was identified by the above mentioned degradome analysis. *MtPt8* encodes a P_i -transporter exclusively transcribed in mycorrhizal roots and its promoter activity was restricted to arbuscule-containing cells. At a low P_i -status, *MtPt8* transcript abundance inversely correlated with a mature miR399 expression pattern. Increased *MtPt8* transcript levels were accompanied by elevated symbiotic P_i -uptake efficiency indicating its impact on balancing plant and fungal P_i -acquisition.

In conclusion, this study provides evidence for a direct link of the regulatory mechanisms of plant P_i -homeostasis and AM symbiosis at a cell-specific level. The results of this study, especially the interaction of miR399 and *MtPt8* provide a fundamental step for future studies of plant-microbe-interactions with regard to agricultural and ecological aspects.

6 Literature

1. Lima, P.T. *et al.* Plant-microbe symbioses: new insights into common roots. *Bioessays* **31**, 1233-1244 (2009).
2. Marschner, H. (ed.) *Mineral Nutrition of Plants*, Edn. 2nd. (Academic Press, London, 1995).
3. Bhat, K.K.S. & Nye, P.H. Diffusion of Phosphate to Plant Roots in Soil .1. Quantitative Autoradiography of Depletion Zone. *Plant and Soil* **38**, 161-& (1973).
4. Bielecki, R.L. Phosphate Pools, Phosphate Transport, and Phosphate Availability. *Annual Review of Plant Physiology and Plant Molecular Biology* **24**, 225-252 (1973).
5. Ozanne, P.G. *Phosphate nutrition in plants-a general treatise*. (American Society of Agronomy, Madison; 1980).
6. Harrison, M.J. Molecular and Cellular Aspects of the Arbuscular Mycorrhizal Symbiosis. *Annu Rev Plant Physiol Plant Mol Biol* **50**, 361-389 (1999).
7. Hause, B. & Fester, T. Molecular and cell biology of arbuscular mycorrhizal symbiosis. *Planta* **221**, 184-196 (2005).
8. Mengel, K. Agronomic measures for better utilization of soil and fertilizer phosphates. *European Journal of Agronomy* **7**, 221-233 (1997).
9. Fujii, H., Chiou, T.J., Lin, S.I., Aung, K. & Zhu, J.K. A miRNA Involved in Phosphate-Starvation Response in *Arabidopsis*. *Curr Biol* **15**, 2038-2043 (2005).
10. Bari, R., Datt Pant, B., Stitt, M. & Scheible, W.R. PHO2, microRNA399, and PHR1 define a phosphate-signaling pathway in plants. *Plant Physiology* **141**, 988-999 (2006).
11. Chiou, T.J. *et al.* Regulation of Phosphate Homeostasis by MicroRNA in *Arabidopsis*. *Plant Cell* **18**, 412-421 (2006).
12. Rubio, V. *et al.* A conserved MYB transcription factor involved in phosphate starvation signaling both in vascular plants and in unicellular algae. *Genes & development* **15**, 2122-2133 (2001).
13. Miura, K. *et al.* The Arabidopsis SUMO E3 ligase SIZ1 controls phosphate deficiency responses. *Proc Natl Acad Sci U S A* **102**, 7760-7765 (2005).
14. Papp, I. *et al.* Evidence for nuclear processing of plant micro RNA and short interfering RNA precursors. *Plant Physiol* **132**, 1382-1390 (2003).
15. Pant, B.D., Buhtz, A., Kehr, J. & Scheible, W.R. MicroRNA399 is a long-distance signal for the regulation of plant phosphate homeostasis. *Plant Journal* **53**, 731-738 (2008).
16. Buhtz, A., Springer, F., Chappell, L., Baulcombe, D.C. & Kehr, J. Identification and characterization of small RNAs from the phloem of *Brassica napus*. *Plant J* **53**, 739-749 (2008).
17. Aung, K. *et al.* pho2, a phosphate overaccumulator, is caused by a nonsense mutation in a microRNA399 target gene. *Plant Physiol* **141**, 1000-1011 (2006).
18. Franco-Zorrilla, J.M. *et al.* Target mimicry provides a new mechanism for regulation of microRNA activity. *Nat Genet* **39**, 1033-1037 (2007).
19. Akiyama, K. & Hayashi, H. Strigolactones: chemical signals for fungal symbionts and parasitic weeds in plant roots. *Ann Bot (Lond)* **97**, 925-931 (2006).
20. Olah, B., Briere, C., Becard, G., Denarie, J. & Gough, C. Nod factors and a diffusible factor from arbuscular mycorrhizal fungi stimulate lateral root formation in *Medicago truncatula* via the DMI1/DMI2 signalling pathway. *Plant J* **44**, 195-207 (2005).

21. Akiyama, K., Matsuzaki, K. & Hayashi, H. Plant sesquiterpenes induce hyphal branching in arbuscular mycorrhizal fungi. *Nature* **435**, 824-827 (2005).
22. Kosuta, S. *et al.* A diffusible factor from arbuscular mycorrhizal fungi induces symbiosis-specific MtENOD11 expression in roots of *Medicago truncatula*. *Plant Physiol* **131**, 952-962 (2003).
23. Kosuta, S. *et al.* Differential and chaotic calcium signatures in the symbiosis signaling pathway of legumes. *Proc Natl Acad Sci U S A* **105**, 9823-9828 (2008).
24. Strack, D., Fester, T., Hause, B., Schliemann, W. & Walter, M.H. Arbuscular mycorrhiza: biological, chemical, and molecular aspects. *Journal of chemical ecology* **29**, 1955-1979 (2003).
25. Pumplun, N. & Harrison, M.J. Live-cell imaging reveals periarbuscular membrane domains and organelle location in *Medicago truncatula* roots during arbuscular mycorrhizal symbiosis. *Plant Physiol* (2009).
26. Benedito, V.A. *et al.* Genomic inventory and transcriptional analysis of *Medicago truncatula* transporters. *Plant Physiol* **152**, 1716-1730 (2010).
27. Javot, H., Pumplun, N. & Harrison, M.J. Phosphate in the arbuscular mycorrhizal symbiosis: transport properties and regulatory roles. *Plant Cell Environ* **30**, 310-322 (2007).
28. Harrison, M.J., Dewbre, G.R. & Liu, J. in *Plant Cell*, Vol. 14 2413-2429 (2002).
29. Liu, J. *et al.* Transcript profiling coupled with spatial expression analyses reveals genes involved in distinct developmental stages of an arbuscular mycorrhizal symbiosis. *Plant Cell* **15**, 2106-2123 (2003).
30. Wulf, A. *et al.* Transcriptional changes in response to arbuscular mycorrhiza development in the model plant *Medicago truncatula*. *Molecular Plant Microbe Interaction* **16**, 306-314 (2003).
31. Frenzel, A. *et al.* Combined transcriptome profiling reveals a novel family of arbuscular mycorrhizal-specific *Medicago truncatula* lectin genes. *Mol Plant Microbe Interact* **18**, 771-782 (2005).
32. Hohnjec, N., Vieweg, M.F., Puhler, A., Becker, A. & Küster, H. Overlaps in the transcriptional profiles of *Medicago truncatula* roots inoculated with two different *Glomus* fungi provide insights into the genetic program activated during arbuscular mycorrhiza. *Plant Physiol* **137**, 1283-1301 (2005).
33. Fiorilli, V. *et al.* Global and cell-type gene expression profiles in tomato plants colonized by an arbuscular mycorrhizal fungus. *New Phytol* **184**, 975-987 (2009).
34. Gomez, S.K. *et al.* *Medicago truncatula* and *Glomus intraradices* gene expression in cortical cells harboring arbuscules in the arbuscular mycorrhizal symbiosis. *BMC Plant Biol* **9**, 10 (2009).
35. Hause, B., Mrosk, C., Isayenkov, S. & Strack, D. Jasmonates in arbuscular mycorrhizal interactions. *Phytochemistry* **68**, 101-110 (2007).
36. Hirsch, A.M., Fang, Y., Asad, S. & Kapulnik, Y. The role of phytohormones in plant-microbe symbioses. *Plant and Soil* **194**, 171-184 (1997).
37. Vierheilig, H., Bago, B., Lerat, S. & Piche, Y. Shoot-produced, light-dependent factors are partially involved in the expression of the arbuscular mycorrhizal (AM) status of AM host and non-host plants. *Journal of Plant Nutrition and Soil Science* **165**, 21-25 (2002).
38. Goicoechea, N., Antolin, M.C. & Sanchez-Diaz, M. The role of plant size and nutrient concentrations in associations between *Medicago*, and *Rhizobium* and/or *Glomus*. *Biologia Plantarum* **43**, 221-226 (2000).

39. Saito, M. Regulation of arbuscular mycorrhiza symbiosis: Hyphal growth in host roots and nutrient exchange. *Jarq-Japan Agricultural Research Quarterly* **31**, 179-183 (1997).
40. Sanders, F.E. (ed.) *The effect of foliar-applied phosphate on the mycorrhizal infection of onion roots*. (Academic Press, 261-276, London; 1975).
41. Menge, J.A., Steirle, D., Bagyaraj, D.J., Johnson, E.L.V. & Leonard, R.T. Phosphorus Concentrations in Plants Responsible for Inhibition of Mycorrhizal Infection. *New Phytologist* **80**, 575-578 (1978).
42. Branscheid, A. *et al.* Expression pattern suggests a role of MiR399 in the regulation of the cellular response to local Pi increase during arbuscular mycorrhizal symbiosis. *Mol Plant Microbe Interact* **23**, 915-926 (2010).
43. Burleigh, S.H. & Harrison, M.J. A novel gene whose expression in *Medicago truncatula* roots is suppressed in response to colonization by vesicular-arbuscular mycorrhizal (VAM) fungi and to phosphate nutrition. *Plant Molecular Biology* **34**, 199-208 (1997).
44. Chen, A. *et al.* Identification of two conserved cis-acting elements, MYCS and P1BS, involved in the regulation of mycorrhiza-activated phosphate transporters in eudicot species. *New Phytol* **189**, 1157-1169 (2011).
45. Lee, Y. *et al.* MicroRNA genes are transcribed by RNA polymerase II. *Embo J* **23**, 4051-4060 (2004).
46. Cai, X., Hagedorn, C.H. & Cullen, B.R. Human microRNAs are processed from capped, polyadenylated transcripts that can also function as mRNAs. *Rna* **10**, 1957-1966 (2004).
47. Vazquez, F., Gascioli, V., Crete, P. & Vaucheret, H. The nuclear dsRNA binding protein HYL1 is required for microRNA accumulation and plant development, but not posttranscriptional transgene silencing. *Curr Biol* **14**, 346-351 (2004).
48. Xie, Z. *et al.* Genetic and functional diversification of small RNA pathways in plants. *PLoS Biol* **2**, E104 (2004).
49. Yu, B. *et al.* Methylation as a crucial step in plant microRNA biogenesis. *Science* **307**, 932-935 (2005).
50. Yang, Z., Ebright, Y.W., Yu, B. & Chen, X. HEN1 recognizes 21-24 nt small RNA duplexes and deposits a methyl group onto the 2' OH of the 3' terminal nucleotide. *Nucleic Acids Res* **34**, 667-675 (2006).
51. Park, W., Li, J., Song, R., Messing, J. & Chen, X. CARPEL FACTORY, a Dicer homolog, and HEN1, a novel protein, act in microRNA metabolism in *Arabidopsis thaliana*. *Curr Biol* **12**, 1484-1495 (2002).
52. Bartel, D.P. MicroRNAs: target recognition and regulatory functions. *Cell* **136**, 215-233 (2009).
53. Llave, C., Kasschau, K.D., Rector, M.A. & Carrington, J.C. Endogenous and silencing-associated small RNAs in plants. *Plant Cell* **14**, 1605-1619 (2002).
54. Baumberg, N. & Baulcombe, D.C. *Arabidopsis* ARGONAUTE1 is an RNA Slicer that selectively recruits microRNAs and short interfering RNAs. *Proc Natl Acad Sci U S A* **102**, 11928-11933 (2005).
55. Qi, Y. & Hannon, G.J. Uncovering RNAi mechanisms in plants: biochemistry enters the foray. *FEBS Lett* **579**, 5899-5903 (2005).
56. Aukerman, M.J. & Sakai, H. Regulation of flowering time and floral organ identity by a MicroRNA and its APETALA2-like target genes. *Plant Cell* **15**, 2730-2741 (2003).

57. Gandikota, M. *et al.* The miRNA156/157 recognition element in the 3' UTR of the Arabidopsis SBP box gene SPL3 prevents early flowering by translational inhibition in seedlings. *Plant J* **49**, 683-693 (2007).
58. Chen, C. *et al.* Real-time quantification of microRNAs by stem-loop RT-PCR. *Nucleic Acids Res* **33**, e179 (2005).
59. Brodersen, P. *et al.* Widespread translational inhibition by plant miRNAs and siRNAs. *Science* **320**, 1185-1190 (2008).
60. Baulcombe, D. Viruses and gene silencing in plants. *Archives of virology* **15**, 189-201 (1999).
61. Navarro, L. *et al.* A plant miRNA contributes to antibacterial resistance by repressing auxin signaling. *Science* **312**, 436-439 (2006).
62. Fahlgren, N. *et al.* High-throughput sequencing of *Arabidopsis* microRNAs: evidence for frequent birth and death of MIRNA genes. *PLoS ONE* **2**, e219 (2007).
63. Rhoades, M.W. *et al.* Prediction of plant microRNA targets. *Cell* **110**, 513-520 (2002).
64. Pruss, G.J., Nester, E.W. & Vance, V. Infiltration with *Agrobacterium tumefaciens* induces host defense and development-dependent responses in the infiltrated zone. *Mol Plant Microbe Interact* **21**, 1528-1538 (2008).
65. Comber, J.P. *et al.* MtHAP2-1 is a key transcriptional regulator of symbiotic nodule development regulated by microRNA169 in *Medicago truncatula*. *Genes Dev* **20**, 3084-3088 (2006).
66. Subramanian, S. *et al.* Novel and nodulation-regulated microRNAs in soybean roots. *BMC Genomics* **9**, 160 (2008).
67. Lelandais-Briere, C. *et al.* Genome-wide *Medicago truncatula* small RNA analysis revealed novel microRNAs and isoforms differentially regulated in roots and nodules. *Plant Cell* **21**, 2780-2796 (2009).
68. Branscheid, A., Devers, E.A., May, P. & Krajinski, F. Stars and symbiosis: microRNA- and microRNA*-mediated transcript cleavage involved in arbuscular mycorrhizal symbiosis. *Plant Physiol* **156**, 1990-2010 (2011).
69. Wang, Y. *et al.* Identification and expression analysis of miRNAs from nitrogen-fixing soybean nodules. *Biochemical and biophysical research communications* **378**, 799-803 (2009).
70. Gaude, N., Bortfeld, S., Duensing, N., Lohse, M. & Krajinski, F. Arbuscule-containing and non-colonized cortical cells of mycorrhizal roots undergo extensive and specific reprogramming during arbuscular mycorrhizal development. *Plant J* (2012).
71. Oldroyd, G.E., Harrison, M.J. & Paszkowski, U. Reprogramming plant cells for endosymbiosis. *Science* **324**, 753-754 (2009).
72. Guether, M. *et al.* Genome-wide reprogramming of regulatory networks, transport, cell wall and membrane biogenesis during arbuscular mycorrhizal symbiosis in *Lotus japonicus*. *New Phytol* **182**, 200-212 (2009).
73. Kistner, C. *et al.* Seven *Lotus japonicus* genes required for transcriptional reprogramming of the root during fungal and bacterial symbiosis. *Plant Cell* **17**, 2217-2229 (2005).
74. German, M.A. *et al.* Global identification of microRNA-target RNA pairs by parallel analysis of RNA ends. *Nat Biotechnol* **26**, 941-946 (2008).
75. German, M.A., Luo, S., Schroth, G., Meyers, B.C. & Green, P.J. Construction of Parallel Analysis of RNA Ends (PARE) libraries for the study of cleaved miRNA targets and the RNA degradome. *Nature protocols* **4**, 356-362 (2009).

76. Addo-Quaye, C., Miller, W. & Axtell, M.J. CleaveLand: a pipeline for using degradome data to find cleaved small RNA targets. *Bioinformatics* **25**, 130-131 (2009).
77. Barker, D.G. *et al.* Growing *M. truncatula*: choice of substrates and growth conditions, in *Medicago truncatula handbook version November 2006* (<http://www.noble.org/MedicagoHandbook/>, 2006).
78. Quandt, H.J., Puehler, A. & I., B. Transgenic root nodules of *Vicia hirsuta*: A fast and efficient system for the study of gene expression in indeterminate-type nodules. *Molecular Plant-Microbe interactions* **6**, 699-706 (1993).
79. Schmidt, R. & Willmitzer, L. High-Efficiency Agrobacterium-Tumefaciens-Mediated Transformation of Arabidopsis-Thaliana Leaf and Cotyledon Explants. *Plant Cell Reports* **7**, 583-586 (1988).
80. Karimi, M., Inze, D. & Depicker, A. GATEWAY vectors for Agrobacterium-mediated plant transformation. *Trends Plant Sci* **7**, 193-195 (2002).
81. Nakagawa, T. *et al.* Improved Gateway binary vectors: high-performance vectors for creation of fusion constructs in transgenic analysis of plants. *Bioscience, biotechnology, and biochemistry* **71**, 2095-2100 (2007).
82. Boisson-Dernier, A. *et al.* Agrobacterium rhizogenes-transformed roots of *Medicago truncatula* for the study of nitrogen-fixing and endomycorrhizal symbiotic associations. *Mol Plant Microbe Interact* **14**, 695-700. (2001).
83. Ramakers, C., Ruijter, J.M., Deprez, R.H. & Moorman, A.F. Assumption-free analysis of quantitative real-time polymerase chain reaction (PCR) data. *Neurosci Lett* **339**, 62-66 (2003).
84. Itaya, K. & Ui, M. A new micromethod for the colorimetric determination of inorganic phosphate. *Clin Chim Acta* **14**, 361-366 (1966).
85. Pena, J.T. *et al.* miRNA in situ hybridization in formaldehyde and EDC-fixed tissues. *Nature methods* **6**, 139-141 (2009).
86. Nuovo, G.J. In situ detection of microRNAs in paraffin embedded, formalin fixed tissues and the co-localization of their putative targets. *Methods (San Diego, Calif)* **52**, 307-315 (2010).
87. Phillips, J.M. & Hayman, D.S. Improved Procedures for Clearing Roots and Staining Parasitic and Vesicular-Arbuscular Mycorrhizal Fungi for Rapid Assessment of Infection. *Transactions of the British Mycological Society* **55**, 158-159 (1970).
88. Berninger, P., Gaidatzis, D., van Nimwegen, E. & Zavolan, M. Computational analysis of small RNA cloning data. *Methods (San Diego, Calif)* **44**, 13-21 (2008).
89. Weese, D., Emde, A.K., Rausch, T., Doring, A. & Reinert, K. RazerS--fast read mapping with sensitivity control. *Genome Res* **19**, 1646-1654 (2009).
90. Rehmsmeier, M. Prediction of microRNA targets. *Methods Mol Biol* **342**, 87-99 (2006).
91. German, M.A., Luo, S., Schroth, G., Meyers, B.C. & Green, P.J. Construction of Parallel Analysis of RNA Ends (PARE) libraries for the study of cleaved miRNA targets and the RNA degradome. *Nature protocols* **4**, 356-362 (2009).
92. Tisserant, E. *et al.* The transcriptome of the arbuscular mycorrhizal fungus *Glomus intraradices* (DAOM 197198) reveals functional tradeoffs in an obligate symbiont. *New Phytol* **193**, 755-769 (2011).
93. Li, Y.F. *et al.* Transcriptome-wide identification of microRNA targets in rice. *Plant J* **62**, 742-759 (2010).
94. Zhou, L. *et al.* Genome-wide identification and analysis of drought-responsive microRNAs in *Oryza sativa*. *J Exp Bot* **61**, 4157-4168 (2010).

95. Gomez, S.K. & Harrison, M.J. Laser microdissection and its application to analyze gene expression in arbuscular mycorrhizal symbiosis. *Pest management science* **65**, 504-511 (2009).
96. Rehmsmeier, M., Steffen, P., Hochsmann, M. & Giegerich, R. Fast and effective prediction of microRNA/target duplexes. *Rna* **10**, 1507-1517 (2004).
97. Usadel, B. *et al.* Extension of the visualization tool MapMan to allow statistical analysis of arrays, display of corresponding genes, and comparison with known responses. *Plant Physiol* **138**, 1195-1204 (2005).
98. Paradi, I. *et al.* Transcription of two blue copper-binding protein isogenes is highly correlated with arbuscular mycorrhizal development in *Medicago truncatula*. *Mol Plant Microbe Interact* **23**, 1175-1183 (2010).
99. Jones-Rhoades, M.W., Bartel, D.P. & Bartel, B. MicroRNAs and their regulatory roles in plants. *Annu Rev Plant Biol* **57**, 19-53 (2006).
100. Voinnet, O. Origin, biogenesis, and activity of plant microRNAs. *Cell* **136**, 669-687 (2009).
101. Meng, Y., Gou, L., Chen, D., Wu, P. & Chen, M. High-throughput degradome sequencing can be used to gain insights into microRNA precursor metabolism. *J Exp Bot* **61**, 3833-3837 (2010).
102. Bologna, N.G., Mateos, J.L., Bresso, E.G. & Palatnik, J.F. A loop-to-base processing mechanism underlies the biogenesis of plant microRNAs miR319 and miR159. *Embo J* **28**, 3646-3656 (2009).
103. Burleigh, S.H. & Harrison, M.J. The down-regulation of Mt4-like genes by phosphate fertilization occurs systemically and involves phosphate translocation to the shoots. *Plant Physiology* **119**, 241-248 (1999).
104. Tadege, M. *et al.* Large-scale insertional mutagenesis using the *Tnt1* retrotransposon in the model legume *Medicago truncatula*. *Plant J* **54**, 335-347 (2008).
105. Corradi, N., Hijri, M., Fumagalli, L. & Sanders, I.R. Arbuscular mycorrhizal fungi (Glomeromycota) harbour ancient fungal tubulin genes that resemble those of the chytrids (Chytridiomycota). *Fungal Genet Biol* **41**, 1037-1045 (2004).
106. Hoagland, D.R. & Arnon, D.I. The water-culture method of growing plants without soil. *Calif. Agr. Expt. Sta. Circ* **347** (1950).
107. Mueller, R., Morant, M., Jarmer, H., Nilsson, L. & Nielsen, T.H. Genome-wide analysis of the Arabidopsis leaf transcriptome reveals interaction of phosphate and sugar metabolism. *Plant Physiol* **143**, 156-171 (2007).
108. Mallory, A.C. & Bouché, N. MicroRNA-directed regulation: to cleave or not to cleave. *Trends Plant Sci* **13**, 359-367 (2008).
109. Doerner, P. Phosphate starvation signaling: a threesome controls systemic P_i homeostasis. *Curr Opin Plant Biol* **11**, 536-540 (2008).
110. Hajdukiewicz, P., Svab, Z. & Maliga, P. The small, versatile pPZP family of Agrobacterium binary vectors for plant transformation. *Plant Mol Biol* **25**, 989-994 (1994).
111. Dai, X., Zhuang, Z. & Zhao, P.X. Computational analysis of miRNA targets in plants: current status and challenges. *Brief Bioinform* (2010).
112. Addo-Quaye, C., Eshoo, T.W., Bartel, D.P. & Axtell, M.J. Endogenous siRNA and miRNA targets identified by sequencing of the Arabidopsis degradome. *Curr Biol* **18**, 758-762 (2008).
113. Pantaleo, V. *et al.* Identification of grapevine microRNAs and their targets using high-throughput sequencing and degradome analysis. *Plant J* **62**, 960-976 (2010).

114. Zhang, W.W., Luo, Y.P., Gong, X., Zeng, W.H. & Li, S.G. Computational identification of 48 potato microRNAs and their targets. *Computational Biology and Chemistry* **33**, 84-93 (2009).
115. Zhou, M. *et al.* Degradome sequencing reveals endogenous small RNA targets in rice (*Oryza sativa* L. ssp. indica). *Frontiers of Biology* **1**, 67-90 (2010).
116. Chen, X. A microRNA as a translational repressor of APETALA2 in Arabidopsis flower development. *Science* **303**, 2022-2025 (2004).
117. Ko, J.H., Prassinos, C. & Han, K.H. Developmental and seasonal expression of PtaHB1, a *Populus* gene encoding a class III HD-Zip protein, is closely associated with secondary growth and inversely correlated with the level of microRNA (miR166). *New Phytol* **169**, 469-478 (2006).
118. Parker, R. & Sheth, U. P bodies and the control of mRNA translation and degradation. *Molecular cell* **25**, 635-646 (2007).
119. Kuester, H. *et al.* Construction and validation of cDNA-based Mt6k-RIT macro- and microarrays to explore root endosymbioses in the model legume *Medicago truncatula*. *J Biotechnol* **108**, 95-113 (2004).
120. Khvorova, A., Reynolds, A. & Jayasena, S.D. Functional siRNAs and miRNAs exhibit strand bias. *Cell* **115**, 209-216 (2003).
121. Schwarz, D.S. *et al.* Asymmetry in the assembly of the RNAi enzyme complex. *Cell* **115**, 199-208 (2003).
122. Pant, B.D. *et al.* Identification of nutrient-responsive Arabidopsis and rapeseed microRNAs by comprehensive real-time polymerase chain reaction profiling and small RNA sequencing. *Plant Physiol* **150**, 1541-1555 (2009).
123. Okamura, K. *et al.* The regulatory activity of microRNA* species has substantial influence on microRNA and 3' UTR evolution. *Nature structural & molecular biology* **15**, 354-363 (2008).
124. Yang, J.H. *et al.* starBase: a database for exploring microRNA-mRNA interaction maps from Argonaute CLIP-Seq and Degradome-Seq data. *Nucleic Acids Res* (2010).
125. Gu, M. *et al.* Expression analysis suggests potential roles of microRNAs for phosphate and arbuscular mycorrhizal signaling in *Solanum lycopersicum*. *Physiologia Plantarum* **138**, 226-237 (2010).
126. Jagadeeswaran, G. *et al.* Deep sequencing of small RNA libraries reveals dynamic regulation of conserved and novel microRNAs and microRNA-stars during silkworm development. *BMC Genomics* **11**, 52 (2010).
127. Zhou, H. *et al.* miR-155 and its star-form partner miR-155* cooperatively regulate type I interferon production by human plasmacytoid dendritic cells. *Blood* **116**, 5885-5894 (2010).
128. Zhang, X. *et al.* Arabidopsis Argonaute 2 regulates innate immunity via miRNA393(*)-mediated silencing of a Golgi-localized SNARE gene, MEMB12. *Molecular cell* **42**, 356-366 (2011).
129. Hsieh, L.C. *et al.* Uncovering small RNA-mediated responses to phosphate deficiency in Arabidopsis by deep sequencing. *Plant Physiol* **151**, 2120-2132 (2009).
130. Chiou, T.J. The role of microRNAs in sensing nutrient stress. *Plant Cell Environ* **30**, 323-332 (2007).
131. Kidner, C.A. & Martienssen, R.A. The developmental role of microRNA in plants. *Curr Opin Plant Biol* **8**, 38-44 (2005).
132. Szittya, G. *et al.* High-throughput sequencing of *Medicago truncatula* short RNAs identifies eight new miRNA families. *BMC Genomics* **9**, 593 (2008).

133. Jones, J.D. & Dangl, J.L. The plant immune system. *Nature* **444**, 323-329 (2006).
134. Glowacki, S., Macioszek, V.K. & Kononowicz, A.K. R proteins as fundamentals of plant innate immunity. *Cellular & molecular biology letters* (2010).
135. Abdel-Fattah, G.M., El-Haddad, S.A., Hafez, E.E. & Rashad, Y.M. Induction of defense responses in common bean plants by arbuscular mycorrhizal fungi. *Microbiological research* (2010).
136. Campos-Soriano, L., Garcia-Garrido, J.M. & San Segundo, B. Activation of basal defense mechanisms of rice plants by *Glomus intraradices* does not affect the arbuscular mycorrhizal symbiosis. *New Phytol* **188**, 597-614 (2010).
137. Lu, X.Y. & Huang, X.L. Plant miRNAs and abiotic stress responses. *Biochemical and biophysical research communications* **368**, 458-462 (2008).
138. Kalo, P. *et al.* Nodulation signaling in legumes requires NSP2, a member of the GRAS family of transcriptional regulators. *Science* **308**, 1786-1789 (2005).
139. Wulff, B.B., Thomas, C.M., Parniske, M. & Jones, J.D. Genetic variation at the tomato Cf-4/Cf-9 locus induced by EMS mutagenesis and intralocus recombination. *Genetics* **167**, 459-470 (2004).
140. Oldroyd, G.E. & Long, S.R. Identification and characterization of nodulation-signaling pathway 2, a gene of *Medicago truncatula* involved in Nod actor signaling. *Plant Physiol* **131**, 1027-1032 (2003).
141. Maillet, F. *et al.* Fungal lipochitooligosaccharide symbiotic signals in arbuscular mycorrhiza. *Nature* **469**, 58-63 (2011).
142. Hirsch, S. *et al.* GRAS proteins form a DNA binding complex to induce gene expression during nodulation signaling in *Medicago truncatula*. *Plant Cell* **21**, 545-557 (2009).
143. Branscheid, A., Devers, E.A., May, P. & Krajinski, F. Distribution pattern of small RNA and degradome reads provides information on miRNA gene structure and regulation. *Plant signaling & behavior* **6**, 1609-1611 (2011).
144. Xie, Z., Kasschau, K.D. & Carrington, J.C. Negative feedback regulation of Dicer-Like1 in *Arabidopsis* by microRNA-guided mRNA degradation. *Curr Biol* **13**, 784-789 (2003).
145. Vaucheret, H., Vazquez, F., Crete, P. & Bartel, D.P. The action of ARGONAUTE1 in the miRNA pathway and its regulation by the miRNA pathway are crucial for plant development. *Genes Dev* **18**, 1187-1197 (2004).
146. Meng, Y. *et al.* Mechanisms of microRNA-mediated auxin signaling inferred from the rice mutant *osaxr*. *Plant signaling & behavior* **5**, 252-254 (2010).
147. Kehr, J. & Buhtz, A. Long distance transport and movement of RNA through the phloem. *J Exp Bot* **59**, 85-92 (2008).
148. Jorgensen, R.A., Atkinson, R.G., Forster, R.L. & Lucas, W.J. An RNA-based information superhighway in plants. *Science* **279**, 1486-1487 (1998).
149. Ham, B.K. *et al.* A polypyrimidine tract binding protein, pumpkin RBP50, forms the basis of a phloem-mobile ribonucleoprotein complex. *Plant Cell* **21**, 197-215 (2009).
150. Wang, C. *et al.* Involvement of OsSPX1 in phosphate homeostasis in rice. *Plant J* **57**, 895-904 (2009).
151. Shin, H., Shin, H.S., Chen, R. & Harrison, M.J. Loss of At4 function impacts phosphate distribution between the roots and the shoots during phosphate starvation. *Plant Journal* **45**, 712-726 (2006).
152. Eamens, A.L., Agius, C., Smith, N.A., Waterhouse, P.M. & Wang, M.B. Efficient silencing of endogenous microRNAs using artificial microRNAs in *Arabidopsis thaliana*. *Molecular plant* **4**, 157-170 (2011).

153. Smith, S.E., Jakobsen, I., Groenlund, M. & Smith, F.A. Roles of arbuscular mycorrhizas in plant phosphorus (P) nutrition: interactions between pathways of P uptake in arbuscular mycorrhizal (AM) roots have important implications for understanding and manipulating plant P acquisition. *Plant Physiol* (2011).
154. deMiranda, J.C.C. & Harris, P.J. Effects of soil phosphorus on spore germination and hyphal growth of arbuscular mycorrhizal fungi. *New Phytologist* **128**, 103-108 (1994).
155. Benabdellah, K., Azcon-Aguilar, C. & Ferrol, N. Plasma membrane ATPase and H⁺ transport activities in microsomal membranes from mycorrhizal tomato roots. *Journal of Experimental Botany* **50**, 1343-1349 (1999).
156. Smith, S.E. & Read, D.J. *Mycorrhizal symbiosis*, Edn. 2. (Academic Press, San Diego and London; 1997).
157. Rosewarne, G.M., Barker, S.J. & Smith, S.E. Production of near-synchronous fungal colonization in tomato for developmental and molecular analyses of mycorrhiza. *Mycological Research* **101**, 966-970 (1997).
158. Rudic, R.D. Time is of the essence: vascular implications of the circadian clock. *Circulation* **120**, 1714-1721 (2009).
159. Liu, J. & Vance, C.P. Crucial roles of sucrose and microRNA399 in systemic signaling of P deficiency: A tale of two team players? *Plant signaling & behavior* **5** (2010).
160. Hammond, J.P. & White, P.J. Sugar signaling in root responses to low phosphorus availability. *Plant Physiol* **156**, 1033-1040 (2011).
161. Lei, M. *et al.* Genetic and genomic evidence that sucrose is a global regulator of plant responses to phosphate starvation in Arabidopsis. *Plant Physiol* **156**, 1116-1130 (2011).
162. Liu, J.Q., Allan, D.L. & Vance, C.P. Systemic signaling and local sensing of phosphate in common bean: cross-talk between photosynthate and microRNA399. *Molecular plant* **3**, 428-437 (2011).
163. Sheng, M. *et al.* Influence of arbuscular mycorrhizae on photosynthesis and water status of maize plants under salt stress. *Mycorrhiza* **18**, 287-296 (2008).
164. Gabriel-Neumann, E., Neumann, G., Leggewie, G. & George, E. Constitutive overexpression of the sucrose transporter SoSUT1 in potato plants increases arbuscular mycorrhiza fungal root colonization under high, but not under low, soil phosphorus availability. *J Plant Physiol* **168**, 911-919 (2011).
165. Olsson, P.A., Hansson, M.C. & Burleigh, S.H. Effect of P availability on temporal dynamics of carbon allocation and glomus intraradices high-affinity P transporter gene induction in arbuscular mycorrhiza. *Appl Environ Microbiol* **72**, 4115-4120 (2006).
166. Lendenmann, M. *et al.* Symbiont identity matters: carbon and phosphorus fluxes between *Medicago truncatula* and different arbuscular mycorrhizal fungi. *Mycorrhiza* **21**, 689-702 (2011).
167. Olsson, P.A., Rahm, J. & Aliasgharzad, N. Carbon dynamics in mycorrhizal symbioses is linked to carbon costs and phosphorus benefits. *FEMS microbiology ecology* **72**, 125-131 (2010).
168. Yoo, B.C. *et al.* A systemic small RNA signaling system in plants. *Plant Cell* **16**, 1979-2000 (2004).
169. Lough, T.J. & Lucas, W.J. Integrative plant biology: role of phloem long-distance macromolecular trafficking. *Annu Rev Plant Biol* **57**, 203-232 (2006).
170. Omid, A., Keilin, T., Glass, A., Leshkowitz, D. & Wolf, S. Characterization of phloem-sap transcription profile in melon plants. *J Exp Bot* **58**, 3645-3656 (2007).

-
171. Molnar, A. *et al.* Small silencing RNAs in plants are mobile and direct epigenetic modification in recipient cells. *Science* **328**, 872-875 (2010).
 172. Tretter, E.M., Alvarez, J.P., Eshed, Y. & Bowman, J.L. Activity range of Arabidopsis small RNAs derived from different biogenesis pathways. *Plant Physiol* **147**, 58-62 (2008).
 173. Alvarez, J.P. *et al.* Endogenous and synthetic microRNAs stimulate simultaneous, efficient, and localized regulation of multiple targets in diverse species. *Plant Cell* **18**, 1134-1151 (2006).
 174. Juarez, M.T., Kui, J.S., Thomas, J., Heller, B.A. & Timmermans, M.C. microRNA-mediated repression of rolled leaf1 specifies maize leaf polarity. *Nature* **428**, 84-88 (2004).
 175. Liu, H., Trieu, A.T., Blaylock, L.A. & Harrison, M.J. Cloning and Characterization of Two Phosphate Transporters From Medicago Truncatula Roots - Regulation in Response to Phosphate and to Colonization By Arbuscular Mycorrhizal (Am) Fungi. *Molecular Plant-Microbe Interactions* **11**, 14-22 (1998).
 176. Bucher, M. Functional biology of plant phosphate uptake at root and mycorrhiza interfaces. *New Phytol* **173**, 11-26 (2007).
 177. Smith, S.E., Smith, F.A. & Jakobsen, I. Mycorrhizal fungi can dominate phosphate supply to plants irrespective of growth responses. *Plant Physiol* **133**, 16-20 (2003).

7 Acknowledgement

At the first place, I would like to acknowledge Prof. Dr. Franziska Krajinski for her supervision and giving me the opportunity to carry out this PhD in her research group at the Max-Planck-Institute of Molecular Plant Physiology.

I would like to thank all members of the AG Krajinski and particularly Emanuel Devers, my closest colleague during my studies and the three years of PhD, for fruitful discussions and support over the whole time. I have learned a lot with his precious input and his scientific advices during the writing of this manuscript.

Many thanks also to Nicole Gaude for her advices at all times and the nice moments especially during coffee breaks. Daniela Zöller, Vinzenz Hofferek, Przemek Cajka for technical and practical support in handling all these huge experimental setups. Thank you all for the great working atmosphere we shared during our time together.

Many thanks to Prof. Dr. Lothar Willmitzer, Dr. Joost van Dongen and Dr. Wolf-Rüdiger Scheible for accepting to be member of my thesis committee and the valuable scientific feedback.

I would also like to thank Ina Talke for recruiting me for the IMPRS, an important source of scientific input, discussions and intercultural communication.

Many thanks to Uschi for her friendship and particularly for the help in taking care of my son during writing my thesis.

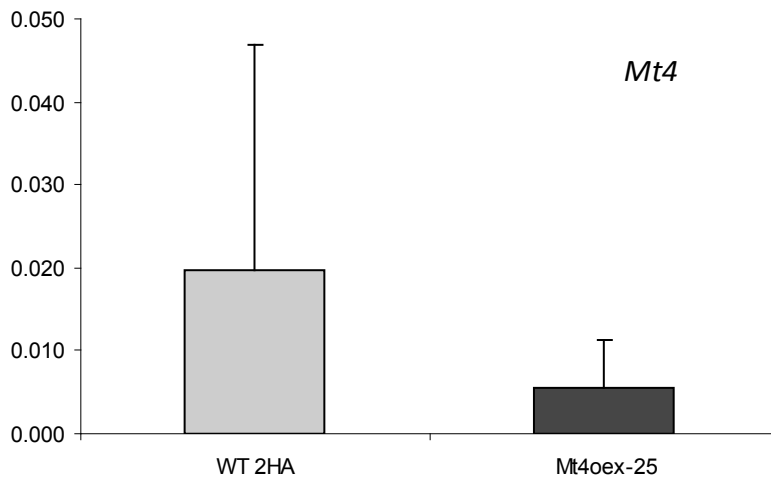
A big thank you to all my friends for the great time we shared, the support and cheering words in stressful times, enduring ups and downs I had during my thesis.

Many many thanks to Derek and Enrico for proofreading of this manuscript.

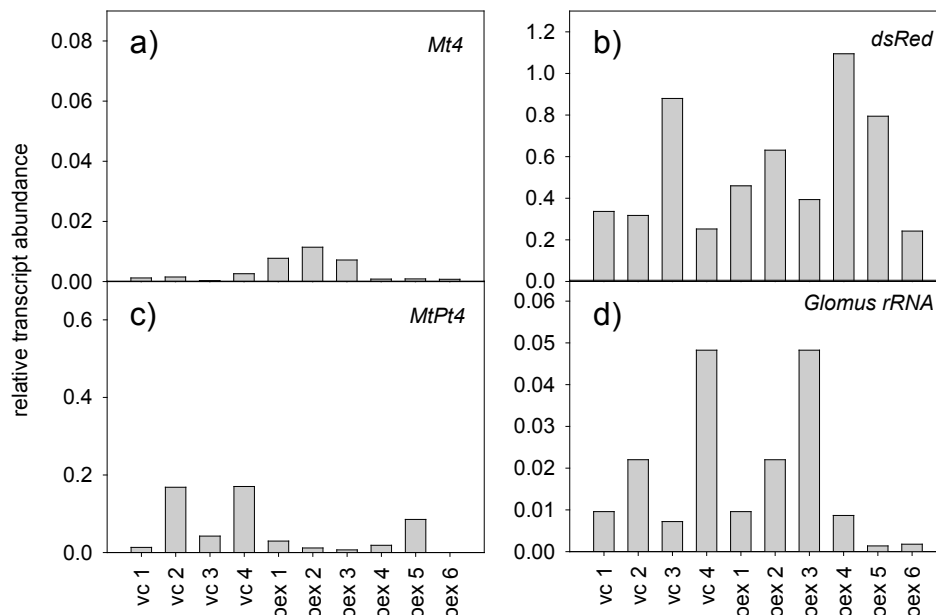
Finally, I would like to thank my family, particularly my sisters Cindy and Diana for their friendship and always believing in me. I am thankful to my mother, who always encouraged and supported me whenever I needed some time to breathe deeply.

A very special thank to Kimi, my lovely son and bright side in my life, I am glad there is you.....

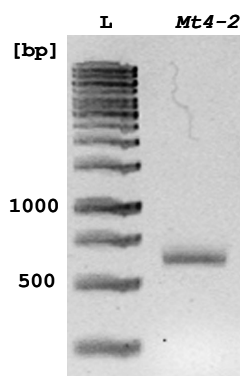
8 Supplementary



Suppl. Fig. 1. qRT-PCR measurements of *Mt4* transcript abundance in *M. truncatula* wild type (WT) and stable *Mt4* overexpression plants (35Spro::*Mt4*). Relative transcript abundance of *Mt4* were calculated relative to the reference gene *MtEf1a*. Each column represents 4 independent biological replicates stdev. Plants were grown at moderate P_i concentrations (1 mM) in Hoagland's solution and harvested 3 weeks after planting.



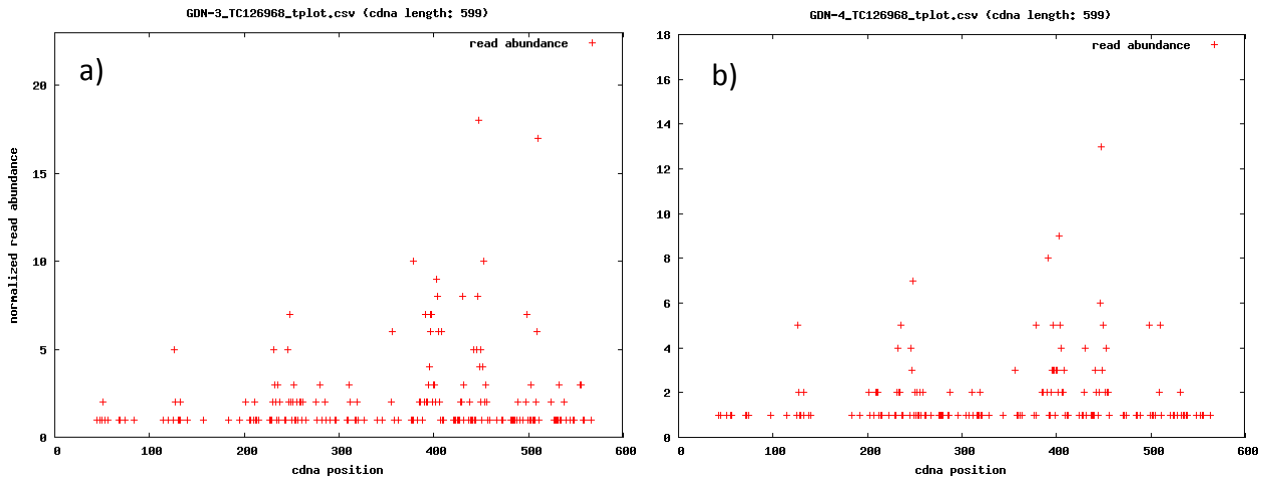
Suppl. Fig. 2. qRT-PCR measurements of *A. rhizogenes* transformed *M. truncatula* roots overexpressing *Mt4* driven by the mycorrhizal specific *MtPt4* promoter (pPT4pro::*Mt4*). Relative transcript abundances of (a) *Mt4*, (b) *dsRed*, (c) *MtPt4*, (d) *GirRNA* were calculated relative to the reference gene *MtEf1a*. Each graphs shows expression levels in 4 independent vector controls (vc) and 6 overexpression lines (oex).



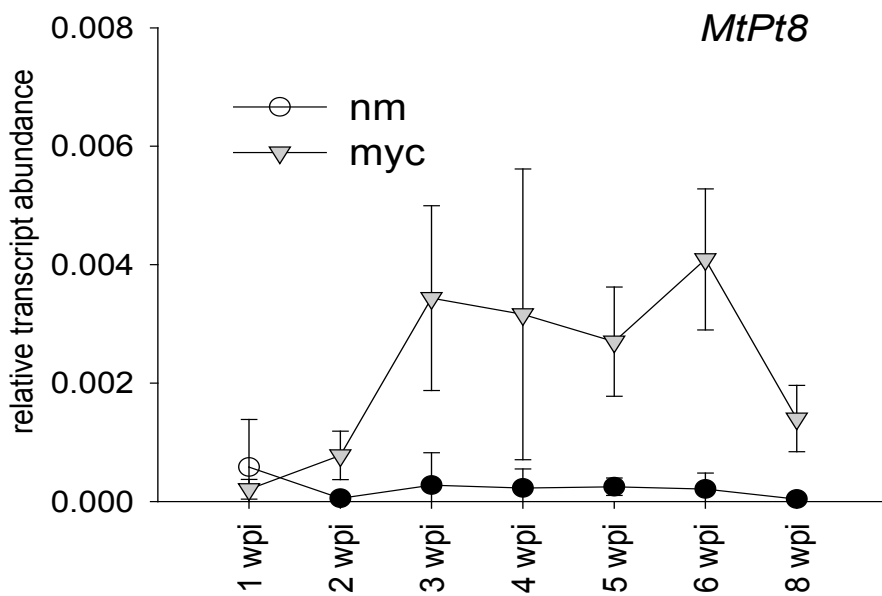
Suppl. Fig 3. RT-PCR validation of *Mt4-2* transcript abundance in cDNA of P_i -depleted *M. truncatula* roots. L: 100 bp DNA ladder, *Mt4-2*: 606 bp PCR fragment resulting from amplification with a primer pair flanking the *Mt4-2* cDNA sequence.

Aco_AcoGoldSmith_v1.003187m		CTGGTCAACTTTT TTTTGGTT
Aco_AcoGoldSmith_v1.003228m		CTGGACAACTCTTCTTTGGGT
Aco_AcoGoldSmith_v1.014549m		CTGGCCAACTCTT TTTTGGCT
Ath_AT1G76430.1		TAGGTCAGCTCATCTTTGGTT
Ath_AT2G32830.1		CAGGCCAGCTCTTCTTCGGTT
Mes_cassava4.1_005221m		CAGGGCAGCTCTTCTTTGGTT
Mes_cassava4.1_005227m		CGGGCAACTCTT TTTTGGTT
Mes_cassava4.1_024814m		TTGGGCAGCTCTTCTTTGGGT
Mes_cassava4.1_031179m		CAGGCCAGCTCTTCTTTGGAT
Cci_clementine0.9_028256m		CTGGGCAACTATTCTTTGGAT
Csa_Cucsa.012870.1		TGGGACAACTTTTCTTTGGGT
Csa_Cucsa.053570.1		CAGGACAACTCTTCTTTGGTT
Csa_Cucsa.383630.1		CTGGCCAACTATTCTTTGGCT
Egr_Eucgr.A02668.1		GAGGCAGATTTCTGTGGCG
Egr_Eucgr.H00162.1		CAGGCCAGATCTTCTTTGGGT
Egr_Eucgr.H03064.1		CAGGCCAGCTCTTCTTTGGCT
Gma_Glyma10g04230.1		CAGGGCAACTCTTCTTTGGCT
Gma_Glyma19g34710.1		CAGGCCAGCTTTTCTTTGGTT
Mtr_Medtr1g089540.1		CAGGACAACTTTTCTTTGGTT
Mtr_Medtr3g106620.1		CAGGCCAACTTTTCTTTGGTT
Mtr_Medtr4g028630.1		CAGGCCAACTTTTCTTTGGTT
Mtr_Medtr5g076920.1	MtPt8	CAGGGCAACTCTTCTTTGGCT
Ptr_POPTR_0001s32590.1		CTGGCCAGCTCTTCTTTGGTT
Ptr_POPTR_0005s15860.1		CGGGACAACTCTTCTTTGGGT
Ptr_POPTR_0005s15880.1		CGGGACAACTCTTCTTTGGGT
Ptr_POPTR_0005s24500.1		CGGGCCAGCTCTTCTTTGGCT
Ptr_POPTR_0005s24500.1		CTGGTCAGCTCTTCTTTGGCT
Ptr_POPTR_0015s06110.1		CAGGC GGATTTTCTTTGGAG
Ptr_POPTR_0019s08990.1		CAGGGCAACTCTTCTTTGGGT
Ppa_Pp1s53_36V6.1		TGGTCAACTCTTCTTTGGAT
Ppe_ppa003959m		CAGGCCAGCTCTTCTTTGGTT
Vvi_GSVIVT01028733001		TGAGGC GGATTTTCTGTGGCG

Suppl. Fig. 4. Sequence alignment of the putative miR399 cleavage sites in P_i -transporter genes of 12 different plant species. Aco – *Aequilegia coerulea*, Mes – *Manihot esculenta*, Ccl – *Citrus clementina*, Csa – *Cucumis sativus*, Egr – *Eucalyptus grandis*, Gma – *Glycine max*, Mtr – *Medicago truncatula*, Ptr – *Populus trichocarpa*, Ppa – *Physcomitrella patens*, Ppe – *Prunus persica*, Vvi – *Vitis vinifera*. The miR399 binding site of *MtPt8* enframed, from this sequence differing nucleotides are shaded in grey. The sequence alignment was carried using the Clustal W algorithm.



Suppl. Fig. 5. Target plots of *Mt4* (TC126968) in nm (a) and myc (b) roots showing the distribution of degradome tag sequences within the *Mt4* transcript.



Suppl. Fig. 6. qRT-PCR measurement of *MtPt8* transcript abundance in *M. truncatula* nm and myc roots 5 wpi dependent on the external P_i treatment (x-axis). Relative transcript abundance was calculated relative to the reference gene *MtEf1a*. Shown values represent 4 independent biological replicates \pm stdev.

cttctggtcaaggctatTTTgagtagtgctaacaaaattctgtccttttattttctcctaattaacttttctctca
 cactaacttttTgtgtagacaagaataaccacctatTTTgggtgacatagagttgagtgatattggTgacattggTca
 atcataatgtcacaatgctTgtgaaagagagagaaatacaagTattgtgacattgtgattgaccaatgtcaccCa
 actctatgtcaccCaagtgtcaccctaattTgacattgtagggcccaccgaaacaatttttattttTgTttgt
 atatgtagacgcaatagaaagcatcattgaaaatacacacataaaatgagagatctTgcgTttgaatccaaaca
 actataaaaaggTtcagtctaacaatctcgccattgtcagTtgagTtttatcttacacataaaaagTtttttaa
 taaaaactaaaagtaattTtaggaatccaaaatgtgTtatatcattaaacatgctcTtatatttccctcattttat
 ttctccctataaccataaaaagtagcattTtgattatTTTaaacattttatataatgtaccatgTaaagtaacaatatga
 aggataaaaaagTaaaaataataaaaaggctTtTgocTtTgtagTttccgaatattattgtgaattcaacaaaatata
 tttTggaactTcatggattTtatctaagaaaagcaaggaattatgattactggTaaaagacagaactatagatgca
 gccagcaatgtgaaagacaacataaaaaacaaacatggctacattatTTTtatcaaatTggaagctTgcttaggg
 TggaagaaactgattgcagcttagccaagagaaagTttTcaaccattaatgccaacaaacaatgtgTtaatatc
 aatgtagTttttcctTgaagaagctgatattTaaataactcgTcactcactatgaaattttTtacagctTtttagaa
 agcaatatcattTgtcaaaaatcccaaaagacaaaaaattatgtTcatatataaaactagcatatttccTtctTttc
 TtctTgtTctcatttttacatcagatacacaacaaacacatattccattgtTcaatgccaat

Suppl. Fig. 7. Breakdown of the 1 kb *MtPt8* promoter region (5'→3') (IMGAG, mt3.0). MYCS binding motif (CTTCTGTTCT) is depicted in a green, the putative transcription start site in a yellow box.

Suppl. Table 1. Oligonucleotides used in this study.

Standard PCR	sequence (forward 5'→3')	sequence (reverse 5'→3')
Mt4_attB	GGGGACAAGTTTGTACAAAAAAGCAGGCTAATCC TATAACAACCAACCAAGC	GGGGACCACTTTGTACAAGAAAGCTGGGTAGAAACGTACA TTTATTGGATATAC
Mt4 (BamHI / HindIII)	GGATCCGTACCAACCTACTTAAGTC	AAGCTTAAATATTAACAACAACAATAG
M4-2_attB	GGGGACAAGTTTGTACAAAAAAGCAGGCTAGCAA CTCCTGTATTTATATATGC	GGGGACCACTTTGTACAAGAAAGCTGGTGTAGCTGCAAATC AGAGATCAATT
pri-miR399d (BamHI/HindIII)	GGATCCTAAAGTAAGCAAATCAGTCATAGGGC	AAGCTTTGTTTAAAGCTAAACACTCGTAGG
MtPt8_Fwd	CTATTCTTATTGTACTTTCCAGC	Nested1 or Nested2
MtPt8_Nested1	CTATTCTTATTGTACTTTCCAGC	GCTGGAAAGTACAATAAGAATAG
MtPt8_Nested2	CTATTCTTATTGTACTTTCCAGC GGGGACAAGTTTGTACAAAAAAGCAGGCTATGGC	CAACGGCTTTCTTGTGATCTCC GGGGACCACTTTGTACAAGAAAGCTGGGTCTAAACCATTG
MtPt8_CDS_attB	CACCAGCCATGGTGTCC	AAGTTTCTGGAG
MtPt8_miR399bs	CACCTAGGTGTTGCGTTGTGTGGC	CTACCAAGCTTGTACCAAGCCAG
MtPt8_mut-miR399bs	CACCGAAT6CCTTATAACAACCAACCAAG	GGATCCAGAAACGTACATTTATTGG
MtPt8_promoter	GGGGACAAGTTTGTACAAAAAAGCAGGCTCGGG GATCCTGATGATAGC	GCTGTGATGCAGAAGAGATCACTGCAGGTGACGGCATTG
MIR399d_promoter	CACCATTATCTTCCAAATACTACCTCCG	GCTAAGTATCAAATGACACTCCC
MtPhr1 (oex)	CACCATGCTGGAGCACTTCCTTC	TTCACTCATCTGCTCTTTGACG
MtPhr1 3'UTR (RNAi)	CACCTTCTGAATCAGCATTGAACCG	ACACTAGAATCTCATCTTAACAG
M13	GTAAACGACGGCCAG	CAGGAAACAGCTATGAC
CaMV-35Spro	CACCAGATTAGCCTTTTCAATTC	CGTGTCTCTCCAAATGAAATGAA
GUS-F	TTAACGATCAGTTCGCCGATGCAG	ACGCAGTTCAACGCTGACATCACC
GUS (XmaI/MluI)	CCCGGGATGTTACGTCCTGTA	ACGCGTCATTGTTGCTCC
RACE 5'Adapter outer	GCTGATGGCGATGAATGAACACTG	
RACE 5'Adapter inner	CGCGGATCCGAACACTGCGTTTGTGGCTTTGATG	
Tnt1-F2	TCTTGTAATTACCGTATCTCGGTGCTACA	

qRT-PCR	sequence (forward 5'→3')	sequence (reverse 5'→3')
MtEF1α	GACAAGCGTGTGATCGAGAGATT	TTTCACGCTCAGCCTTAAGCT
MtPDF2	GTGTTTTGCTTCCGCCGTT	CCAAATCTTGCTCCCTCATCTG
MtUbi intron	GTCCTCTAAGGTTTAATGAACCGG	GAAAGACACAGCCAAGTTGCAC
qRT_MtPhr1_3'UTR	TCTTATCAACATCCTACGACCT	ATGACTCTAATCCAACAAACGG
qRT_MtPhr1_ORF	TTGGCAGGAGTGGGCTGACC	ATGGAGCGACGCCAACATGG
qRT_Mt4	AATGATTGCTGGGAATGAACCTT	TTCCAAAGAGAAAATCCCATCAA
qRT_Mt4/H1	TTCTTTCTCCAGCCACAAAT	AGGATACATAAATTGCCAAAGGAT
qRT_pri-miR399d	TAAGCAAATCAGTCATAGGGCATG	TAGGGCAGCTCTCCTTTGGC
qRT_mat-miR399_GCT	CGGATTGAAAAAGGAGAGC	CCAGTGCAGGGTCCGAGGT
qRT_mat-miR399_TTT	GCGGATTGCCAAAGGAGATT	CCAGTGCAGGGTCCGAGGT
qRT_mat-miR399_GTT	CGGATTGCCAAAGGAGAGT	CCAGTGCAGGGTCCGAGGT
qRT_mat-miR399_K	GCGGATCGCCAAAGAAGATT	CCAGTGCAGGGTCCGAGGT
qRT-Pho2_rev	AACCAGAAGGGAACTTCAACAGG	ATGTCAACAACTGGGAGCAATCG
qRT_MtPID	TTGATGAATGGAAGCCGTGG	GCGGAGGCTATGGGAAAATTT
qRT_MtPT4	CAAGAAAGATTAGACGCGCAA	GTTTCCGTCACCAAGAACGTG
qRT_Gi rRNA	GTATGCCTGTTTGAGGGTCAGTATT	AAACTCCGGAACGTCACTAAAGAG
qRT_GiαTubulin	TGTCCAACCGGTTTTAAAGT	AAAGCACGTTTGGCGTACAT
qRT_MtGst1	CGGAAAATGCAAACTCGTCTC	GACGTCGATAACACTTAGCGACAA
qRT_nptII	CGCCAGCCGAAGTGTTCG	CGATACCGTAAAGCACGAGGAAGC
qRT_mRFP	ATGGCCTCCTCCGAGGACGT	TTAGGCGCCGGTGGAGTGGC
qRT_eGFP	TCAAGGTGAACTTCAAGATCC	TCCTTCTGTACAGCTCGTC
qRT_Hygromycin	GCTGCGTAAAAGATACGGAAGGAATG	CATCATGCCGTTCAAAGTGC
qRT_DsRed	ATGCAGATCTTTGCCATGGCGC	AGGGGGCCGCCCTTGGTCACT
cDNA synthesis	sequence (5'→3')	
stemloop_miR399-GCT	GTCGTATCCAGTGCAGGGTCCGAGGTATTCGCAC TGGATACGACCAGGGCA	
stemloop_miR399-TTT	GTCGTATCCAGTGCAGGGTCCGAGGTATTCGCAC TGGATACGACTGGGCA	
stemloop_miR399-GTT	GTCGTATCCAGTGCAGGGTCCGAGGTATTCGCAC TGGATACGACCAGGGCA	
stemloop_miR399k	GTCGTATCCAGTGCAGGGTCCGAGGTATTCGCAC TGGATACGACTAGGGCA	
Oligo_dT(30)	TTTTTTTTTTTTTTTTTTTTTTTTTTTTTTTT	

9 Eidesstattliche Erklärung

Ich versichere hiermit, die vorliegende Arbeit selbstständig angefertigt und keine anderen als die angegebenen Quellen und Hilfsmittel verwendet zu haben. Ich versichere ebenfalls, dass die Arbeit an keiner anderen Hochschule als der Universität Potsdam eingereicht wurde.

29.02.2012

Anja Branscheid